Bioengineered in vitro Model for Peri-implantation Human Embryogenesis

by

Yue Shao

A dissertation submitted in partial fulfillment
of the requirements for the degree of
Doctor of Philosophy
(Mechanical Engineering)
in the University of Michigan
2017

Doctoral Committee:

Associate Professor Jianping Fu, Chair
Professor Deborah L. Gumucio
Assistant Professor Allen P. Liu
Professor K. Sue O'Shea

ACKNOWLEDGEMENTS

I am grateful to innumerable people for their help and guidance during my time at the University of Michigan. First and foremost, I would like to express my deepest and most sincere gratitude to my advisor, Prof. Jianping Fu, for his enthusiastic encouragement, immense support, and wise advice during my entire PhD study. His open-mindedness and unconditional support have provided me with the best environment to cultivate my creativity. His great mentoring has taught me many invaluable lessons on my path to be an independent researcher.

My greatest gratitude also goes to Prof. Deborah L. Gumucio, for her heartwarming support of my work in her lab and her wise and meticulous advice on my PhD research. Her mentoring in the last two years is irreplaceable to me and has given me great ideas of the skill-set and mind-set needed for the pursuit of top-notch science.

I also owe special thanks to Prof. Allen P. Liu and Prof. K. Sue. O'Shea for their constant warm and firm support of my research and their insightful advice that have come at many different places during my time of PhD study. I would also like to extend my special gratitude to Prof. Jason R. Spence, Prof. Sundeep Kalantry, Prof. Toshio Miki (USC), and Dr. William Shawlot (UT-Austin) for their help and constructive suggestions to my research. I also want to thank the Virtual Human Embryo project for providing the Carnegie stage human embryo section images (http://virtualhumanembryo.lsuhsc.edu) that are used in my studies.

My special thanks also go to all members and alumni of the Fu lab, who have generously lent me their help through my PhD study. I would also like to thank all members and alumni of the Gumucio lab for their help, suggestions, and hospitality during my work there in the last two years. I want to specially thank Dr. Kenichiro Taniguchi and Mr. Ryan F. Townshend from the Gumucio lab, as well as Dr. Yu-Hwai Tsai and Ms. Sha Huang from the Spence lab for their invaluable assistance in my research. I would also like to extend my special thanks to every colleague who I have worked with during my PhD study, for our fruitful and memorable work together.

I would like to thank the University of Michigan, for supporting top-class research facilities, professional and friendly staff, as well as a highly interdisciplinary research atmosphere, which were all indispensible for my PhD research. I want to specially thank the Microscopy and Image Analysis Laboratory (MIL; University of Michigan Medical School), the University of Michigan DNA Sequencing Core, the Flow Cytometry Core (University of Michigan Medical School), the University of Michigan MStem Cell Laboratories, the University of Michigan Pluripotent Stem Cell Core, and the University of Michigan Lurie Nanofabrication Facility, for their assistance.

I also want to thank the Department of Mechanical Engineering, the College of Engineering, and the Rackham Graduate School for their support on various levels. I want to specially thank the Alexander Azarkhin Scholarship, I.K. McIvor Award, Richard and Eleanor Towner Prize for Outstanding PhD Research, and the Rackham Predoctoral Fellowship for supporting my studies.

In the end, I want to express my utmost gratitude to my beloved wife and our parents, whose steady, unshakable, unconditional, and unlimited love and support have made this dissertation possible. Last but not the least, I thank all my friends, nearby or afar, for your caring and keen friendship as always, and I hope our paths will cross again in the years to come.

TABLE OF CONTENTS

LIST OF FIGURES

LIST OF TABLES

LIST OF APPENDICES

ABSTRACT

Implantation is a critical developmental milestone for early human embryogenesis and successful pregnancy. During implantation, the pluripotent epiblast gives rise to the squamous amnion and the columnar embryonic disc, which together enclose the amniotic cavity to form an asymmetric cystic structure called the amniotic sac. Amniogenesis - the development of amnion - marks the first differentiation of the epiblast during implantation; in parallel, the formation of the amniotic sac delineates the morphology of the human embryo and prepares it for subsequent gastrulation. Despite its fundamental and clinical importance, the development of the amnion and the amniotic sac in humans remains mysterious due to the scarcity and restricted availability of *in vivo* human embryo specimens and the lack of *in vitro* models.

In this dissertation, we report the first *in vitro* model for peri-implantation human amniogenesis and amniotic sac development, by culturing human pluripotent stem cells (hPSCs) in a bioengineered niche that mimics the physical microenvironment experienced by human embryos during implantation. Specifically, we find that hPSCs cultured in such implantation-like niche undergo self-organized development and form three dimensional (3D) structures *in vitro* that molecularly and morphologically resemble human amnion and human amniotic sac *in vivo*. We further show that implantation-like physical niche cues - a soft tissue bed and a 3D extracellular matrix (ECM) - are both necessary and sufficient for triggering the amniogenic development in an otherwise self-renewal-permissive biochemical context. We also demonstrate

that the hPSC-derived amniotic sac embryoid can model human amniotic sac development beyond the peri-implantation stage with primitive streak-like development. Additionally, we unveil an endogenous BMP-SMAD signaling underlying peri-implantation human amniogenesis and amniotic sac patterning.

Furthermore, we demonstrate an integrative mechanotransduction that can induce amniogenesis of hPSCs by integrating multiple upstream signals including substrate rigidity, cell cluster size, and cell spreading. Enabled by such new knowledge, we have developed a novel micro-engineered array of hPSC-derived amnion-like tissues, as a potential high-throughput screening platform for regenerative medicine.

Together, findings in this dissertation provide innovative *in vitro* systems for investigating early human embryogenesis during implantation and early gastrulation, thereby helping advance human embryology and reproductive and regenerative medicine.

CHAPTER I

Introduction

After fertilization, the human embryo embarks on a 40-week journey that gradually reveals the complexity and beauty of life (Figure 1-1). Starting from a fertilized egg, the human embryo first develops into a hollow structure called blastocyst during the first week of pregnancy. This pre-implantation embryo next undergoes implantation, gastrulation, and body folding in an orchestrated manner to establish the overall body plan of the human embryo by the end of the first month. Organogenesis, which initiates near the end of the first month, gives rise to a variety of organ rudiments that evolve into organ systems with a myriad of functions, constituting the sophisticated biological machinery for the development and intrauterine life of a human fetus. Together, these early developmental events lay the foundations that are indispensible for human embryo development.

Ever since the bewilderment manifested by ancient philosophers, "the development of the human" has been a question that not only stimulates philosophical thoughts on human nature but

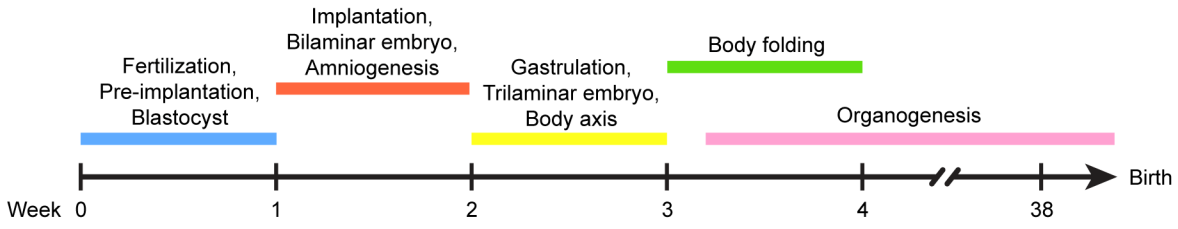

Figure 1-1 Timeline of human embryonic development.

also drives the advancement of modern science and medicine. Despite of such importance, our understanding of human development, especially the aforementioned early stages, is still limited, largely due to the ethical controversies surrounding *in vivo* experimentation and the lack of technologies for *in vitro* studies. The goal of this dissertation is therefore to fill such a gap in knowledge and technology, by taking advantage of the recent rise of human pluripotent stem cell engineering to develop *in vitro* methods for studying human development during implantation - a critical developmental milestone that ensues during the second week of pregnancy.

In this chapter, I will briefly summarize the background and the outline of this dissertation.

1.1 Human Embryogenesis in the First Two Weeks of Pregnancy

Herein, I present a concise summary of our current understanding of early human development[1] during the first two weeks of pregnancy (Figure 1-2), with a focus on the peri-/post-implantation development of the embryo during the second week, when it forms the

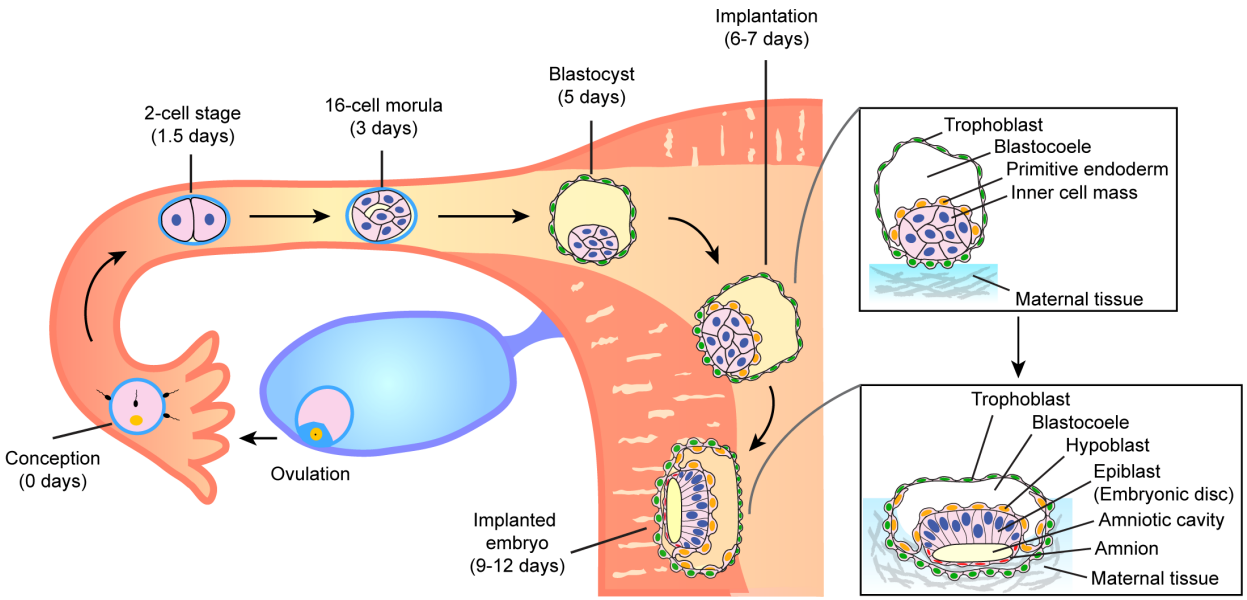

Figure 1-2 Schematic summarizing the development of human embryo during the first two weeks of pregnancy. The epiblast, amnion, and the amniotic cavity constitute the amniotic sac.

amniotic sac - a key developmental structure that delineates the rudimentary morphology of the human embryo enveloped by the amnion.

1.1.1 Pre-implantation Development of the Human Embryo

After the union of egg and sperm upon fertilization/conception in the oviduct, the zygote travels down the oviduct and undergoes its fist cleavage (Figure 1-2). With a series of cleavages that follow, the embryo develops into a solid cluster of multiple cells (Figure 1-2). Cells in the embryo at this stage are called blastomeres and each blastomere has the so-called "totipotency" - the capability of differentiating and becoming any cell type in the human body. Upon further development, the morula differentiates into two distinct populations of cells with different localization and destiny. Specifically, through a process called compaction, some cells in the morula are excluded from the surface and internalized into the embryo to form the inner cell mass (ICM). In the meantime, the outer cells of the morula compact into a thin epithelial layer called the trophectoderm (TE), which contains cells named trophoblast and surrounds the inner cell mass with a cavity - the blastocoele (Figure 1-2). During further development, the ICM will give rise to the embryo proper and embryo-associated extraembryonic tissues such as the amnion and the yolk sac; in contrast, the TE will develop into part of the placenta and some other extraembryonic tissues. At this stage, cells residing in the ICM, but not TE, have the characteristic of "pluripotency" - the capability of generating all human cell types including the three germ layers that constitute the embryo proper. By days post fertilization (d.p.f.) 5 - 6, the embryo develops into a hollow fluid-filled structure called a blastocyst and enters the uterine cavity, ready for the next step - implantation (Figure 1-2). More extensive summary of human pre-implantation embryo development can be found in a recent review by others[2].

1.1.2 Peri- and Post-implantation Development of the Human Embryo

At d.p.f. 5 - 6, shortly before the human embryo (blastocyst) attaches to the endometrial lining of the uterine wall and begins its invasion into the maternal tissue (Figure 1-2) - a process named implantation, the embryo initiates a transformation *via* sorting the ICM into two distinct cell groups: the epiblast and the hypoblast (or primitive endoderm). Hypoblast - a differentiated cell type originating from ICM and lining one side of the ICM and later epiblast - will give rise to theprimary and secondary yolk sac. The epiblast, which retains the pluripotency from the ICM, will continue to generate the embryo proper and an important extraembryonic tissue that envelops the embryo till birth - the amnion. Together, the amnion and the epiblast enclose a fluid-filled cavity called the amniotic cavity, and thereby form an asymmetrically patterned sac-like structure called the amniotic sac. The development of amnion and amniotic sac is of particular importance and represents the focus of this dissertation because it generates the basic morphology of a human embryo, which is the indispensable foundation for any later development of the embryo.

The development of the human embryo during implantation, commonly referred to as peri-implantation or post-implantation development, is understood based on histological sections of

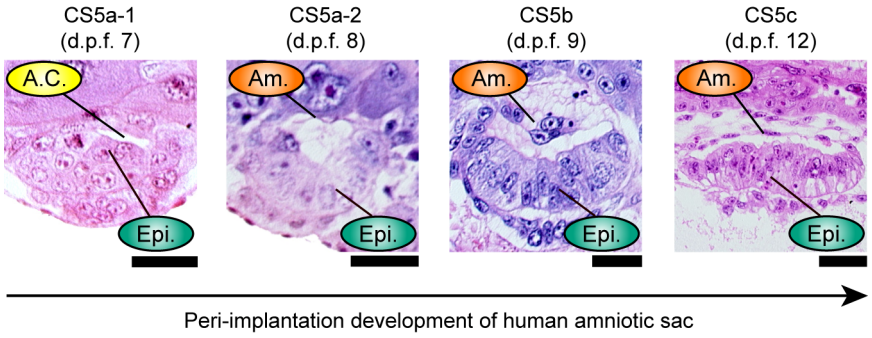

Figure 1-3 Human amniotic sac development *in vivo*. Carnegie stage (CS) 5a-1[3], 5a-2[4], 5b[3], and 5c[5] human embryos at d.p.f. 7, 8, 9, and 12, respectively. A.C., pro-amniotic cavity; Epi., epiblast; Am., amnion. Sections are obtained from the Virtual Human Embryo project.

historically acquired human embryo samples accumulated in collections of human embryos, such as the Carnegie collection. As shown in Figure 1-3, sections obtained from the Carnegie collection demonstrate the histological changes during human amniotic sac development. Specifically, at d.p.f. 7 - about 1 day after implantation initiates - the embryo invades into the uterine wall and the cluster of epiblast cells undergoes polarization and forms a distinct cavity - the pro-amniotic cavity. Other than the establishment of epiblast polarity, there is no distinct sign of differentiation within the epiblast at this point. Interestingly, at d.p.f. 8, the columnar epiblast cells appear to align only along one side of the cavity, sitting next to the hypoblast layer; while seemingly flattened cell(s) enclose the cavity on the other side. The appearance of such flattened cells with a squamous morphology implies the differentiation towards presumptive amniotic cells (amnioblasts) from the epiblast in the embryo. Further development between d.p.f. 9 and 12 clearly demonstrates the expansion of the squamous tissue on one side of the amniotic cavity with a paralleled expansion of columnar epiblast on the other side. Together, they organize into an asymmetrically patterned amniotic sac, whose amniotic pole nestles beside the developing trophoblast invading into the uterine wall while the epiblast pole sits next to the developing hypoblast. Such histogenesis of amnion and morphogenesis of amniotic sac is also observed in non-human primates, such as cynomolgus monkey and rhesus monkey[6-8].

1.2 Current Understanding of Peri-implantation Human Embryogenesis is Limited

In the past decade, rapid development of "omics" sciences and the availability of pre-implantation human embryos for research purposes (*via* cryopreserved samples from in vitro fertilization clinics) have significantly advanced our understanding of pre-implantation human embryo development[9-13]. In contrast, our understanding of peri-implantation human

embryogenesis remains limited, due to the inaccessibility to peri-implantation human embryo samples. So far, knowledge about peri-implantation human embryogenesis is largely drawn from interpretations of images of sectioned human and primate embryos that were deposited in embryo collections more than 50 years ago. Despite recent excitement in developing *in vitro* systems for studying early human embryogenesis[14-17], the induction of two key peri-implantation developmental structures - the amnion and the amniotic sac - in humans remains mysterious to date. Here, a brief summary is provided to highlight the gap in our current knowledge about peri-implantation human amniogenesis and amniotic sac development.

1.2.1 Different Hypotheses Suggested for Human and Non-human Primate Amniogenesis

At the commencement of implantation, the epiblast undergoes prominent cellular reorganization. Specifically, it transforms from an irregularly packed cell aggregate to a spherical cell cluster showing evidence of cell polarity, with the basal surface facing the basal lamina (which is deposited at the epiblast/hypoblast interface as well as the epiblast/trophoblast interface) and the apical surface oriented towards the interior (Figure 1-4). The epiblast cluster next undergoes lumenogenesis and form a cavity inside the cluster (Figure 1-4). Although it has been commonly accepted that such epiblast "cyst" is the precursor that further gives rise to the amnion and the amniotic sac, it is still under debate that how the subsequent induction and morphogenesis of amnion occurs in peri-implantation human embryos[18] (Figure 1-4).

For example, in an early study published in 1975, Luckett conducted a histological analysis of archived images of sectioned human and monkey embryos[6]. In this study, Luckett proposed the hypothesis that the amniogenesis in primates initiates after a transient opening of the epiblastic cavity (cavity within the epiblast cyst) to the trophoblast, forming an epiblastic-trophoblast cavity (Figure 1-4); upon further development, the proliferation, differentiation, and

migration of epiblast cells at the margins of the epiblast disc results in the up-folding of the epiblast layer and generates precursors of amniotic cells, which eventually enclose a permanent cavity ("the amniotic cavity") with the roof made of squamous cells destined to become the amnion. This hypothesis has been taken as a textbook dogma in human embryology[1].

However, another study by Enders *et al*. in 1986 reported that they did not find signs of transiently opened epiblastic cavity after analyzing peri-implantation rhesus monkey embryos, thereby challenging the Luckett hypothesis. Instead, their findings implied a possible alternative route for primate amniogenesis, wherein the epiblast cells that face the trophoblast undergo a continuous "thinning" process and eventually become the squamous amniotic epithelium (Figure 1-4), which does not involve a transiently opened epiblastic cavity. This hypothesis is also consistent with recent findings by Sasaki *et al*. in post-implantation cynomolgus monkey embryos[19]. These different conclusions and hypotheses about closely related primate species obscure our understanding of the development of human amnion and amniotic sac.

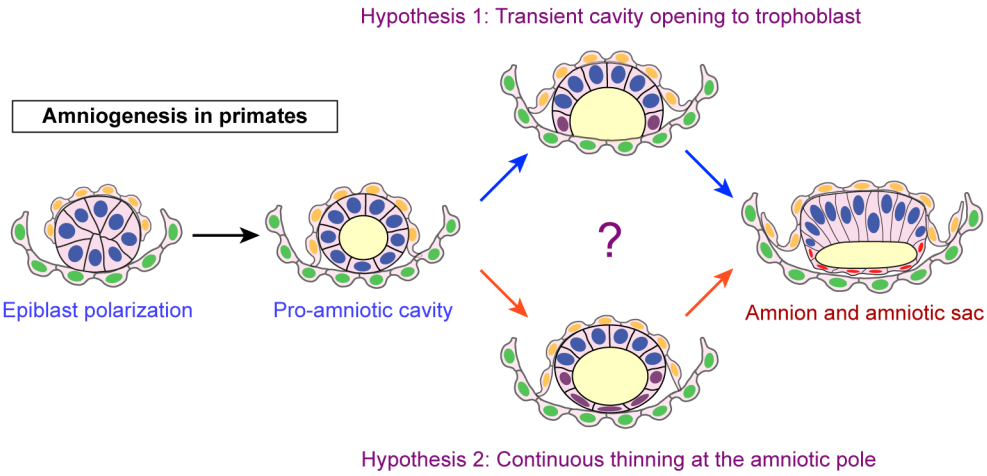

Figure 1-4 Schematic illustrating two different hypotheses for the amniogenesis in human/primates. The process through which the amnion emerges remains mysterious to date.

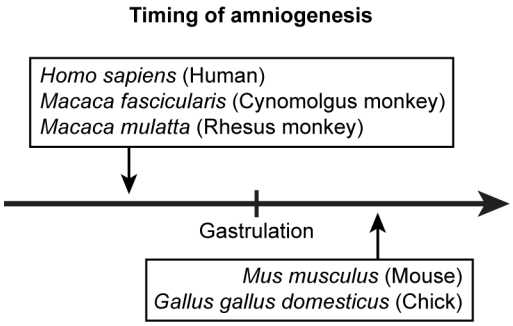

Figure 1-5 Interspecies differences in the timing of amniogenesis between human/primates and other commonly used non-primate animal models.

1.2.2 Interspecies Differences in Amniogenesis Limit the Relevance of Common Animal Models

For centuries, scientists have utilized various kinds of model organisms to study the fundamental principles underlying the development of the human embryo. Although the use of animal models has generated a large amount of fruitful results and significantly advanced our understanding of the fundamentals of development, it might fall short to serve for the study of human amnion development due to non-negligible interspecies differences. Specifically, in humans as well as non-human primates such as cynomolgus monkeys and rhesus monkeys, the amnion is the first tissue to differentiate from the pluripotent epiblast. Amniogenesis in primates occurs along with implantation and precedes the initiation of primitive streak development and gastrulation[6,18,19]. In drastic contrast, in mouse and chick, which are commonly used animal models in developmental biology, the development of amnion occurs after the initiation of primitive streak and takes place during the gastrulation[18,20,21]. Such distinct differences in the timing of amniogenesis might reflect different, species-specific strategies for cell fate allocation and embryonic patterning, thereby limiting the relevance of common animal models in the study of human amnion development.

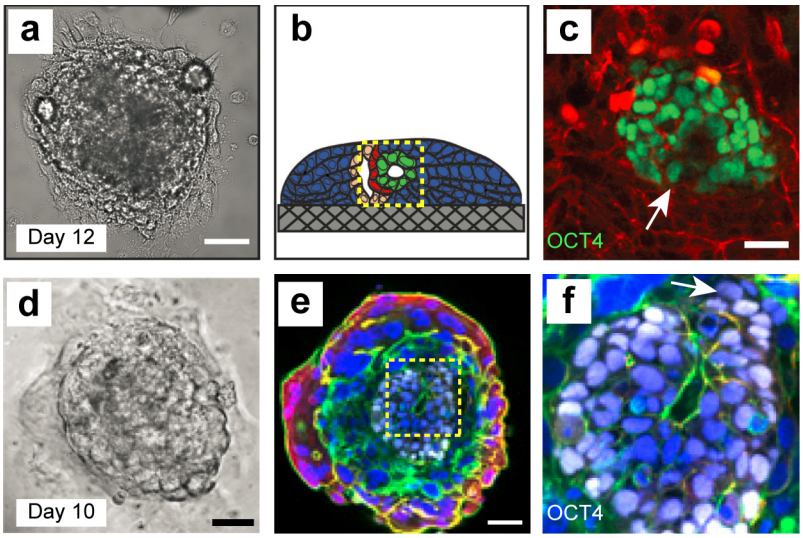

Figure 1-6 *In vitro* cultured human embryos. Recent work by Deglincerti *et al*.[16] (**a-c**) and Shahbazi *et al*.[17] (**d-f**) cultured human blastocysts *in vitro*. (**a,d**) Phase contrast images of the cultured human embryo at day 12 (**a**) and day 10 (**b**), respectively. (**b,e**) Schematic (**b**) and immunofluorescence analysis (**e**) of the cultured human embryo. Yellow boxes highlight the amniotic cavity. (**c,f**) Zoom-in views of the amniotic cavity boxed in **b** and **e**, respectively. Scale bars, 50 μm in **a**, **d**, **e**; 20 μm in **c**. Reproduced with permission.

1.2.3 In vitro Cultured Human Embryos Lack Definitive Amnion Development and Amnion-Epiblast Patterning

In order to overcome the inaccessibility of peri-implantation human embryo samples for investigating human developmental biology during implantation, two research groups recently took advantage of discarded pre-implantation human blastocysts from in vitro fertilization clinics and cultured them *in vitro* to induce further development that recapitulates implantation (Figure 1-6). In the study by Deglincerti *et al*., the authors cultured human embryos *in vitro* to develop and form two primary cavities: the amniotic cavity and the yolk sac, which are hallmarks of per-implantation human embryos[16]. Similarly, another study by Shahbazi *et al*. also cultured human embryos to generate an amniotic cavity and a prospective yolk sac[17]. Despite their success in culturing human embryos *in vitro* to undergo implantation-like development for the first time,

neither study identified the development of definitive amniotic tissue, as reflected by the absence of OCT4- squamous amnion cells at the prospective amniotic pole (white arrows in Figure 1-6c&f). Those cultured human embryos also lacked a clear amnion-epiblast patterning that resembles the human amniotic sac *in vivo*. Importantly, studies such as these still require the use of live human embryos and therefore are subjected to ethical controversies and additional limitations on the scale and efficiency of such studies.

1.3 Human Pluripotent Stem Cells: a Promising Resource for Modeling Human Development in a Culture Dish

Compared with the valuable yet largely inaccessible/inefficient studies on human embryos both *in vivo* and *ex vivo*, the rise of human stem cells and stem cell engineering in recent years has provided us with a promising route to study human development in an efficient and scalable fashion *in vitro*[22]. In particular, human pluripotent stem cells (hPSCs), which share molecular similarity with human epiblast[8,9,23] and have the potential to develop to many cell types in human embryos, are under the spotlight due to their capability of modeling human development and diseases in a culture dish[24-28]. However, at the time of initiation of this dissertation, it was still unexplored whether hPSCs have the potential to be applied to recapitulate peri-implantation human developmental events such as amniogenesis. The work herein explores such a potential and uses hPSCs as the cellular tool for developing *in vitro* models for peri-implantation human embryogenesis. Next, I present a brief summary of our current understanding of hPSCs and a concise review of recent applications of hPSCs to model human organogenesis in culture.

1.3.1 Derivation of Human Pluripotent Stem Cells

Historically, the term "human pluripotent stem cells" was originally used to unify the description of two kinds of cells: human embryonic stem cells (hESCs) and human induced pluripotent stem cells (hiPSCs), which are derived from different origins with different methods but share similar levels of pluripotency - the competence to differentiate into all three germ layers and their progenies (Figure 1-7). Specifically, hESCs are derived from the outgrowth of the human ICM after the ICM is isolated from the blastocyst and cultured in a dish[29]; while hiPSCs are derived from adult tissue cells, such as skin cells[30] and blood cells[31], *via* a process called reprogramming which can be achieved by forced expression of key transcription factors associated with pluripotency. Both hESCs and hiPSCs are regulated by the same set of pluripotency-associated transcriptional circuitry including key pluripotency factors NANOG, OCT4, and SOX2[32]. Nevertheless, hESCs and hiPSCs are not identical. The extent to which hiPSCs are similar to their embryonic counterparts - hESCs - is often dependent on the protocol

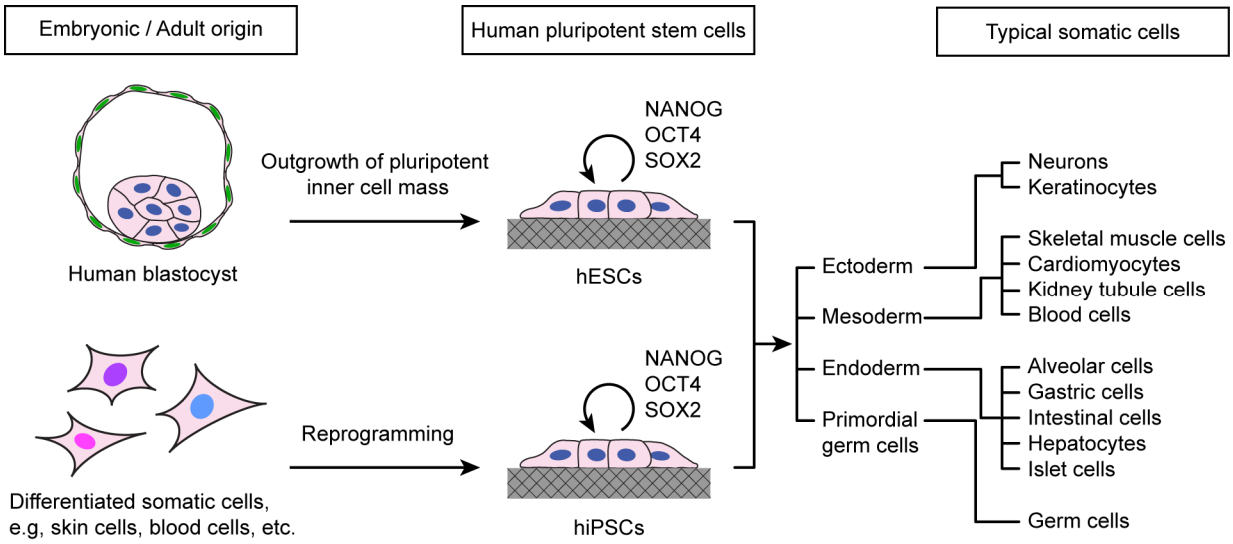

Figure 1-7 Derivation and application of hPSCs. Schematic showing the derivation of human embryonic stem cells (hESCs) and human induced pluripotent stem cells (hiPSCs), which together constitute hPSCs, as well as the typical application of hPSCs for generating human somatic cells *via* directed differentiation.

used for hiPSC derivation[33,34]. Therefore, it typically requires side-by-side comparisons to confirm the similarity of hiPSCs and hESCs in a context-dependent manner. It also calls for caution when attempting to extrapolate properties of hESCs to hiPSCs, or *vice versa*.

Since the discovery of hESCs and hiPSCs, researchers have been endeavoring to develop standardized culture systems for maintaining and expanding hPSCs, as well as a multitude of methods for directed differentiation of hPSCs towards somatic cells that are progenies of the three embryonic germ layers - ectoderm, mesoderm, and endoderm (Figure 1-7). Intriguingly, recent findings indicate that hPSCs are also competent for generating cells that resemble human primordial germ cells (hPGCs)[35] as well as germ cells[36], which, according to a recent report by Sasaki *et al*., originate from extraembryonic nascent amnion in cynomolgus monkey embryos[19]. Therefore, the above findings suggest that hPSCs might also be competent for generating cells of extraembryonic lineages, *e.g.*, the amniotic lineage, as well.

1.3.2 Pluripotency in Human Cells: a Developmental Spectrum

As mentioned in section 1.1, pluripotent cells exist at multiple early developmental stages in human embryos *in vivo* (Figure 1-8). For example, the ICM and the early epiblast in pre-implantation embryos both exhibit pluripotency. The epiblast in post-implantation, pre-gastrulation embryos also carries pluripotency. Given such a developmental spectrum of pluripotent states *in vivo*, the embryonic developmental stage to which hESCs and hiPSCs match *in vitro* has been a matter of intense debate for a long time.

Because it originates from the outgrowth of human ICM, hESCs were thought to reside in an ICM-like developmental stage, and so were hiPSCs because of their similarity to hESCs. However, hESCs and hiPSCs (referred to henceforth as conventional hPSCs in this section) were soon found to exhibit characteristics of the post-implantation epiblast instead of that of the ICM,

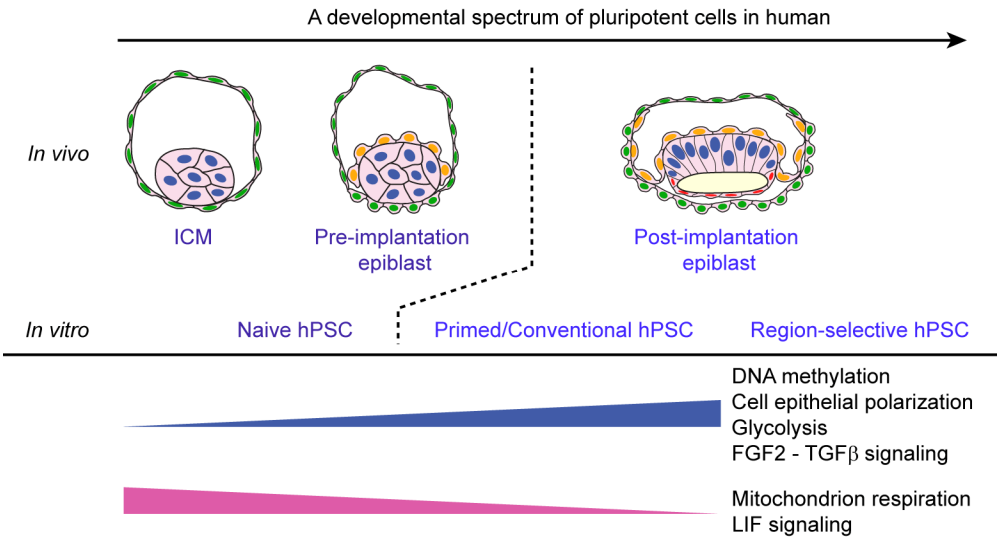

Figure 1-8 Developmental spectrum of pluripotent states in human embryos and cultured human cells.

including a high level of DNA methylation[12], prominent epithelial polarity, increased glycolysis[37], and dependence on FGF2/ERK and TGFβ signaling for self-renewal[38]. A recent study by Nakamura *et al*. in post-implantation cynomolgus monkey embryos further indicates that conventional hPSCs are most similar to the post-implantation epiblast[8].

In past years, researchers have also been actively exploring the possibility of generating hPSCs of alternative pluripotent states other than that of the post-implantation epiblast. For example, by expressing NANOG and KLF2 for a short time, Takashima *et al*. successfully reset conventional hPSCs to a "ground-state" that resembles the pre-implantation human blastocyst ICM[39]. These alternative hPSCs, typically called naive hPSCs or ground-state hPSCs, exhibit distinct molecular signatures compared with conventional hPSCs, e.g., largely reduced DNA methylation (a state called hypomethylation), activation of mitochondrial respiration, and self-renewing maintenance in the absence of ERK signaling, which are hallmarks of the ICM in pre-implantation human embryos. Recently, Guo *et al*. successfully derived native hPSCs directly

from human ICM[40], further confirming the existence of an alternative, human ICM-like pluripotent state in cultured human cells *in vitro*.

In another recent study by Wu *et al*., the authors identified an alternative epiblast-like pluripotent state in cultured hPSCs[41]. Specifically, by removing TGFβ1 from conventional hPSC culture medium and supplementing a small molecule inhibitor for WNT signaling, IWR1, they successfully reset conventional hPSCs to a different pluripotent state, which features more efficient generation of post-implantation interspecies chimaeric embryos and higher cloning efficiency when compared with conventional hPSCs. Because those alternative hPSCs show most efficient integration into the posterior region of post-implantation interspecies chimaeric embryos, they were named region-selective hPSCs (rs-hPSCs or human rsPSCs)[41]. These human rsPSCs were therefore also hypothesized to reside in a late, yet still pluripotent, epiblast-like developmental state.

Together, such a developmental spectrum of pluripotent states and their distinct *in vitro* counterparts in cultured hPSCs could provide us with a comprehensive set of resources for modeling diverse early human embryogenic events *in vitro*.

1.3.3 3D Organotypic Culture of hPSCs for Modeling Human Organogenesis

The fate and organization of cells in the human body are tightly regulated in the three-dimensional (3D) cell microenvironment through intricate interactions with neighboring cells, the surrounding extracellular matrix (ECM), and soluble biochemical cues[42,43]. Thus, to recapitulate *in vivo*-like cellular structures, properties, and organizations using hPSCs, it is critical to control and modulate the 3D cell microenvironment mimicking tissue- and organ-specific niches[24]. By leveraging the self-organizing cytodifferentiation of hPSCs in properly designed tissue-mimicking microenvironments, biologists and bioengineers have developed a

range of 3D hPSC culture systems for modeling the development of various human organs in the last ten yesrs[25,44]. A brief summary of these hPSC-derived organ developmental models, commonly called the organoids, is provided here[24].

The late developmental biologist Yoshiki Sasai and his colleagues have done pioneering work that utilizes hPSCs to model the development of organs of neuroectodermal lineage. Using serum-free culture of embryoid body-like aggregates (SFEB), Sasai and colleagues recapitulated 3D optic cup morphogenesis using hESCs (Figure 1-9a)[45]. In another work from Sasai and colleagues, hESCs were induced toward neuroepithelial lineages and cortical tissues exhibiting distinct zones along the apical-basal axis (*e.g.*, ventricular, early and late cortical plate, and Cajal-Retzius cell zones) were generated (Figure 1-9b)[46]. Recently, Mariani *et al.* extended the SFEB method to hiPSCs and generated human cortical organoids mimicking the developing human telencephalon[47]. In addition, *via* co-induction of hypothalamic neuroepithelium and oral ectoderm in a 3D culture system, Ozone *et al*. generated anterior pituitary organoids from hESCs[48]. In another exciting study, Lancaster *et al*. successfully applied 3D hPSC culture to generate cerebral organoids with distinct brain regions (Figure 1-9c)[49]. Intriguingly, early corticogenesis and subsequent patterning of forebrain, midbrain, and hindbrain regions were observed in cerebral organoids. Importantly, using hiPSCs derived from patients of microcephaly, Lancaster *et al*. successfully modeled critical pathological phenotypes of microcephaly in cerebral organoids.

3D organotypic culture methods have also been successfully applied to generate organoids with mesodermal and endodermal origins. By inducing hESCs toward the primitive streak-intermediate mesodermal lineage, Takasato *et al*. generated self-organized human kidney organoids that exhibited ureteric buds, metanephric mesenchyme, and nephron formation (Figure

1-9d)[50]. Recently, Takasato *et al*. reported an improved method for inducing kidney organoids that contain nephrons associated with a collecting duct network surrounded by renal interstitium and endothelial cells, which shows high similarity to the first trimester human kidney[51]. In another work from Kusuma *et al*., an hPSC-derived microvascular network was demonstrated through co-differentiation with vascular endothelial cells and pericytes and subsequent encapsulation in HA-based hydrogel (Figure 1-9e)[52]. A relevant work to engineer functional human blood vessels in 3D culture using hiPSC-derived endothelial cells and mesenchymal precursor cells was recently reported by Samuel *et al* [53].

Following endodermal commitment, Spence *et al*. successfully generated human intestinal organoids (HIOs) from hPSCs using a Matrigel-based 3D culture system (Figure 1-9f)[54]. Through temporally controlling growth factors to dictate sequential definitive endoderm, posterior endoderm, and hindgut specification and morphogenesis, Spence *et al*. created *in vitro* intestines containing villus-like structures and crypt-like proliferative zones. Such HIOs was further utilized for studying the roles of WNT3a and FGF4 in intestine development and NEUROG3 (a pro-endocrine transcription factor) in human enteroendocrine cell development and disease. More recently, Watson *et al*. successfully implanted human intestinal organoids generated from hPSCs *in vitro* into mice, and observed significant maturation of HIO to form human adult-like small intestinal tissue with vasculature integration with the mouse host. This work supports the feasibility of using human intestinal organoids to study human small intestine maturation and relevant adult intestinal diseases[55]. Based on the hindgut organoid model, McCracken *et al*. developed a method to generate posterior foregut organoid that eventually gives rise to human gastric organoid (hGO) by manipulating the BMP, retinoic acid, and EGF

signaling pathways (Figure 1-9g). This hGO model was used to study the fundamentals of human stomach development as well as gastric pathogenesis caused by *H. pylori* infection[56].

In a separate study, Takebe *et al*. recreated human liver buds *in vitro* by leveraging 3D self-organization of hiPSC-derive immature hepatic cells and human endothelial and mesenchymal stem cells under coculture (Figure 1-9h)[57]. Interestingly, such *in vitro* engineered human liver buds matured and functioned like adult human liver after transplantation and could even rescue drug-induce lethal liver failure mouse models. By differentiating hPSCs to NKX6.1+/PDX1+ pancreatic exocrine progenitor cells and culturing those progenitor cells in a 3D environment, Huang *et al*. generated pancreatic organoids containing ductal and acinar structures both *in vitro* and after transplantation (Figure 1-9i)[58]. Using progenitors with mutant *KRAS* and *TP53*, the pancreatic organoid was used to model pancreatic ductal adenocarcinoma for drug screening. Recently, Dye *et al*. induced hPSCs into ventral anterior foregut spheroids, which were then expanded to form human lung organoids (HLO)[59,60]. HLO contains epithelial and mesenchymal compartments and exhibits airway-like structures resembling human lung when grown both *in vitro* and after transplantation.

Together, recent developments of various human organoids using 3D biomaterial-based culture methods highlight the great potential of hPSCs in conjunction with conductive 3D culture environment for fundamental organ development studies, critical for identifying therapeutic targets for treating complex developmental or degenerative diseases. However, it is noteworthy that despite the extensive and successful utilization of hPSCs for modeling organogenesis, which is a post-gastrulation developmental period, it remains undetermined whether hPSCs can be applied to model pre-gastrulation, peri-implantation human embryogenic events such as amniogenesis and the formation of the amniotic sac.

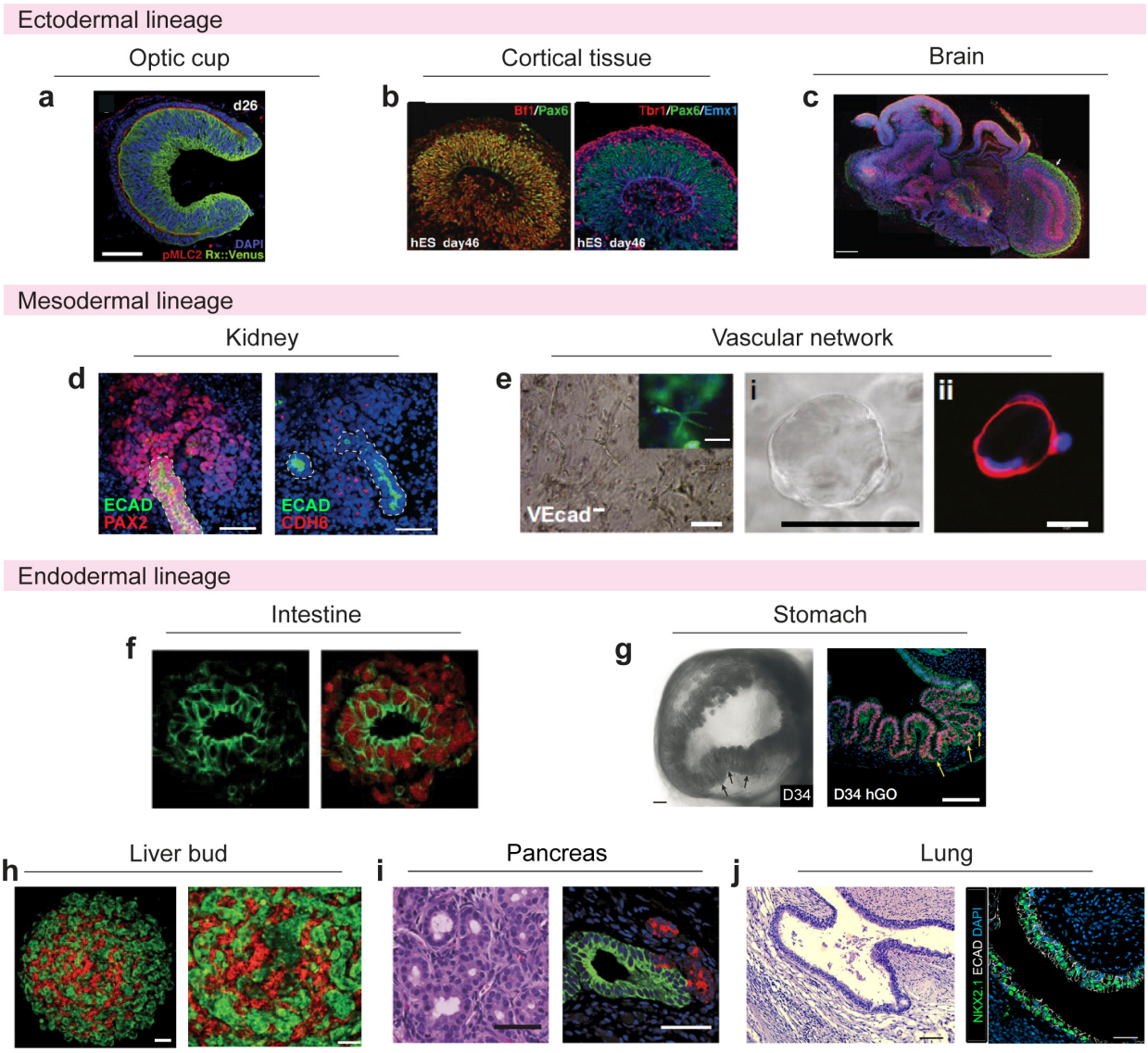

Figure 1-9 hPSC-derived 3D organoid models for human organogenesis. Reproduced with permissions[45,46,49,50,52,54,56,57,60,61].

1.4 Dissertation Outline

Given: (1) the intense interest and significance in advancing our understanding of early human embryogenesis; (2) the current gap in knowledge and technology for understanding peri-implantation human development, especially the development of amnion and amniotic sac; (3) successful precedents utilizing hPSCs to model post-gastrulation organogenesis by providing rationally designed, biomimetic 3D culture environments, and (4) the similarity between hPSCs and the peri-/post-implantation epiblast that gives rise to amniotic cells during the second week of pregnancy, the goal of this dissertation is to leverage 3D hPSC bioengineering to develop the first *in vitro* models for studying peri-implantation human amniogenesis and amniotic sac development. Specifically, I will first develop a biomimetic implantation-like biophysical niche for inducing amniogenesis from hPSCs in Chapter II. In Chapter III, this implantation-like niche will be further applied to generate an asymmetric cystic structure resembling human amniotic sac at implantation and early gastrulation. Chapter IV will summarize a pilot study that aims at translating the hPSC amniogenesis system to a micro-array platform that is potentially useful for high-throughput screening for reproductive medicine in the future. Finally, Chapter V will summarize the contributions of this dissertation and suggest avenues for future researches.

CHAPTER II

Self-organized Amniogenesis by Human Pluripotent Stem Cells in a Biomimetic Implantation-like Biophysical Niche

2.1 Introduction

Development of amnion, which occurs between d.p.f. 6 and 12, is the first - although poorly studied - differentiation event that happens in the human epiblast and is indispensible for further developmental events such as gastrulation[6,18]. Abnormal amnion development can evolve into critical pregnancy complications, such as oligohydramnios or amniotic band syndrome. Amnion also has anti-inflammatory and pro-regenerative functions that have been leveraged in clinics for facilitating wound healing[62]. Despite its fundamental and clinical significance, amnion development in the human remains little understood, due to the inaccessibility to 6-12 d.p.f. human embryos and the drastic difference in amnion development between human and other common animal models. Recently, there has been significant progress in developing *in vitro* culture systems, including *in vitro* cultured human embryos as published by Deglincerti *et al*.[16] and Shahbazi *et al*.[17] to expand our knowledge of early human development. While such studies using live human embryos are valuable, they are inefficient, non-scalable, and ethically controversial. Thus, human-specific amnion development remains mysterious and poorly approachable.

In past years, hPSCs have been successfully utilized for modeling post-gastrulation human embryonic development[14,49]. However, the applicability of hPSCs for modeling peri-implantation, pre-gastrulation developmental events, such as amniogenesis, remains undetermined. Inspired by the recently implicated cell biological and transcriptomic similarities between hPSCs and peri-/post-implantation epiblast[8,17,23,63], which gives rise to nascent amnion, the goal of this chapter is to adapt a biomimicry approach to engineer a biomaterial-based *in vitro* hPSC culture system for efficient generation of early human amniotic tissue.[†]

2.2 Biomimetic Implantation-like Biophysical Niche: Rationale and Design

Because the *in vivo* milieu of the embryo implantation site is complex and has not yet been fully elucidated, it is not practical at this point to fully recapitulate all aspects of the peri-implantation microenvironment to reconstruct a biomimetic implantation-like amniogenic niche *in vitro*. Instead, here I chose to concentrate on two central concepts that address key features of the peri-implantation environment.

Firstly, during the implantation of human embryo, amniotic differentiation initiates in parallel with self-renewing expansion of the pluripotent epiblast. Therefore, it is hypothesized here that a biochemical context permissive for maintaining the pluripotent epiblast might also be permissive for initial amnion development. Such a biochemical context can be mimicked by conditions that have been used extensively in the feeder-free culture system for maintaining hPSCs: the mTeSR1 medium and a basement membrane matrix (herein Geltrex™), of which the

[†] The results presented in this chapter are adapted from my recent publication: Shao et al., *Nature Materials*, in press, DOI: 10.1038/NMAT4829.

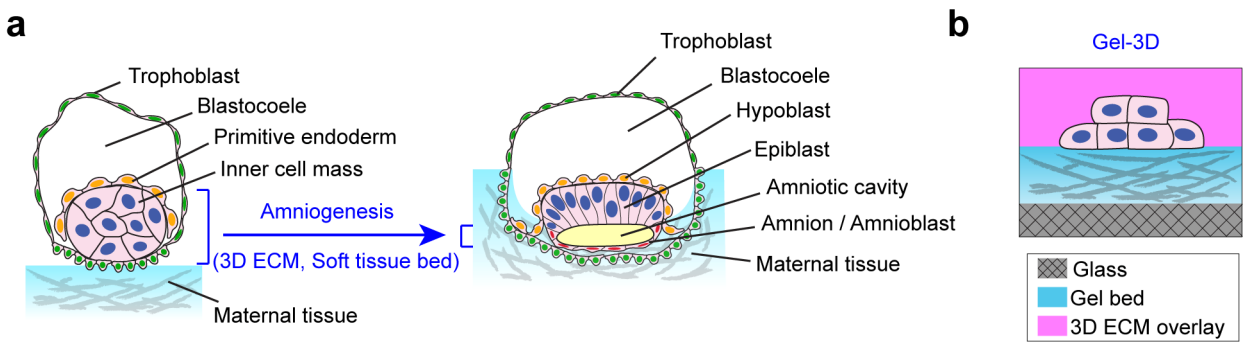

Figure 2-1 Rationale of the biomimetic implantation-like niche. (**a**) Development of amnion/amnioblasts from epiblasts in a peri-implantation human embryo[18]. Amniogenesis *in vivo* occurs in a biophysical niche featuring a soft tissue bed (maternal tissue and invading trophoblasts) and a 3D ECM environment provided by the overlying primitive endoderm/hypoblasts. (**b**) Schematic of the implantation-like "Gel-3D" culture system, which contains a thick, soft gel bed and a 3D ECM overlay.

latter is also the first type of extracellular matrix formed surrounding the epiblast in primate embryos at implantation[7].

Secondly, the conventional cell culture system for hPSCs utilizes a two dimensional (2D) setting in which cells are plated on a stiff plastic/glass substrate thinly coated by basement membrane matrix proteins. In contrast, the *in vivo* peri-implantation environment has notably different physical properties (Figure 2-1a). For example, implantation occurs as the embryo nestles against a bed of maternal tissue and trophoblast cells. This environment should be mechanically more similar to a soft hydrogel than to a rigid piece of plastic. In addition, the hypoblast and underlying basement membrane matrix surround the epiblast with a 3D extracellular matrix (ECM) environment *in vivo*. To mimic these two physical features of the peri-implantation niche, a thick soft gel bed made of basement membrane matrix (Geltrex^{TM}) and an ECM overlay (also containing basement membrane matrix protein) are incorporated in the implantation-like culture system *in vitro* (Figure 2-1b).

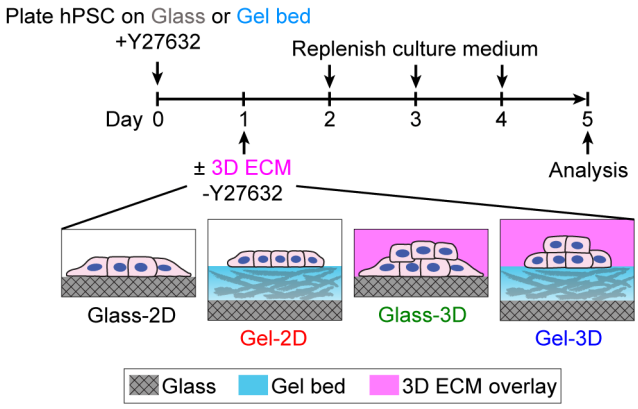

Figure 2-2 Schematic showing the hPSC amniogenesis assay.

In this culture system, H9 human embryonic stem cells (hESCs) were plated as single cells at 30,000 cells cm^{-2} onto a thick and soft basement membrane matrix gel bed (Geltrex™, with thickness ≥ 100 µm, bulk *Young*'s modulus ~900 Pa[64], coated on glass coverslip) in mTeSR1 medium supplemented with Y27632, a ROCK inhibitor that prevents dissociation-induced apoptosis[65] (Figure 2-2). At 24 h (day 1), Y27632 was removed and 4% (*v* : *v*) Geltrex™ was added in mTeSR1 to establish a 3D implantation-like niche (referred to henceforth as "Gel-3D" condition). To assess the effect of ECM dimensionality and matrix rigidity, respectively, several modifications of this Gel-3D condition were also tested (Figure 2-2). First, the Geltrex™ supplement was excluded from the medium, with the gel bed retained (referred to henceforth as "Gel-2D" condition). Second, the soft gel bed was replaced with a 1% Geltrex™-coated glass coverslip (referred to henceforth as "Glass-3D" condition). Finally, a standard 2D culture, using a 1% Geltrex™-coated glass coverslip (referred to henceforth as "Glass-2D" condition), was examined as a control that maintains hPSC self-renewal. Culture medium was replenished daily. Analyses were performed for all conditions at day 5 unless otherwise noted (Figure 2-2).

2.3 Materials and Methods

2.3.1 Fabrication of Basement Membrane Matrix Gel Beds

Fabrication protocol for the Geltrex™ gel bed was based on a "sandwich" setup previously developed for generating polyacrylamide gel substrates[66-68]. To prepare a substrate that the gel bed could attach to, a 22 × 22 mm^2 glass coverslip was first treated with air plasma (Harrick Plasma) for 2 min before coated with 0.1 mg ml^{-1} poly-(L-lysine) (PLL) solution (Sigma-Aldrich) for 30 min, and 1% glutaraldehyde solution (Electron Microscopy Sciences) for another 30 min. To prepare a substrate that could "sandwich" and release the gel bed, a pre-cleaned glass slide was treated with air plasma for 2 min before coated with 0.1 mg ml^{-1} poly-(L-lysine)-graft-poly-(ethylene glycol) (PLL-g-PEG; SuSoS) solution for 1 h. To obtain gel beds with nominal thickness of 20, 60, and 100 μm, undiluted Geltrex™ (10, 30 and 50 μl, respectively) was sandwiched between the pre-treated glass coverslip and glass slide on ice before incubated at 37°C for 30 min for gelation. The gel bed, which was attached to the glass coverslip, was then removed from the glass slide and submerged in DMEM/F12 medium (Thermo Fisher Scientific) and incubated at 37°C overnight before plating cells.

To prepare gel beds with a nominal thickness larger than 100 μm, spacers with the desired thickness were placed between the glass coverslip and the glass slide when preparing the gel bed sandwich. Specifically, spacers were made of polydimethylsiloxane (PDMS; Dow Corning) films. The film was made by spin-coating liquid phase PDMS (mixed at 10:1 of base:curing agent ratio) onto a petri-dish at 500 rpm for 40 s (for generating 150 μm thick film) and cured at 70°C for at least 24 h before use. A previously published "PDMS film thickness - spin coating parameter" chart[69] can be referred to when preparing PDMS films of desired thicknesses.

2.3.2 Fabrication of Elastomeric Artificial Matrices

The elastomeric artificial matrix consisted of a regular PDMS micropost array generated using a microfabrication protocol previously published[70]. To functionalize inert PDMS surfaces for cell attachment, the PDMS micropost array was treated with air plasma for 2 min and coated with 1% Geltrex™ solution for 2 h. The Geltrex™ solution was aspirated, and the PDMS micropost array was rinsed with DMEM/F12 before plating hPSCs.

Finite element analysis was performed to determine the nominal spring constant, K, of the PDMS micropost under lateral force applied at the micropost top as previously described[71]. The nominal spring constant K was converted to an "effective in-plane substrate rigidity E_{eff}", by $E_{eff} = 9K / 2\pi D$[72], where D = 1.83 μm was the micropost diameter.

2.3.3 3D Amniogenesis Assay

Three different kinds of substrates were used in this study: glass coverslip coated with 1% Geltrex™ solution for 1 h at room temperature, Geltrex™ beds of different nominal thicknesses (as described below), and artificial matrices of different effective rigidities (as described below). Cultured hPSC colonies were first incubated with Accutase (Sigma-Aldrich) at 37°C for 10 min before triturated and suspended in PBS as single cells. hPSCs were then centrifuged and the cell pellet was resuspended in mTeSR1 containing 10 μM Y27632 (Tocris). hPSCs were plated as single cells at 30,000 cells cm^{-2} onto the indicated substrate. After 24 h (on day 1), culture medium was changed to fresh mTeSR1 without Y27632. For 3D culture conditions, 4% (v : v) Geltrex™ was supplemented in mTeSR1 medium on day 1, as previously described[63]. Thereafter, mTeSR1 medium was replenished daily, and 4% (v : v) Geltrex™ was supplemented daily for all 3D culture conditions.

2.3.4 BMP Inhibition Assay

500 nM BMP receptor ALK2/3 inhibitor LDN193189 (LDN; STEMCELL Technologies) was added to the culture medium, either on day 2 only or on both days 2 and 3. DMSO (Sigma-Aldrich) was added to control groups on both days 2 and 3. In experimental groups treated with LDN on day 2 only, DMSO was supplemented on day 3. No LDN or DMSO was added to the culture medium on days other than those specified above.

2.3.5 Derivation of Primitive Streak Cells

Primitive streak (PS) cells were derived from hPSCs according to a previously published protocol[73]. In brief, hPSCs (H9 line) were dissociated and plated as single cells at 20,000 cells cm^{-2} onto glass coverslips coated with 1% Getlrex^{TM} solution in mTeSR1 medium containing 10 μM Y27632. After 24 h (on day 1), culture medium was replaced by fresh mTeSR1 without Y27632. On day 2, mTeSR1 was replaced by PS-differentiation medium containing Essential 6^{TM} medium (Thermo Fisher Scientific), 20 ng ml^{-1} FGF2 (Peprotech), and 8 μM CHIR99021 (Tocris). PS cell differentiation was induced for 48 h before performing downstream assays.

2.4 Results and Discussion

2.4.1 hPSCs Self-organize into Squamous Cystic Tissue with Amnion-like Epithelial Morphology in the Implantation-like Niche

In the Glass-2D condition, as expected, apico-basally polarized hESC colonies were observed at day 5. Strikingly, in Gel-2D, Glass-3D, and Gel-3D conditions, hESCs formed 3D cysts with EZRIN+ lumenal apical surfaces facing inward (Figure 2-3a), reflecting the intrinsic lumenogenic property of hESCs[17,63]. In both Gel-2D and Glass-3D conditions, > 90% of lumenal cysts are made of tall, columnar E-CADHERIN+ (ECAD+) epithelial cells with apico-basally

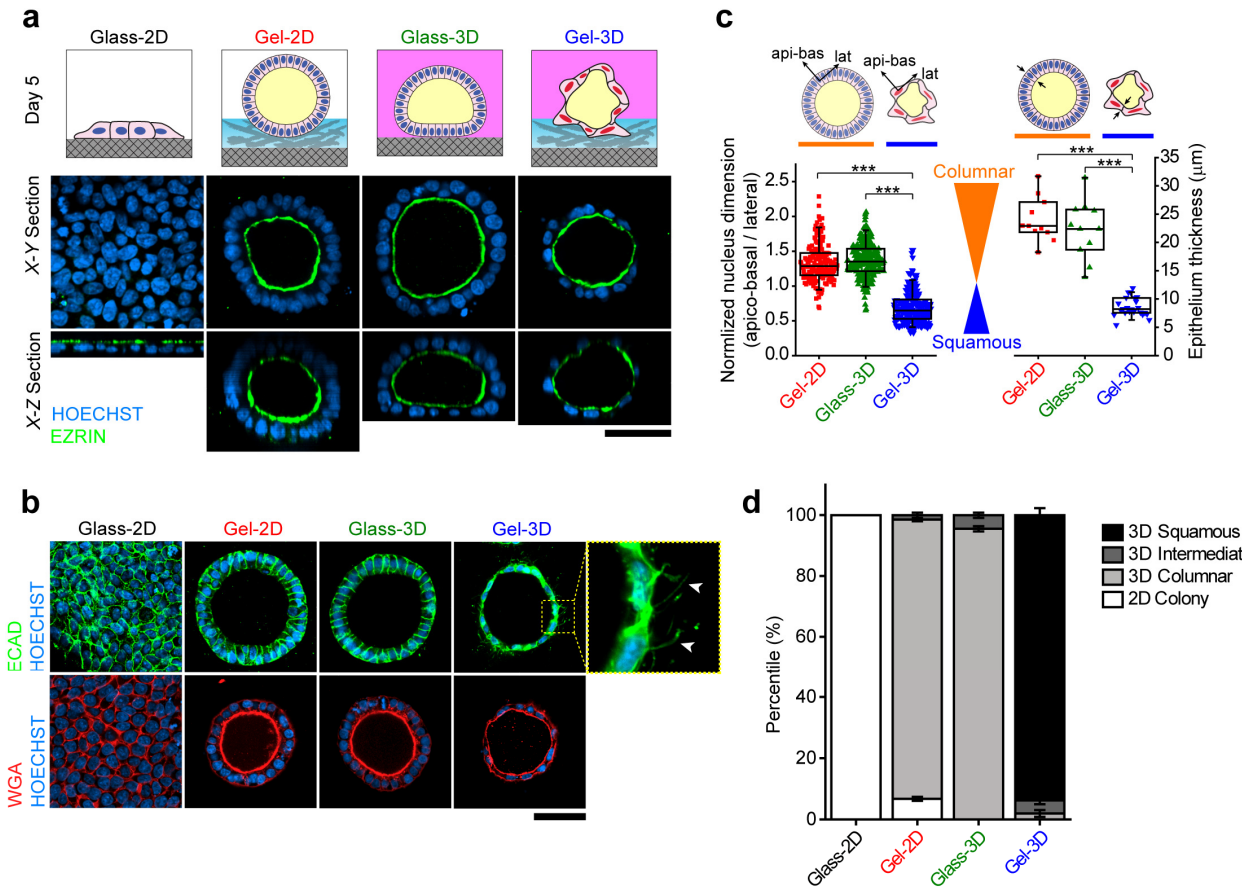

Figure 2-3 hPSCs self-organize to form squamous epithelial cystic tissues in the implantation-like niche. (**a**) Cartoons showing hPSC morphogenesis under different culture conditions (*top*). Confocal micrographs showing the *X-Y* (*middle*) and *X-Z* (*bottom*) sections of the hPSC monolayer and cysts formed in indicated conditions at day 5. EZRIN (green) demarcates apical surfaces. HOECHST (blue) counterstains nuclei. (**b**) Confocal micrographs showing staining of E-CADHERIN (ECAD, green; *top*), wheat germ agglutinin (WGA, red; *bottom*), and HOECHST (blue, nucleus) in hPSCs cultured under indicated conditions. Squamous cells exhibit basal ECAD+ protrusions, highlighted by white arrowheads. (**c**) Box charts showing normalized nucleus dimension (*left*) and epithelium thickness (*right*) for hPSC cysts in indicated conditions (box: 25% - 75%, bar-in-box: median, and whiskers: 1% and 99%). Cartoons show columnar versus flat, squamous cyst morphologies and the apico-basal (api-bas) and lateral (lat) directions. n_{cell} = 179, 254, and 243, and n_{cyst} = 11, 11, and 23, for Gel-2D, Glass-3D, and Gel-3D, respectively. Quantitation was performed on n = 4 independent experiments. *P*-values were calculated using unpaired, two-sided Student's *t*-test. ***: $P < 0.001$. (**d**) Stacked bar plots showing percentages of hPSC colonies or hPSC-derived epithelial cysts with different morphologies under different culture conditions as indicated. n_{cyst} (n_{colony}) = 100, 502, 469, and 694 for Glass-2D, Gel-2D, Glass-3D, and Gel-3D conditions, respectively. Data represent the mean ± s.e.m with n = 3 biological replicates from n = 2 independent experiments. Same observation has been successfully repeated in total n = 16 independent experiments. Scale bars in **a&b**, 50 μm.

elongated nuclei and thick epithelium (Figure 2-3b,c,d). In distinct contrast, > 90% of cysts formed in Gel-3D show a squamous epithelial morphology featuring flattened, laterally elongated cell nuclei and reduced epithelium thickness, as well as unique ECAD+ cellular protrusions extending from basal surfaces (Figure 2-3b,c,d). Intriguingly, this spontaneously developed squamous epithelial cystic tissue is morphologically reminiscent of the developing amnion in peri-implantation human embryos[17,18].

2.4.2 The Squamous Cystic Tissue is Spontaneously Differentiated in a Self-renewal Permissive Biochemical Context

Notably, all 3D columnar epithelial cysts that formed in both Gel-2D and Glass-3D conditions express pluripotency markers NANOG, OCT4, and SOX2[32], consistent with the well-known association between columnar epithelial morphology and pluripotent epiblasts *in vivo*[6,8,16]

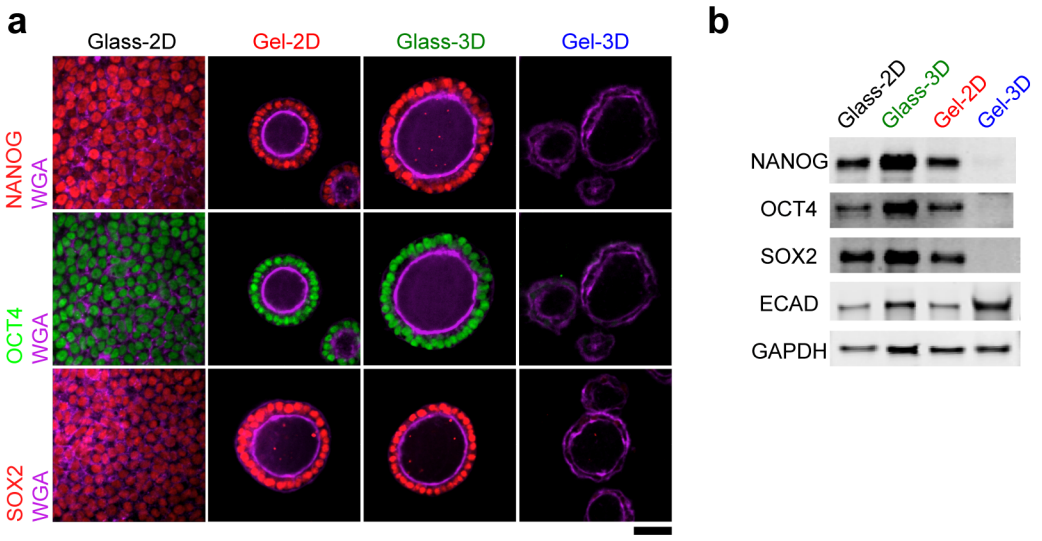

Figure 2-4 hPSC-derived squamous cystic tissues undergo spontaneous differentiation and lose pluripotency markers. (**a**) Confocal micrographs showing NANOG (*top*), OCT4 (*middle*), and SOX2 (*bottom*) immunostaining in hPSCs cultured under indicated conditions. WGA co-staining shows cell morphology. $n = 9$ independent experiments. Scale bar, 50 µm. (**b**) Western blot showing protein levels of NANOG, OCT4, SOX2, ECAD, and GAPDH in hPSCs cultured under indicated conditions. $n = 3$ independent experiments.

(Figure 2-4a). However, in the squamous cysts that formed in Gel-3D condition, expression of NANOG, OCT4, and SOX2 protein is lost, suggesting that they are composed of a differentiated cell type (Figure 2-4b). Interestingly, qRT-PCR analysis shows reduction in mRNA expression for *NANOG* and *SOX2*, but not *OCT4* (also known as *POU5F1*), in the Gel-3D condition (Figure 2-5a), suggesting a blunted transcriptional regulation of *OCT4*. Despite loss of pluripotency markers, the squamous cyst maintains an epithelial phenotype, retaining expression of ECAD/*CDH1* and *CLDN6*[74] (Figure 2-4b, 2-5b). Interestingly, such loss of pluripotency in parallel with squamous epithelial morphogenesis is also recently observed by

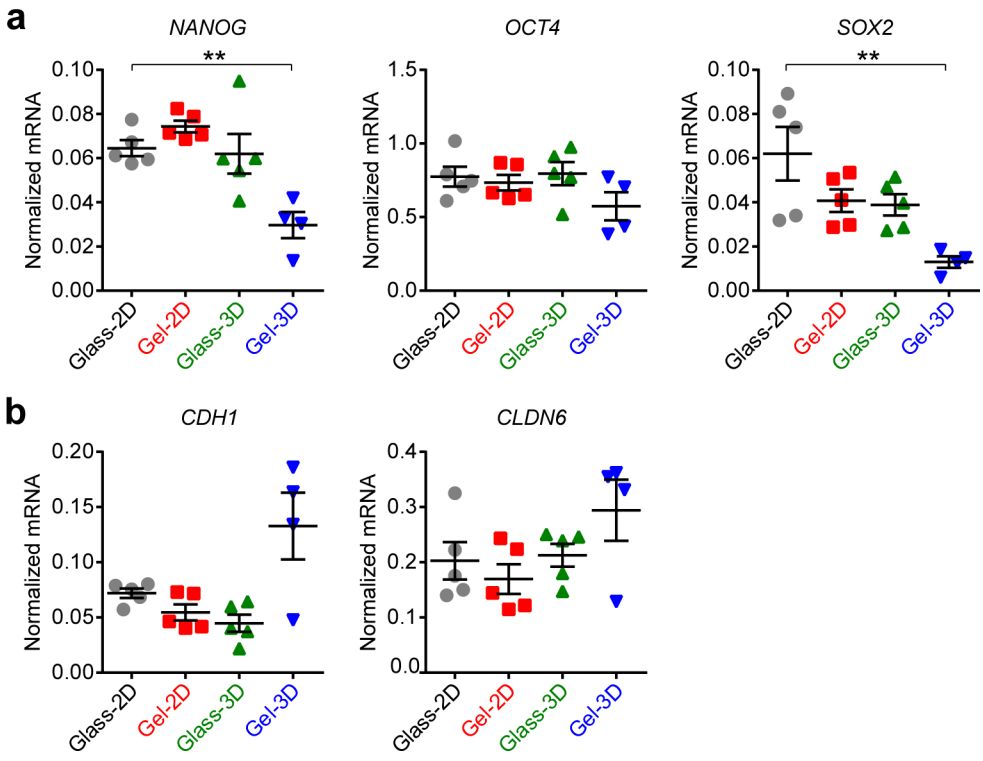

Figure 2-5 Squamous epithelial cysts derived from hPSCs show blunted transcriptional suppression of pluripotency genes while maintaining epithelial features. qRT-PCR analysis of pluripotency genes *NANOG*, *OCT4*, and *SOX2* (**a**), as well as epithelial markers *CDH1* and *CLDN6* (**b**), for hPSCs cultured in indicated conditions. Data were normalized against *GAPDH* and plotted as the mean ± s.e.m, with $n = 4$ - 5 biological replicates indicated by individual dots under each condition. $n = 2$ independent experiments. *P*-values were calculated using unpaired, two-sided Student's *t*-test. **: $P < 0.01$.

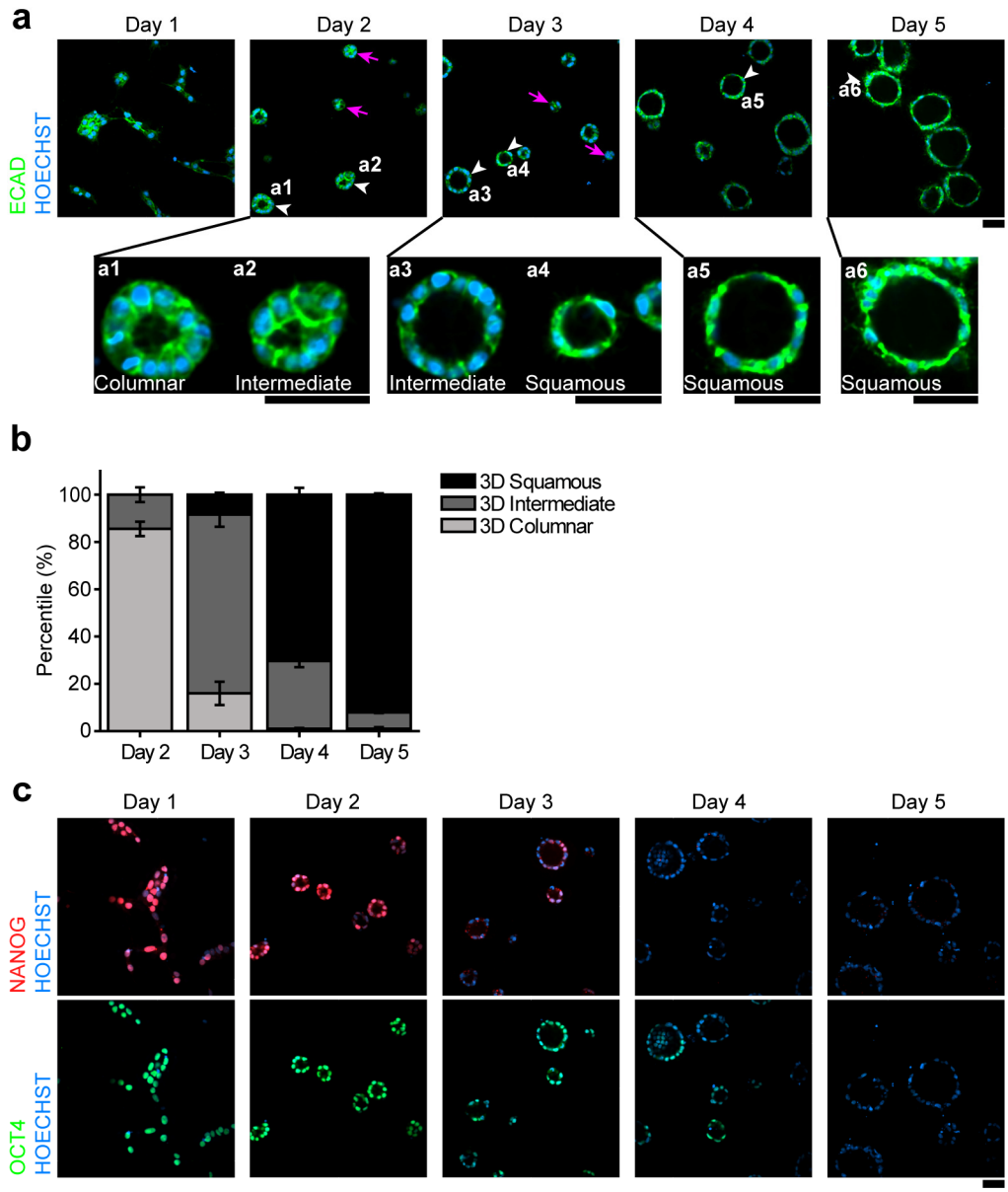

Figure 2-6 Morphogenic cytodifferentiation of hPSCs over time in the implantation-like Gel-3D niche. (**a**) Confocal micrographs taken at different days (as indicated), showing immunostaining of ECAD (green) and counterstaining by HOECHST (blue) to examine morphological evolution of hPSCs cultured in the implantation-like Gel-3D niche. Magnified views of individual cysts (marked by white arrowheads) at different time points reveal a morphological transition from columnar to intermediate, to squamous cysts (**a1-a6**). Some hPSC clusters (marked by magenta arrows) did not form recognizable open lumens at day 2 or day 3. Such clusters were excluded from the quantification of time-dependent cyst morphological change in **b**. (**b**) Stacked bar plot showing percentages of hPSC-derived epithelial cysts with different morphologies in the implantation-like Gel-3D niche at days 2, 3, 4, and 5. Data represent the mean ± s.e.m with n_{cyst} = 424 (day 2), 534 (day 3), 652 (day 4),

and 542 (day5). *n* = 3 biological replicates for each condition. (**c**) Confocal micrographs showing co-staining of NANOG (red) and OCT4 (green) for hPSCs cultured in the implantation-like Gel-3D niche at different days as indicated. HOECHST (blue) counterstains the nucleus. Scale bars in **a&c**, 50 μm. *n* = 2 independent experiments.

Sasaki *et al*. in the development of nascent amnion in monkey embryos[19].

Furthermore, the dynamics of squamous epithelial cyst development in Gel-3D condition was also examined (Figure 2-6). On day 2, majority of epithelial cysts were lumenal and columnar (Figure 2-6a,b). Such columnar cyst morphology was transient, however, and by day 4, most cysts had become flat and squamous (Figure 2-6a,b). During morphological evolution of lumenal epithelial cysts, NANOG and OCT4 were gradually lost, with most dramatic changed observed between day 2 and day 4 (Figure 2-6c). These findings suggest concurrent squamous epithelial morphogenesis and spontaneous cytodifferentiation.

Spontaneous self-organized development of squamous epithelial cysts was also observed in two additional hESC lines (UM63-1 and H7) and an hiPSC line (1196a) cultured in Gel-3D, but not under Glass-2D, Gel-2D, or Glass-3D conditions (Figure 2-7). Thus, uniquely among all conditions examined, the implantation-like Gel-3D biophysical niche is both necessary and sufficient for efficiently inducing spontaneous self-organization and differentiation of hPSCs to a cystic epithelial tissue with amnion-like squamous morphology, under biochemical conditions that permit hPSC self-renewal.

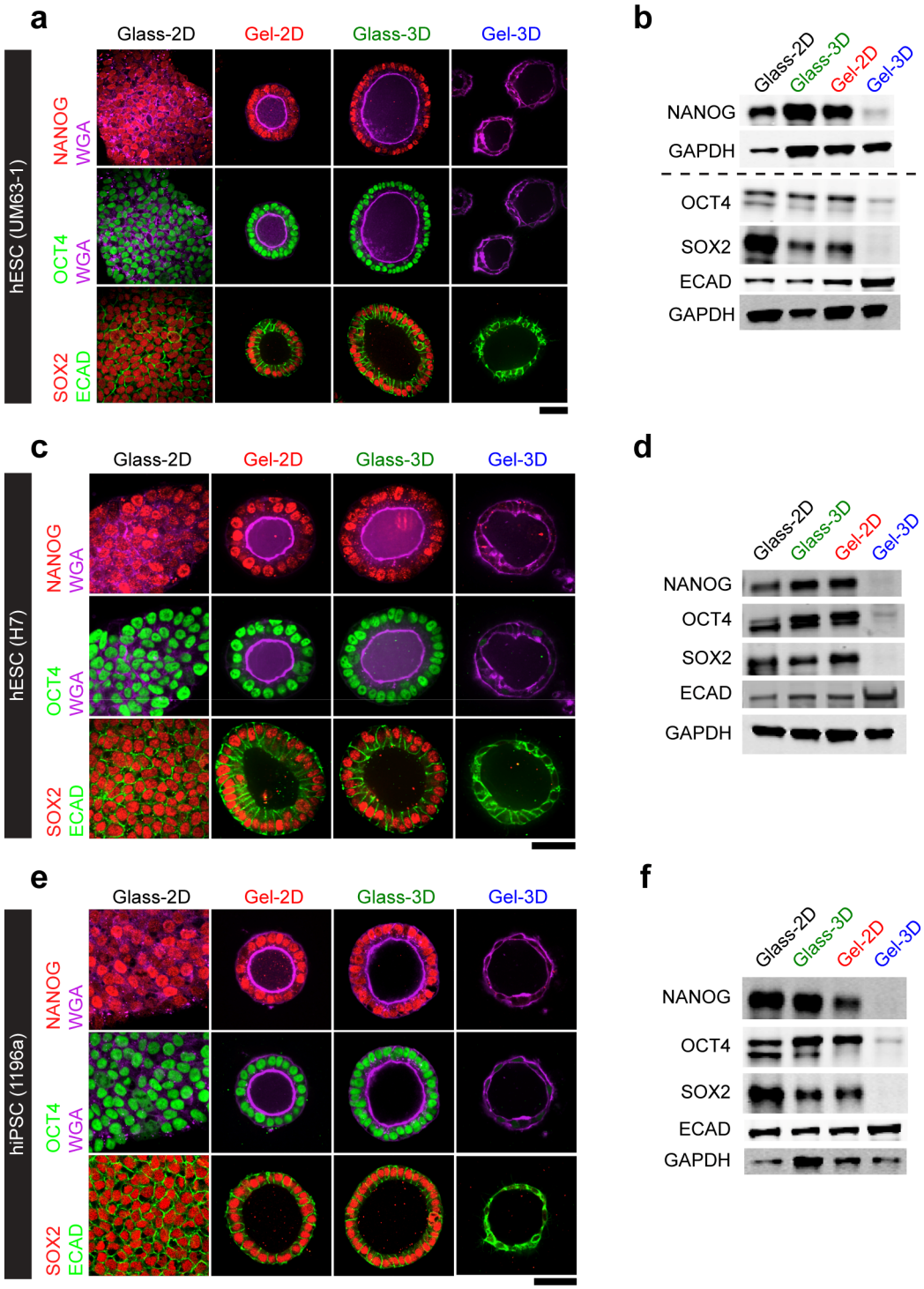

Figure 2-7 The implantation-like Gel-3D niche induces spontaneous, self-organized development of squamous epithelial cysts from multiple hPSC lines. Confocal micrographs showing immunostaining of NANOG (red; *top*), OCT4 (green; *middle*), and SOX2 (red; *bottom*), with WGA (purple; *top and middle*), and ECAD (green; *bottom*), in the UM63-1 hESC line (**a**), H7 hESC line (**c**), and 1196a hiPSC line (**e**) cultured under indicated

conditions. Scale bars, 50 μm. Western blot showing expression levels of NANOG, OCT4, SOX2, ECAD, and GAPDH in the UM63-1 hESC (**b**), H7 hESC (**d**), and 1196a hiPSC (**f**) cultured under indicated conditions. Immunofluorescence staining and Western blotting for each cell line was conducted for $n = 2$ independent experiments.

2.4.3 Development of the Squamous Cyst is Sensitive to the Mechanical Property of the Niche

Since the thickness of a soft gel bed coated on glass coverslip is negatively correlated with the apparent substrate rigidity[75], above results suggest that the development of the squamous

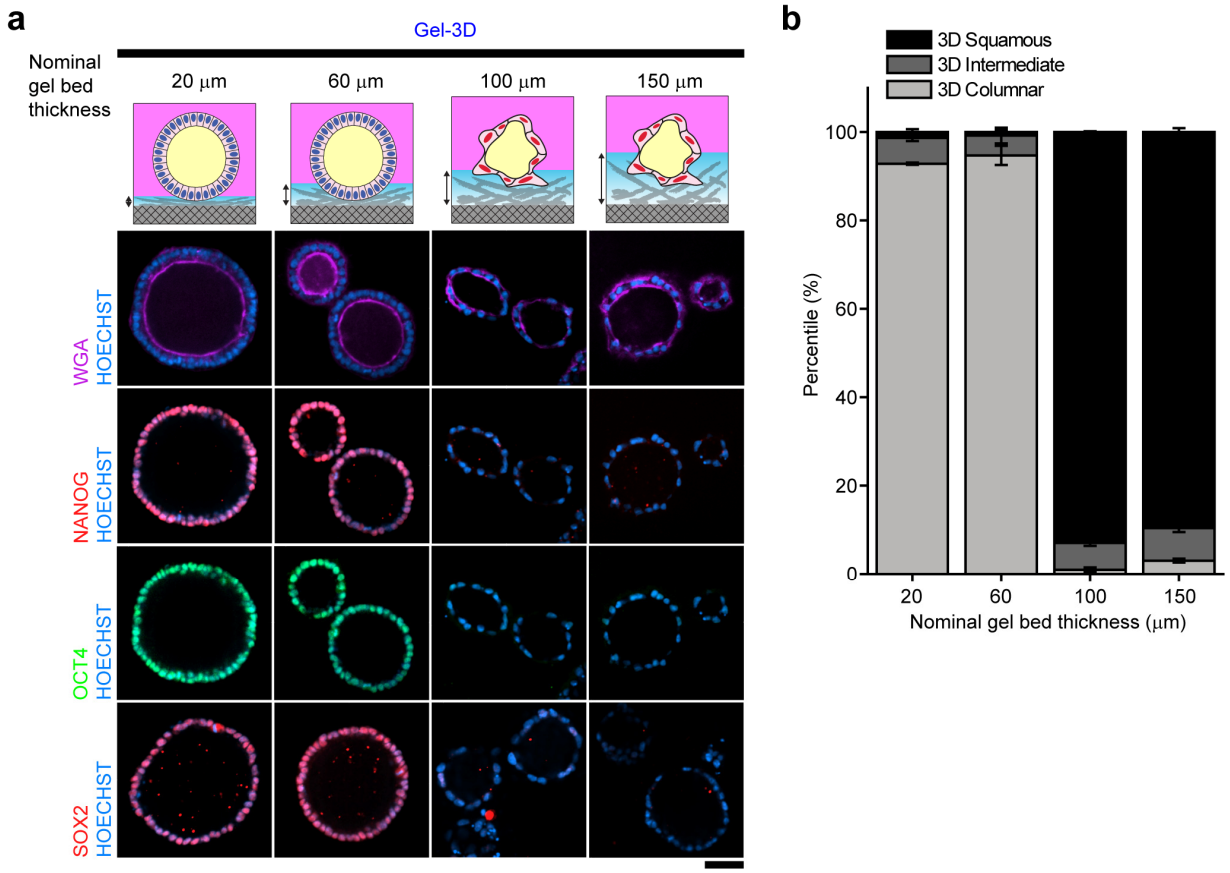

Figure 2-8 Development of squamous cystic tissues from hPSCs in the Gel-3D niche requires a thick gel bed. (**a**) Confocal micrographs showing staining of WGA (purple), NANOG (red), OCT4 (green), and SOX2 (red) and counterstaining by HOECHST (blue) for hPSCs cultured in Gel-3D with varying nominal gel bed thicknesses as indicated. Cartoons show the typical epithelial cyst morphology observed under each condition. Scale bar, 50 μm. (**b**) Stacked bar plot showing percentages of hPSC-derived epithelial cysts with different morphologies in Gel-3D as a function of the nominal gel bed thickness. Data represent the mean ± s.e.m with n_{cyst} = 306, 361, 694, and 492 for gel beds of 20, 60, 100, and 150 μm thickness, respectively. $n = 3$ biological replicates for each condition. $n = 2$ independent experiments.

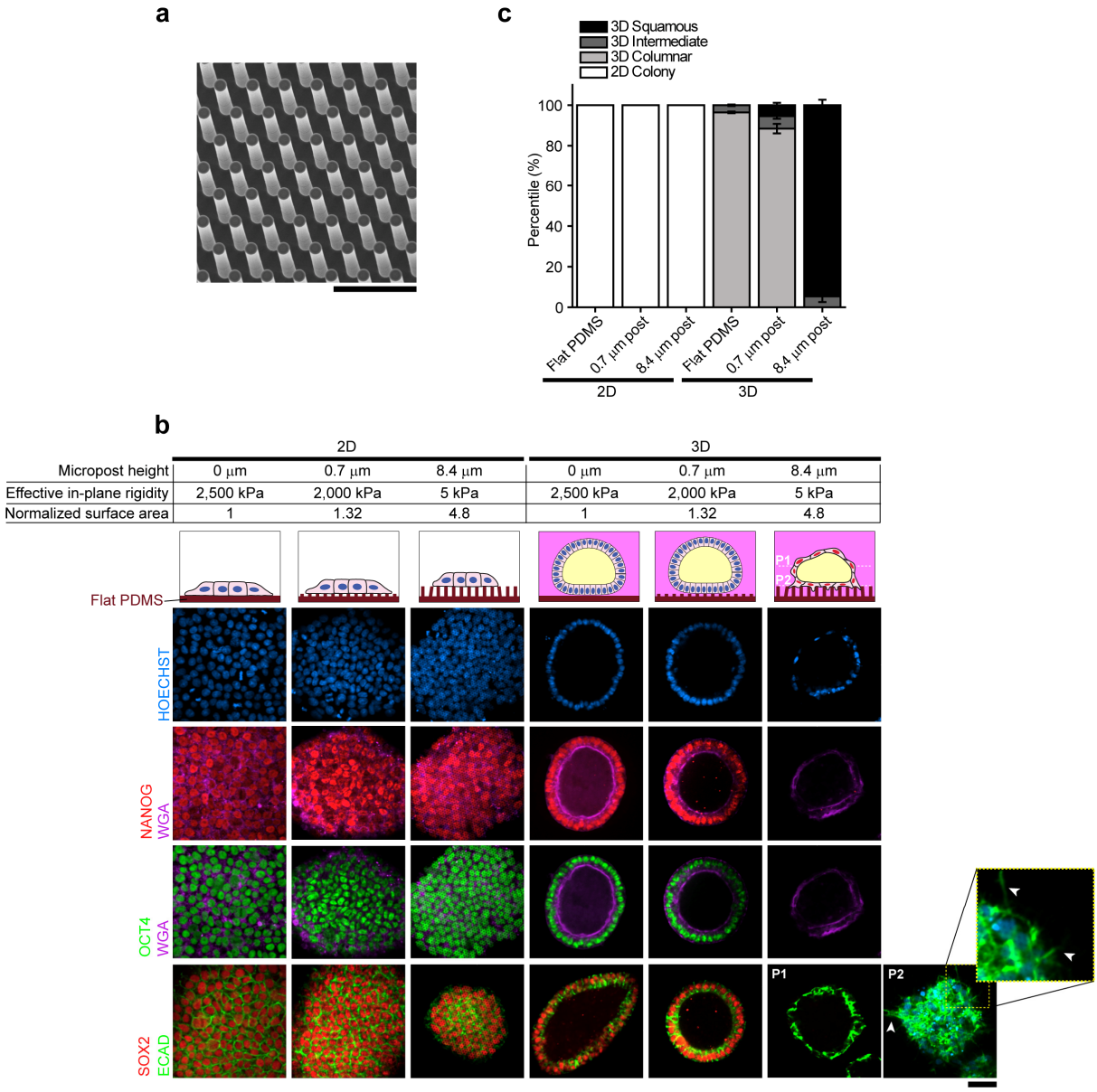

Figure 2-9 Self-organized development of epithelial cystic tissue with squamous, human amnion-like morphology by hPSCs cultured on an artificial matrix containing an elastomeric micropost array. (**a**) Scanning electron microscopy (SEM) image of the elastomeric polydimethylsiloxane (PDMS) micropost array with a post diameter of 1.83 μm, a post height of 8.4 μm, and a post center-to-center distance of 4 μm. Scale bar, 10 μm. (**b**) Specifics (*top*) and cartoons (*middle*) showing culture conditions containing an artificial matrix made of PDMS microposts with different post heights to modulate substrate rigidity. Confocal micrographs (*bottom*) showing epithelial morphology (stained by WGA, purple, or ECAD, green) and co-staining of NANOG (red), OCT4 (green), and SOX2 (red) for hPSCs cultured in indicated conditions. HOECHST (blue) counterstains the nucleus. For the squamous cyst formed in 3D on 8.4 μm tall microposts (*right*), confocal micrographs taken at two planes passing the middle (**P1**) and bottom (**P2**) of the cyst (white dashed lines in cartoon) are

shown. The yellow square highlights ECAD+ protrusions (white arrowheads) at the interface between the cyst and microposts. Scale bar, 50 μm. (**c**) Stacked bar plot showing percentages of hPSC colony or hPSC-derived epithelial cysts with different morphologies as a function of PDMS micropost height and ECM dimensionality. Flat PDMS surfaces without microposts (thus with a micropost height of 0 μm) were included for comparison. Data represent the mean ± s.e.m with n_{colony} = 100 for all three 2D culture conditions and n_{cyst} = 250, 270, and 282 for 3D cultures using flat PDMS, 0.7 μm tall micropost, and 8.4 μm tall micropost, respectively. n = 3 biological replicates for each condition. n = 3 independent experiments.

cysts might be sensitive to the apparent mechanical stiffness of the gel bed. In order to test this hypothesis, gel beds of different thickness, namely, 20, 60, 100, and 150 μm, were used in the Gel-3D culture condition. Interestingly, at day 5, lumenal epithelial cysts formed by hPSCs on gel beds of 100 μm and 150 μm thickness exhibited predominantly a flat, squamous morphology; while those cultured on thinner gel beds of 20 and 60 μm thickness displayed mainly columnar epithelial morphology (Figure 2-8). This observation supports that the squamous cystic tissue morphogenesis is mechano-sensitive and requires a soft 3D ECM environment.

To further confirm the physical niche-dependency of hPSC morphogenic cytodifferentiation, we adopted an artificial matrix, made of a regular array of elastomeric polydimethylsiloxane (PDMS) microposts[70] whose height can be precisely modulated to control substrate rigidity and surface area (Figure 2-9a,b). Consistently, spontaneous development of squamous cysts occurred only in hPSCs cultured on 8.4 μm tall microposts (a soft matrix), but not on 0.7 μm tall microposts or on flat PDMS surfaces (rigid matrices), even though all included a 3D Geltrex™ overlay (Figure 2-9b,c). Interestingly, hPSCs cultured on soft 8.4 μm tall microposts in 2D (*i.e.*, without the Geltrex™ overlay) did not form cysts (Figure 2-9b), in contrast to columnar cysts formed in Gel-2D (Figure 2-3a,b). The mechanism underlying this differential morphogenesis is yet unknown, but it is speculated to be due to the mechanical property difference between an isotropic gel bed and an anisotropic micropost array. This question is worthy of further study.

2.4.4 The Squamous Cystic Tissue is Not of Other Non-Amniotic Lineages

In order to elucidate the cell fate of the hPSC-derived squamous cystic tissue, its molecular signature was examined and compared with that of other embryonic and extraembryonic lineages possibly existing in a peri-implantation embryo, including primitive streak (PS), neuroectoderm, primordial germ cells (PGCs), primitive endoderm (PE)/hypoblast, trophectoderm (TE)/trophoblast, and amnion.

Primitive streak development is associated with an epithelial-to-mesenchymal transition (EMT) accompanied by the up-regulation of transcription factors including BRACHYURY (BRA), SNAIL, and SLUG[76]. Indeed, basal protrusions observed in the squamous cysts (Figure 2-3b) suggest the possible involvement of EMT. Compared with control hPSCs in Glass-2D, up-regulation of BRA/*BRA* and SLUG/*SNAI2*, but not SNAIL/*SNAI1*, were observed in squamous cysts in Gel-3D; no up-regulation of these transcription factors was seen in Gel-2D or Glass-3D conditions (Figure 2-10). In contrast, hPSC-derived PS cells (*via* a 2D culture protocol[73]; referred to henceforth as PS-2D cells) showed up-regulation of BRA/*BRA*, SNAIL/*SNAI1*, and SLUG/*SNAI2* (Figure 2-10). PS-2D cells also showed a pronounced decrease in ECAD/*CDH1* and loss of ECAD organization, accompanied by increased NCAD/*CDH2*; none of these changes were seen in hPSC-derived squamous cysts (Figure 2-11). These data suggest that while PS-2D cells exhibit molecular signatures of canonical EMT (Figure 2-12a), the development of squamous cysts activates a unique subset of EMT-related transcription factors, notably without SNAIL, and elicits a columnar-to-squamous epithelial transition with ECAD/NCAD regulation

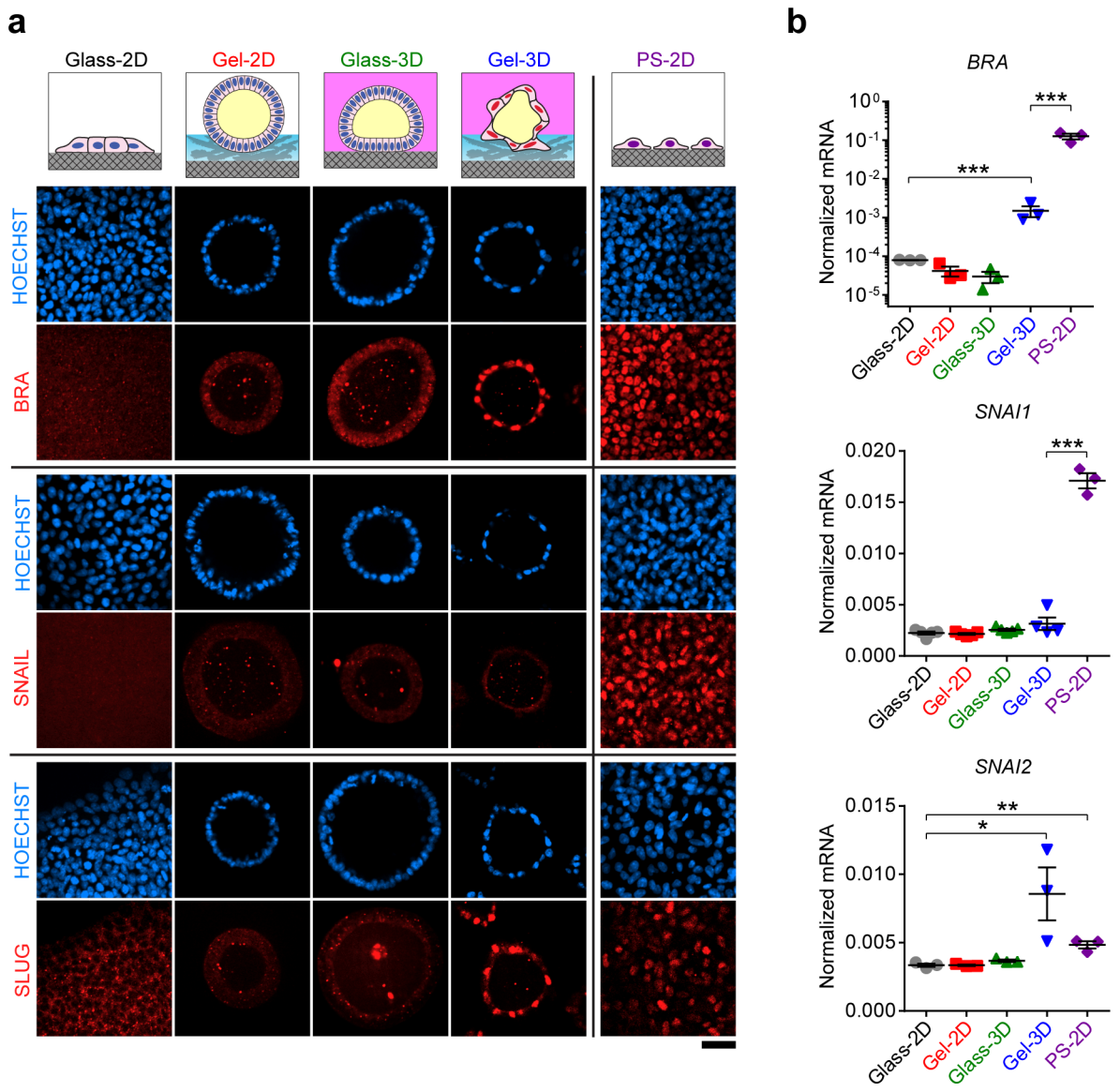

Figure 2-10 The development of squamous cystic tissues activates a unique subset of epithelial-to-mesenchymal transition related transcription factors. (**a**) Confocal micrographs showing immunostaining of BRACHYURY (BRA, red; *top*), SNAIL (red; *middle*), and SLUG (red; *bottom*) in hPSCs cultured under indicated conditions and corresponding staining of primitive streak (PS) cells derived from hPSCs under 2D culture[73] (PS-2D). HOECHST (blue) counterstains the nucleus. Scale bar, 50 μm (**b**) qRT-PCR analysis of *BRACHYURY* (*BRA*), *SNAI1*, and *SNAI2*, for hPSCs cultured in indicated conditions. Data were normalized against *GAPDH* and plotted as the mean ± s.e.m, with $n = 3$ - 5 biological replicates indicated by individual dots under each condition, $n = 2$ independent experiments. *P*-values were calculated using unpaired, two-sided Student's *t*-tests. *: $P < 0.05$; **: $P < 0.01$; ***: $P < 0.001$.

distinct from that observed in canonical EMT and PS lineage differentiation (Figure 2-12b). Additionally, FOXA2/*FOXA2* , a PS/endoderm marker, was undetectable in squamous cysts (Figure 2-13), further excluding the PS lineage. Absence of SOX2 - a marker of human neuroepithelium[77] - in squamous cysts (Figure 2-4) excludes the neuroectodermal lineage. A recent publication suggests that PGCs develop by canonical EMT from nascent amniotic cells in the monkey embryo[19]. As shown above, the molecular profile of squamous cysts indicates the absence of a canonical EMT program, excluding the PGC lineage. In addition, expression of SOX17, which is another marker of PGCs, was not observed in the squamous cyst either (data not shown). However, it remains a future goal to determine whether PGCs can be derived from the squamous cysts with a suitable protocol.

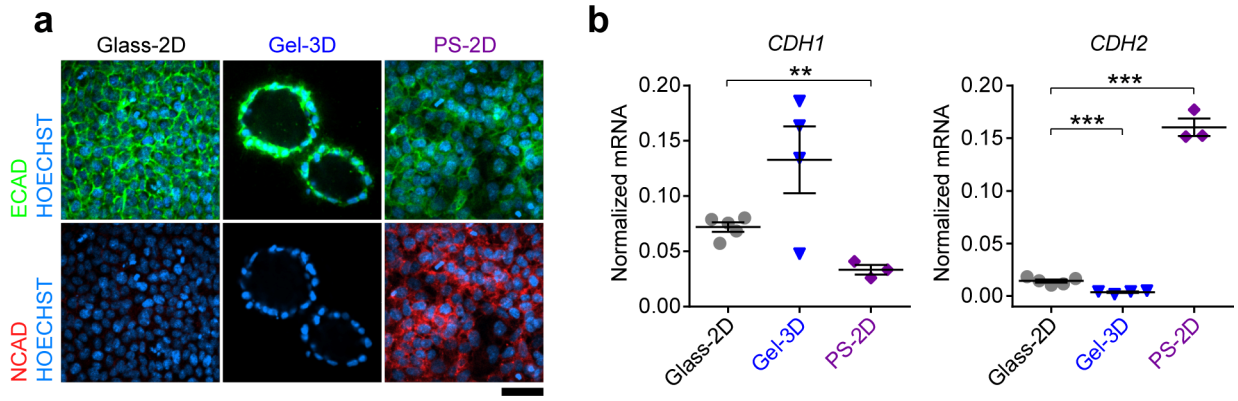

Figure 2-11 Squamous cysts exhibit distinct regulation on CADHERINs. (**a**) Confocal micrographs showing immunostaining of ECAD (green; *top*) and N-CADHERIN (NCAD, red; *bottom*) for hPSCs under indicated culture conditions. HOECHST (blue) counterstains the nucleus. Scale bar, 50 µm. $n = 2$ independent experiments. (**b**) qRT-PCR analysis of *CDH1*, and *CDH2*, for hPSCs cultured in indicated conditions. Data were normalized against *GAPDH* and plotted as the mean ± s.e.m, with $n = 3$ - 5 biological replicates indicated by individual dots under each condition, $n = 2$ independent experiments. Data in **b** for *CDH1* under both Glass-2D and Gel-3D conditions are the same as those in Figure 2-5b. *P*-values were calculated using unpaired, two-sided Student's *t*-tests. **: $P < 0.01$; ***: $P < 0.001$.

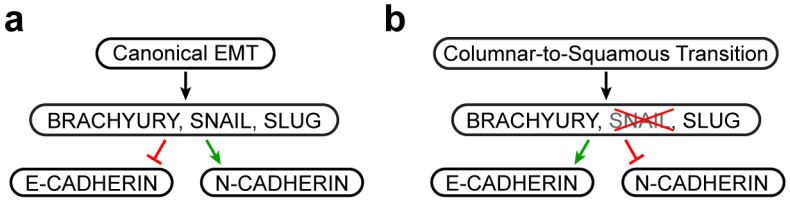

Figure 2-12 Schemes summarizing the paradigms of canonical epithelial-to-mesenchymal transition (EMT). (**a**) and the columnar-to-squamous transition reminiscent of human amnion development (**b**).

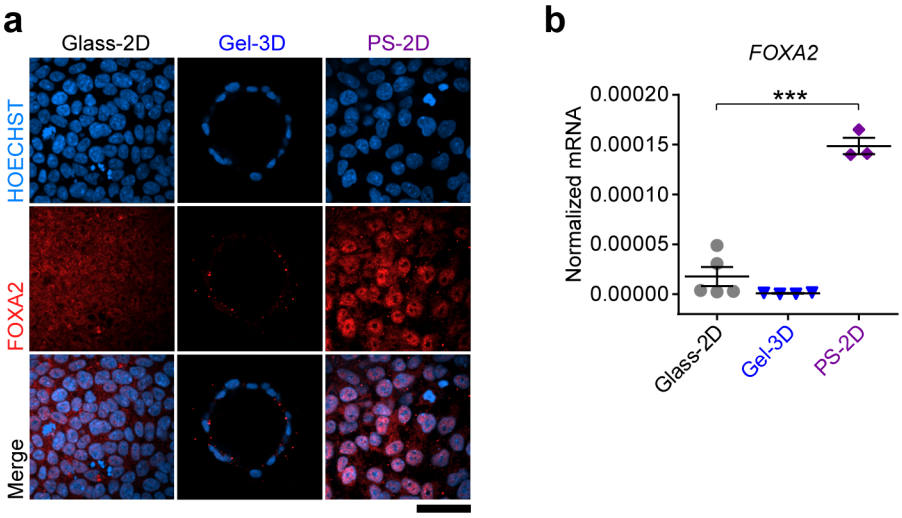

Figure 2-13 The squamous cystic tissue does not express FOXA2, a PS/endoderm marker. (**a**) Confocal micrographs showing immunostaining of FOXA2 (red) and counterstaining by HOECHST (blue) for hPSCs cultured in Glass-2D, Gel-3D, and PS-2D conditions as indicated. Scale bar, 50 µm. $n = 2$ independent experiments. (**b**) qRT-PCR analysis of *FOXA2* for hPSCs cultured in different conditions as indicated. Data were normalized against *GAPDH* and plotted as the mean ± s.e.m, with $n = 3$ - 5 biological replicates indicated by individual dots under each condition. *P*-values were calculated using unpaired, two-sided Student's *t*-test. ***: $P < 0.001$. $n = 2$ independent experiments.

In addition, PE/hypoblast markers *GATA4* and *GATA6*[16] were not up-regulated in squamous cysts either, compared with hPSCs, excluding the PE lineage (Figure 2-14a). Interestingly, several TE/trophoblast markers - *GATA2*, *GATA3*,*CDX2*, and *TP63*[16,78] - were highly up-regulated in squamous cysts compared with hPSC colonies and columnar cysts (Figure 2-14b). However, other known trophoblast markers - *KRT7*, *CGA*, *HLA-G*[78,79] - were not up-regulated in

squamous cysts (Figure 2-15a). The squamous cysts showed heterogeneous staining of CDX2 and GATA3, both of which co-localize with BRA (Figure 2-15b,c), combinations not seen in hPSC-derived trophoblasts[78]. SSEA-4, a surface antigen associated with the inner cell mass, but not TE[80], is also retained in squamous cysts (Figure 2-15d). Importantly, other studies have reported *GATA2*, *GATA3*[78,81], and SSEA-4[18,82] expression in human amnion. Together, these results contradict known molecular features of trophoblasts, and suggest that the hPSC-derived squamous cysts formed in the implantation-like Gel-3D niche might resemble human amnion.

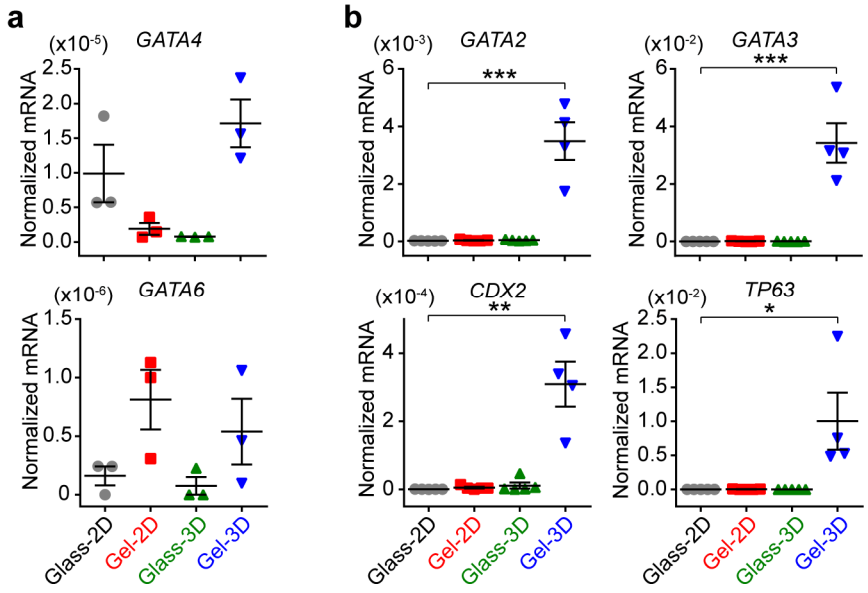

Figure 2-14 The squamous cystic tissue express extraembryonic tissue markers. qRT-PCR analysis of primitive endoderm/hypoblast markers *GATA4* and *GATA6* (**a**), and conventional trophectoderm and trophoblast markers *GATA2*, *GATA3*, *CDX2*, and *TP63* (**b**).

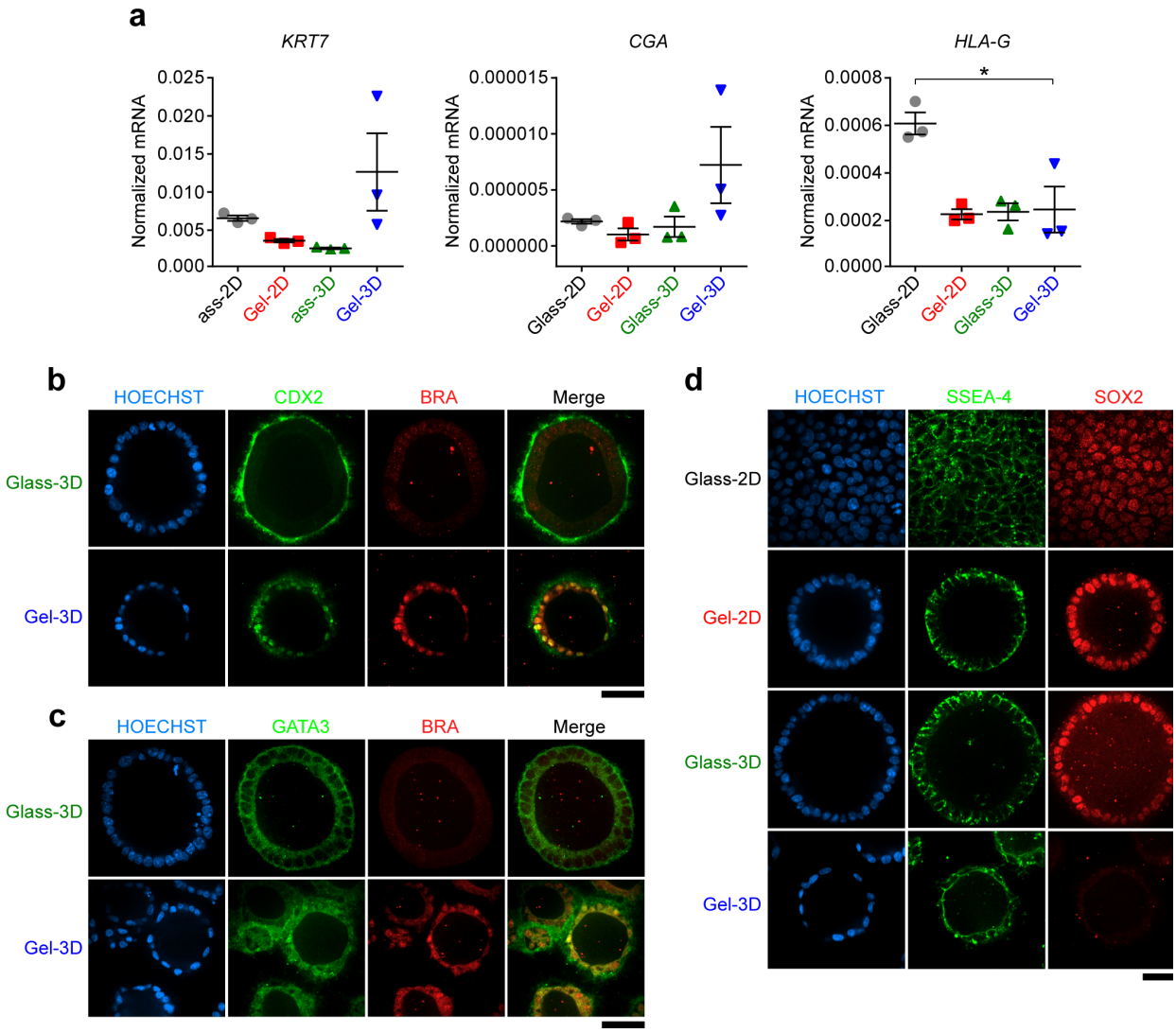

Figure 2-15 hPSC-derived squamous cystic tissue lacks molecular features associated with trophoblasts. (**a**) qRT-PCR analysis of trophoblast markers *KRT7*, *CGA*, and *HLA-G*, for hPSCs under different culture conditions as indicated. Data were normalized against *GAPDH* before being plotted as the mean ± s.e.m, with $n = 3$ biological replicates indicated by individual dots for each condition. $n = 2$ independent experiments. *P*-values were calculated using unpaired, two-sided Student's *t*-test. *: $P < 0.05$. (**b&c**) Confocal micrographs showing co-staining of BRA (red) with CDX2 (green; **b**) or GATA3 (green; **c**), for hPSCs under both Glass-3D and Gel-3D culture conditions. HOECHST (blue) counterstains the nucleus. $n = 2$ independent experiments. (**d**) Confocal micrographs showing co-staining of SSEA-4 (green) with SOX2 (red) for hPSCs cultured in different conditions as indicated. HOECHST (blue) counterstains the nucleus. $n = 2$ independent experiments. Scale bars in **b-d**, 50 µm.

2.4.5 The Squamous Cystic Tissue Exhibits Molecular Signatures of Early Human Amnion

As shown in Figure 2-16a, mRNA expression of a set of key fate-identifying genes recently reported for first trimester human amnion - *ITGB6*, *VTCN1*, *GABRP* and *MUC16*[81] - are all significantly up-regulated in squamous cysts compared with control hPSCs. Additionally, squamous cysts exhibit up-regulated expression of *HAND1*, *POSTN*, *TFAP2A*, and *TFAP2B* (Figure 2-16b); *HAND1*, *POSTN*, and *TFAP2A* are early amnion markers in the mouse embryo[83], and *POSTN*, *TFAP2A*, and *TFAP2B* are reported first trimester human amnion markers[81,83,84]. The squamous cysts also show up-regulation of *KRT17* and *KRT18* (Figure 2-16c), which are observed in week 10 human amnion[85]. Together, these data demonstrate that, among all the candidate lineages, the hPSC-derived squamous cysts exhibit a molecular signature most closely matching known aspects of human amnion at the first trimester (*e.g.*, week 9-10), the earliest stage reported so far in the literature.

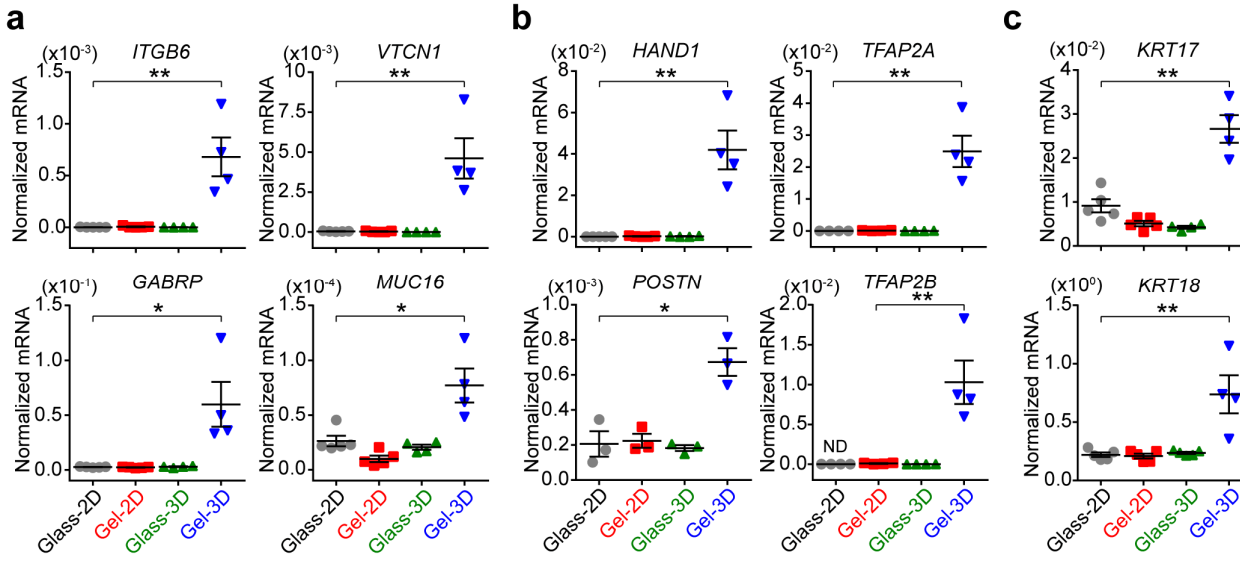

Figure 2-16 qRT-PCR analysis of squamous cysts for first trimester human amnion markers *ITGB6*, *VTCN1*, *GABRP*, *MUC16*, *HAND1*, *POSTN*, *TFAP2A*, *TFAP2B*, *KRT17*, and *KRT18*. All data were normalized against *GAPDH* and plotted as the mean ± s.e.m, with $n = 3$ - 5 biological replicates indicated by individual dots, $n = 2$ independent experiments. *P*-values were calculated using unpaired, two-sided Student's *t*-tests. *: $P < 0.05$; **: $P < 0.01$.

2.4.6 Profiling the Transcriptome of hPSC-derived Amnion-like Tissue by RNA-sequencing

To establish the transcriptome of the hPSC-derived amnion-like tissue (referred to henceforth as hPSC-amnion), we performed RNA-sequencing (RNA-seq) (see GEO deposit GSE89479). Although the transcriptome of hPSC-amnion differs substantially from that of control hPSCs, the expression levels of a cohort of putative pluripotency genes[86] (Table D-1) are remarkably similar in both; only *CUZD1* and *CCL26* are substantially down-regulated in hPSC-amnion compared with control hPSCs (Figure 2-17). This observation suggests that hPSC-amnion develops with only slight down-regulation of the transcriptional circuitry maintaining pluripotency, consistent with the emergence of amnion from expanding pluripotent epiblasts in a self-renewal-permissive environment *in vivo* and here *in vitro*.

We next selected ~4,000 genes with higher expression in hPSC-amnion than in hPSCs or in previously examined fetal extraembryonic tissues, including amnion, chorion, and umbilical cord (GEO access number GSE66302)[81] (Figure 2-18), and subjected them to hierarchical clustering. This revealed a gene set uniquely enriched in hPSC-amnion and relatively depleted in hPSCs and

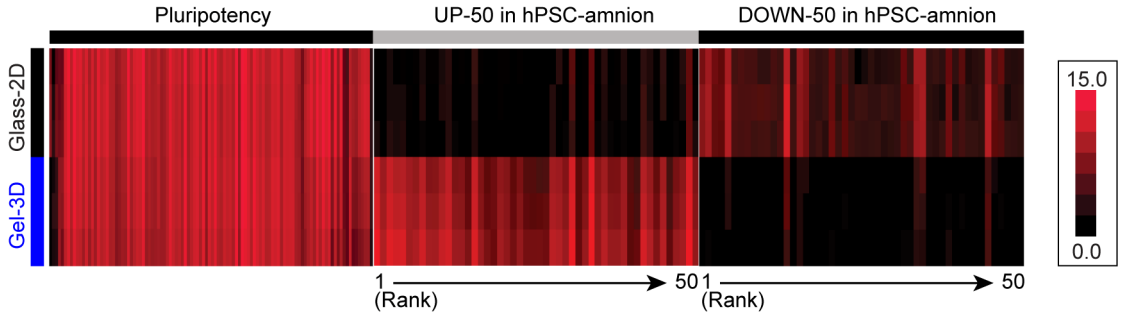

Figure 2-17 The development of squamous cysts shows limited perturbation on putative pluripotency genes. Heat map showing expression levels of 108 putative pluripotency genes[86] (Table D-1), 50 most up-regulated genes (UP-50), and 50 most down-regulated genes (DOWN-50) (Table E-1) in hPSC-amnion derived in Gel-3D relative to hPSC colonies in Glass-2D. $n = 3$ biological replicates. The color scale represents levels of normalized gene expression.

other extraembryonic fetal tissues (Figure 2-18). Thus, this unique molecular signature probably reflects the fact that the peri-implantation stage represented by hPSC-amnion is developmentally earlier than any of previously examined amnion tissues[78,81,84]. We also compared the genes enriched in hPSC-amnion with the recently reported single cell transcriptomes of 197 non-amniotic cells obtained from post-implantation monkey embryos[8]. This analysis did not reveal any single monkey cell that displays a transcriptome similar to hPSC-amnion (data not shown), further supporting our contention that the hPSC-amnion described here represents a distinct lineage. We should also note that the hPSC-amnion, which resembles the initial stage of amnion

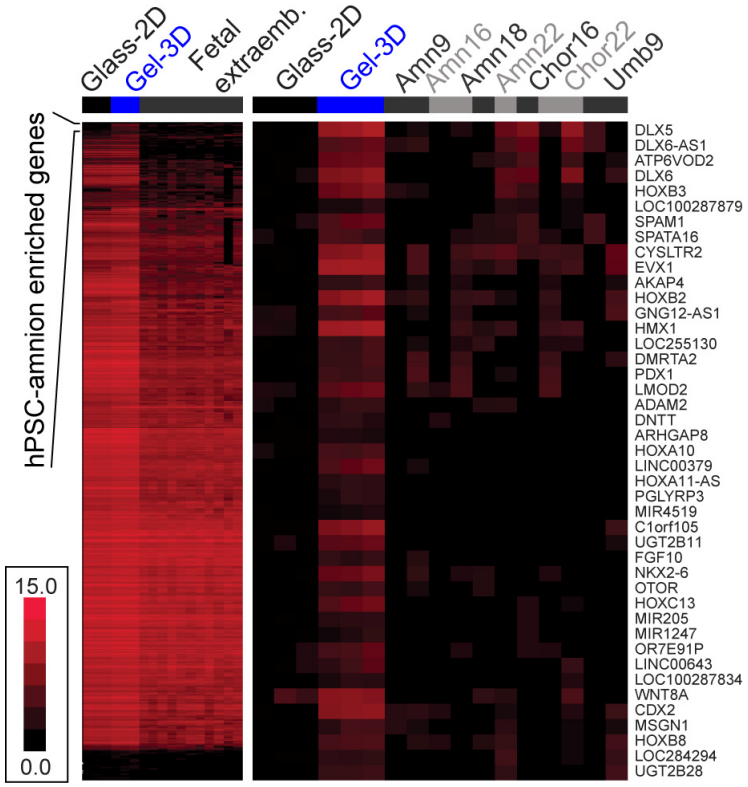

Figure 2-18 A unique gene set enriched in hPSC-amnion. (*left*) Hierarchical clustering of ~4,000 hPSC-amnion-enriched genes among hPSC colonies (Glass-2D), hPSC-amnion (Gel-3D), and published fetal extraembryonic tissues including week 9 amnion and umbilical cord (Amn9, Umb9), week 16 amnion and chorion (Amn16, Chor16), week 18 amnion (Amn18), and week 22 amnion and chorion (Amn22, Chor22)[81]. (*right*) Zoom-in view of hPSC-amnion enriched genes. The color scale represents levels of normalized gene expression.

development in human, is the end-point phenotype in the current culture system (data not shown), suggesting that it may require additional factors for further development of the amnion-like tissue *in vitro*.

To further characterize the hPSC-amnion, we performed gene ontology (GO) functional annotation clustering for genes enriched in hPSC-amnion relative to hPSCs. GO terms for genes enriched in 9-week human amnion as well as human chorion and placenta (relative to hPSCs) were similarly clustered. Strikingly, three most enriched annotation clusters in hPSC-amnion were transcription factors, primarily those of the homeobox classes (Figure 2-18). Interestingly, HOX genes comprised the highest ranked cluster in 9-week amnion as well (Figure 2-18).

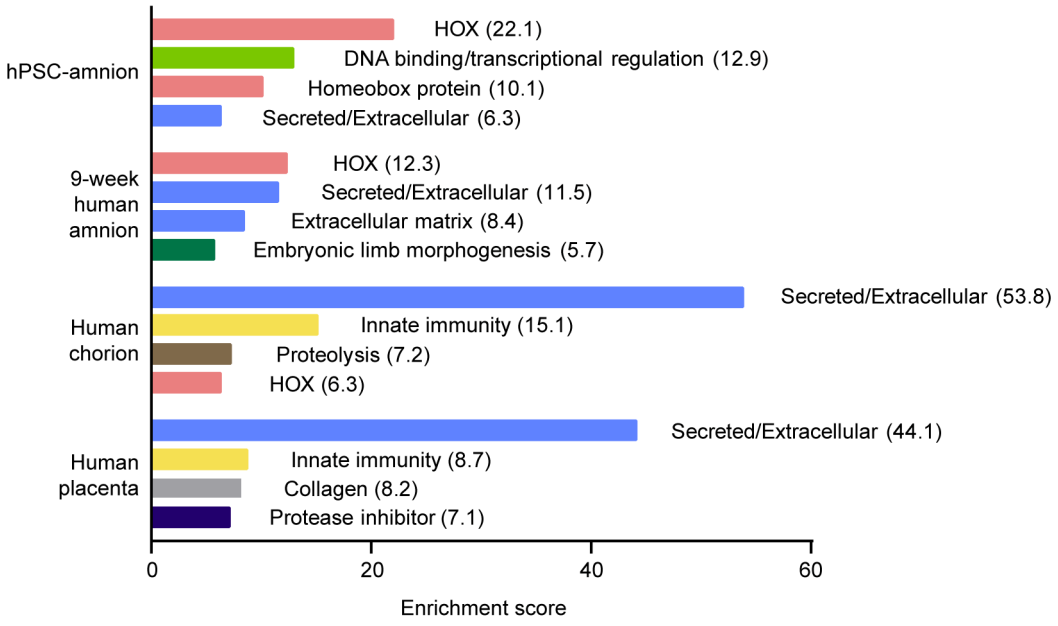

Figure 2-19 Gene ontology (GO) functional annotation clustering. Genes enriched in hPSC-amnion, 9-week human amnion, human chorion, and human placenta, respectively, relative to hPSCs, were subjected to functional annotation clustering analysis using DAVID. For each data set, the four annotation clusters with the highest enrichment scores (plotted along the *x*-axis and also listed in parentheses following the annotation term) are presented. The data sets used for 9-week human amnion, human chorion, and human placenta are from a previous publication (GEO accession number GSE66302)[81].

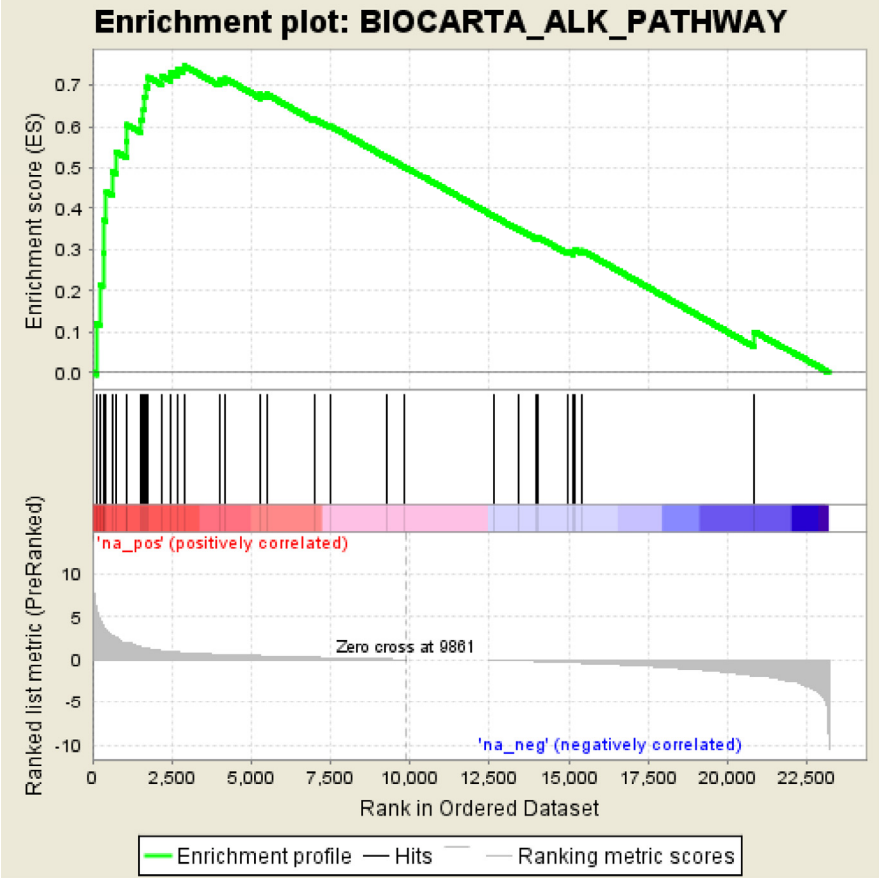

Figure 2-20 Gene set enrichment analysis (GSEA) for ALK-pathway hPSC-amnion. The entire ranked list of genes, ordered by fold change of expression level in hPSC-amnion relative to hPSCs (as shown in GEO deposition GSE89479), was queried using the gene set, BIOCARTA_ALK_PATHWAY, which contains 35 genes associated with BMP signaling. Significant enrichment of ALK-pathway related genes was observed in hPSC-amnion. (see Table F-1 for tabulated enrichment analysis results).

2.4.7 BMP-SMAD Signaling is Endogenously Activated and Required for hPSC Amniogenesis

Among genes enriched in hPSC-amnion were several potential BMP targets including *DLX5/6* and *EVX1* (Figure 2-18, Table E-1). Gene set enrichment analysis (GSEA) also revealed significant enrichment of genes related to the ALK-pathway, which is associated with BMP signaling, in hPSC-amnion compared with hPSCs (Figure 2-20). Indeed, we observe prominent nuclear staining and up-regulated protein level of phosphorylated SMAD1/5 (pSMAD1/5), a

downstream target of BMP-SMAD signaling, in hPSC-amnion, compared with control hPSC colonies and columnar cysts (Figure 2-21). It suggests that BMP-SMAD signaling is activated during hPSC-amnion development, consistent with findings in early mouse embryos[83,87,88] and post-implantation monkey embryos[19]. Consistently, both RNA-seq and qRT-PCR analysis (Figure 2-22a) show up-regulated *BMP2/4/7* in hPSC-amnion. Western blotting further confirms significantly increased BMP4 protein level in hPSC-amnion (Figure 2-22b), consistent with endogenously activated BMP-SMAD signaling during the development of hPSC-amnion in the implantation-like biophysical niche.

To examine whether BMP-SMAD signaling is required for hPSC-amnion development, hPSCs cultured in Gel-3D were treated with a small molecule inhibitor LDN193189 (LDN), which inhibits ALK2/3 receptors that bind to BMP2/4/7. Strikingly, short-term treatments with LDN (on day 2 only or on both days 2 and 3) were sufficient to inhibit hPSC-amnion development (Figure 2-23, 2-24). The development of hPSC-amnion is also inhibited by treatment with NOGGIN, a BMP-specific antagonist protein (**Supplementary Fig. 11d&e**). Together, these results implicate the requirement of endogenous BMP-SMAD signaling for hPSC-amnion development. It remains to be determined how physical signals from the 3D implantation-like niche activate BMP-SMAD signaling to elicit the development of hPSC-amnion.

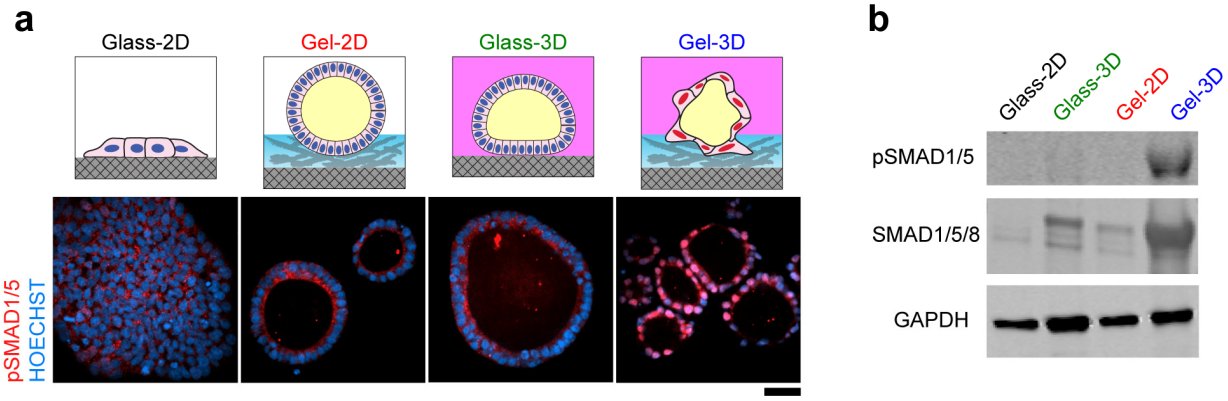

Figure 2-21 The development of hPSC-amnion activates BMP-SMAD signaling. (**a**) Confocal micrographs showing immunostaining of phosphorylated SMAD1/5 (pSMAD1/5, red) in hPSCs cultured under indicated conditions. HOECHST (blue) counterstains the nucleus. $n = 2$ independent experiments. Scale bar, 50 µm. (**b**) Western blot showing protein levels of pSMAD1/5, SMAD1/5/8, and GAPDH for hPSCs cultured under indicated conditions. $n = 3$ independent experiments.

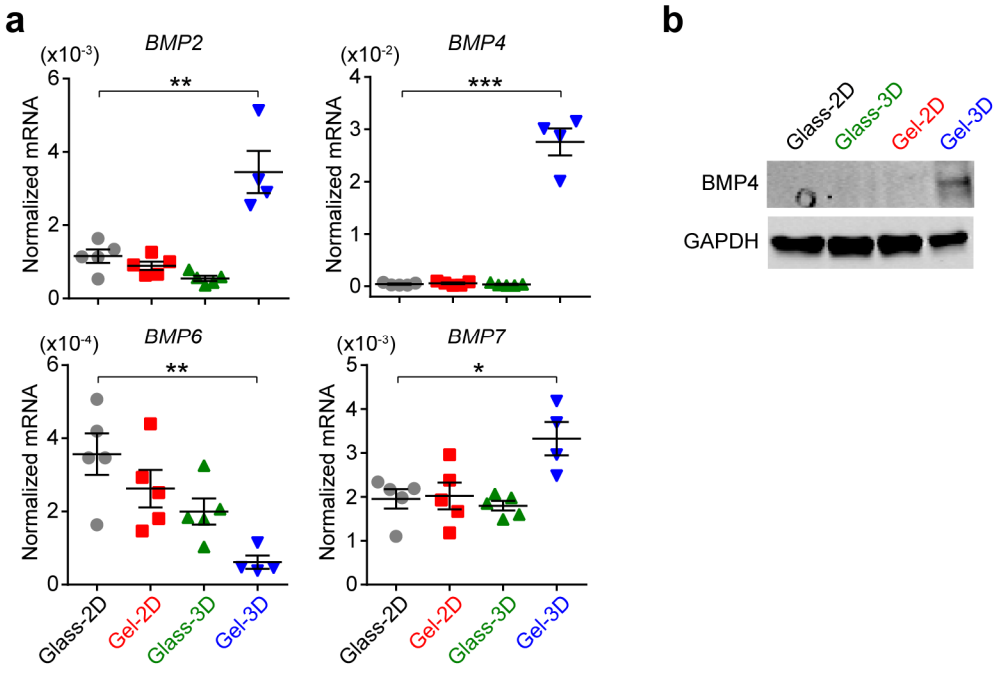

Figure 2-22 The development of hPSC-amnion activates endogenous BMP production. (**a**) qRT-PCR analysis of *BMP2*, *BMP4*, *BMP6*, and *BMP7* for hPSCs cultured under indicated conditions. Data were normalized against *GAPDH* and plotted as the mean ± s.e.m, with $n = 4$ - 5 biological replicates indicated by individual dots, $n = 2$ independent experiments. *P*-values were calculated using unpaired, two-sided Student's *t*-tests. *: $P < 0.05$; **: $P < 0.01$; ***: $P < 0.001$. (**b**) Western blot showing expression levels of BMP4 and GAPDH in hPSCs cultured under different conditions as indicated.

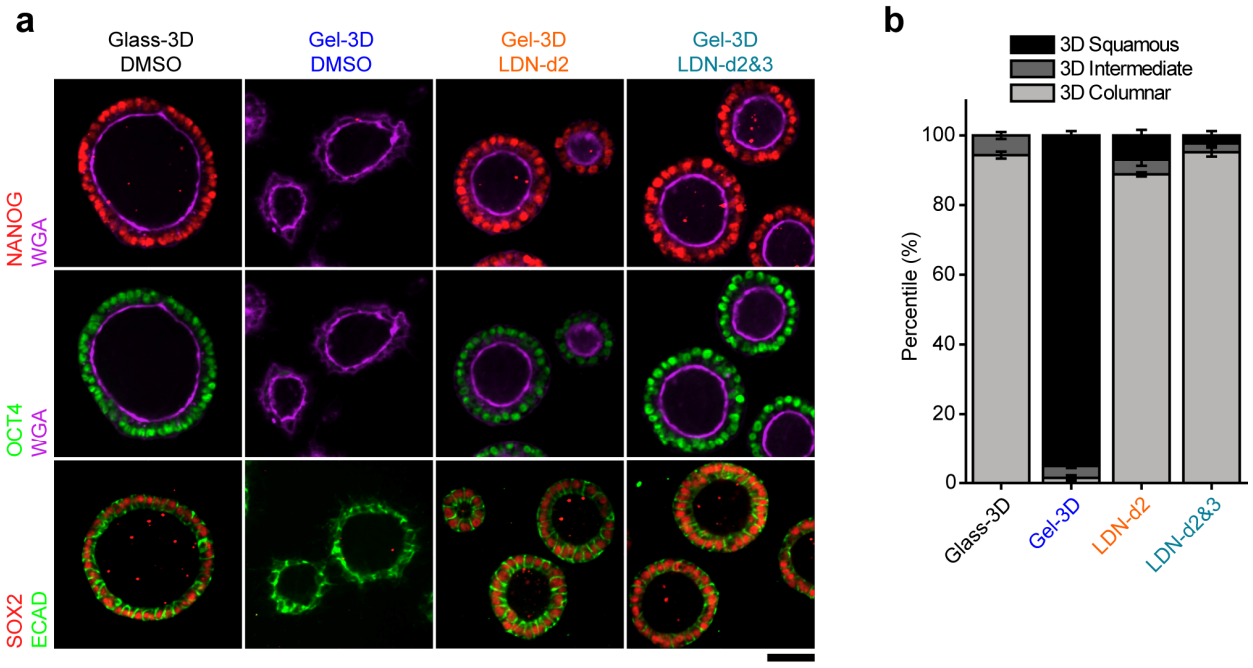

Figure 2-23 Inhibition of BMP receptors prevents the spontaneous differentiation of hPSC-amnion. (**a**) Confocal micrographs showing immunostaining of NANOG (red; *top*), OCT4 (green; *middle*), SOX2 (red; *bottom*), pan-cell membrane marker WGA (purple; *top* and *middle*), and basolateral membrane marker ECAD (green; *bottom*), in hPSC-derived epithelial cysts under Glass-3D and Gel-3D conditions with or without supplementation of BMP inhibitor LDN193189 (LDN) as indicated. LDN was supplemented on either day 2 only (LDN-d2) or on both days 2 and 3 (LDN-d2&3). $n = 4$ independent experiments. Scale bar, 50 μm. (**b**) Stacked bar plot showing percentages of hPSC-derived epithelial cysts with different morphologies in Glass-3D supplemented with DMSO (Glass-3D; negative control), in Gel-3D supplemented with DMSO (Gel-3D; positive control), and in Gel-3D supplemented with LDN193189 (LDN; 500 nM) on day 2 only (LDN-d2) or on both days 2 and 3 (LDN-d2&3). $n_{cyst} = 144$, 311, 365, and 320 for Glass-3D, Gel-3D, LDN-d2, and LDN-d2&3, respectively. $n = 3$ biological replicates for each condition. $n = 2$ independent experiments.

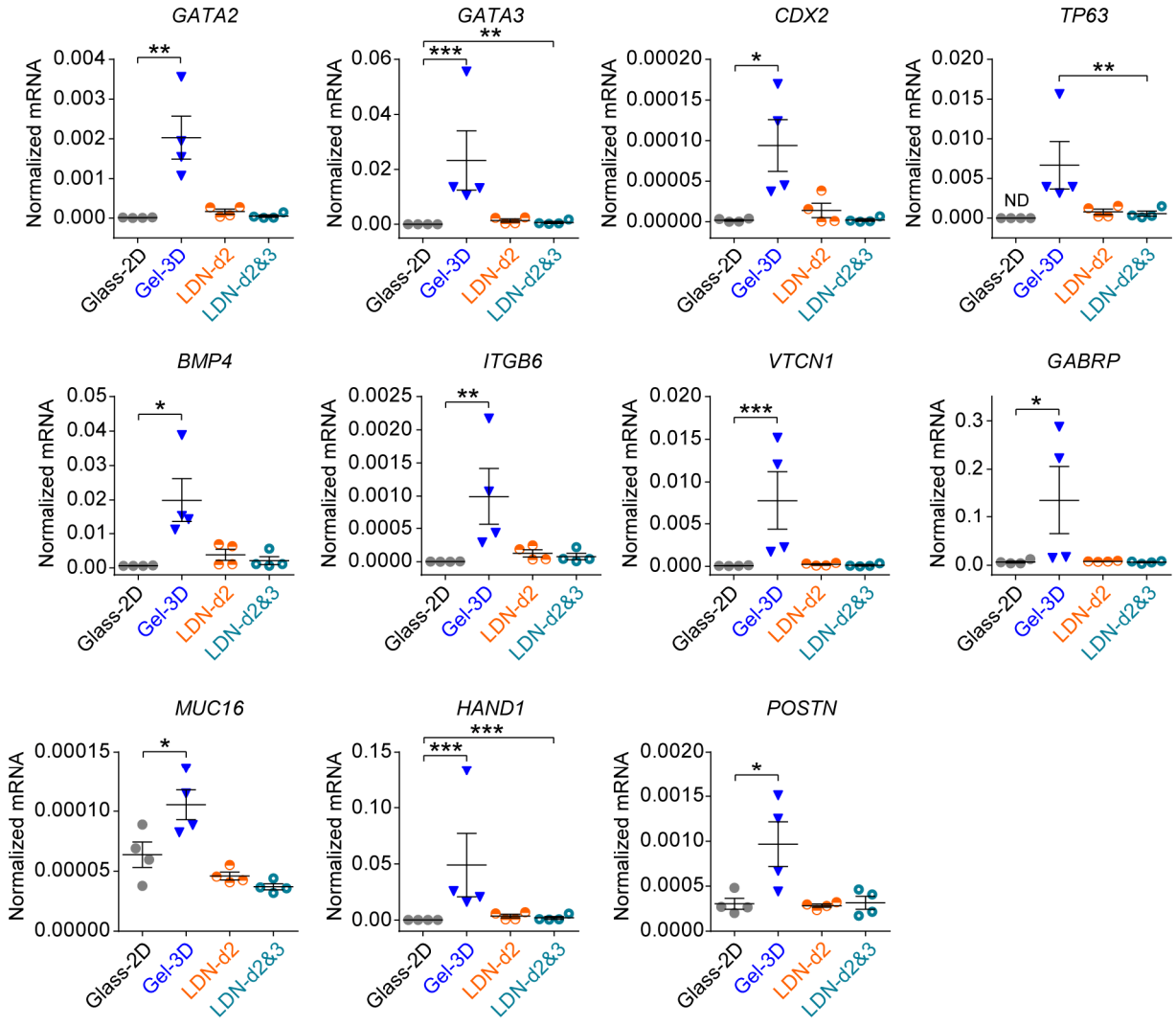

Figure 2-24 Inhibition of BMP receptors suppresses the up-regulation of amniotic markers in Gel-3D condition. qRT-PCR analysis of *GATA2*, *GATA3*, *CDX2*, *TP63*, *BMP4*, *ITGB6*, *VTCN1*, *GABRP*, *MUC16*, *HAND1*, and *POSTN* under Glass-3D, Gel-3D, LDN-d2, and LDN-d2&3 conditions. Data were normalized against *GAPDH* and plotted as the mean ± s.e.m, with $n = 4$ biological replicates indicated by individual dots for each condition. $n = 2$ independent experiments. *ND*, not detected, with its normalized value set to zero. *P*-values were calculated using unpaired, two-sided Student's *t*-test. *P*-value calculation was not performed against "*ND*" result. *: $P < 0.05$; **: $P < 0.01$; ***: $P < 0.001$.

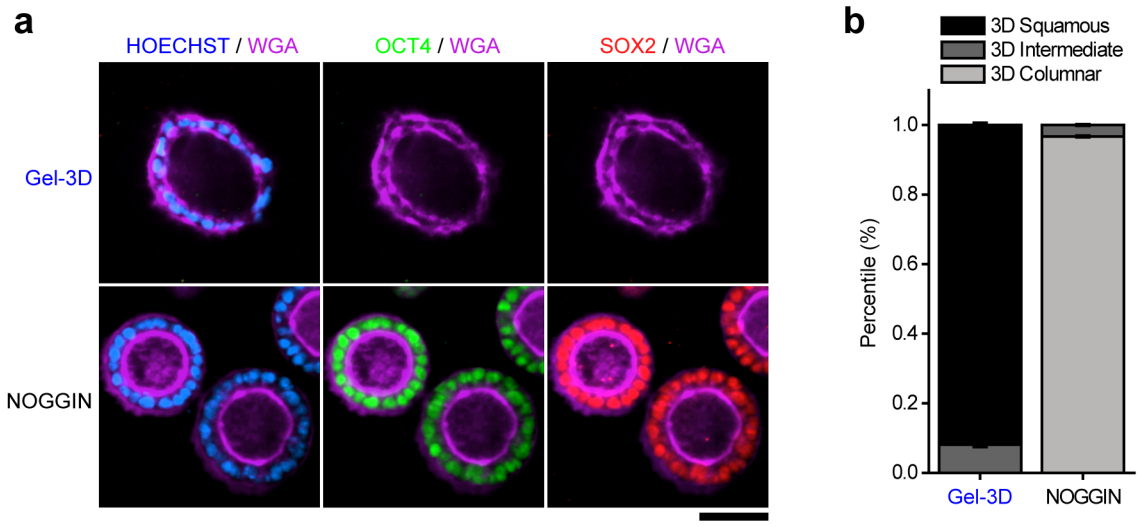

Figure 2-25 Development of hPSC-amnion can be inhibited by NOGGIN, a BMP antagonist protein. (**a**) Immunofluorescence analysis of cysts cultured under Gel-3D condition without (*top*) or with (*bottom*) NOGGIN treatment. Cysts were stained for OCT4 (green), SOX2 (red), and WGA (purple). HOECHST (blue) counterstains the nucleus. Scale bar, 50 μm. (**b**) Stacked bar plots show percentages of hPSC-derived epithelial cysts with different morphologies in the Gel-3D system without ("Gel-3D" group) or with ("NOGGIN" group) NOGGIN treatment. n_{cyst} = 131 and 241 for Gel-3D and NOGGIN groups, respectively. Data represent the mean ± s.e.m. with n = 3 biological replicates from n = 2 independent experiments.

2.4.8 Discussion

Although the histology of early human amnion development has been documented for more than half a century in the Carnegie collection of human embryos, it remains mysterious thus far how amniogenesis is induced from the epiblast and what developmental signaling is involved in such process. Findings reported in this work have brought new insights to answer those questions. Specifically, this work showed that amnion-like epithelial cells can arise from hPSCs through an apparent columnar-to-squamous morphological transition, suggesting that a similar process, which does not elicit canonical EMT but a unique subset of EMT-related transcription factors, might be involved during the emergence of amnion from pluripotent epiblast. In addition, this work showed that the amniogenic differentiation requires endogenous BMP production and

subsequent BMP-SMAD signaling within the amniotic cells, suggesting a potentially self-organizing and self-sustaining development of amnion in humans. This finding could challenge the traditional dogma that exogenous BMP ligand, likely from extraembryonic tissues (such as trophoblast) adjacent to the epiblast, is required for inducing amnion development in humans[17]. It also suggests that peri-implantation amnion could be a source of BMP ligand for additional embryonic induction of other tissues. This is consistent with recent report by Sasaki *et al*. that nascent amnion might be a paracrine center providing BMP ligand for PGC induction in monkey embryos[19].

In the last 5 years, there has been intensive interest and rapid progress in developing human organogenesis models *in vitro* using cultured hPSCs[26,49]. Paradoxically, it remains unclear whether hPSCs, which reside in a peri-implantation epiblast-like state, can be applied to model human-specific, peri-implantation developmental events *in vitro*. This work provides the first successful demonstration of applying hPSCs to study pre-gastrulation, peri-implantation human embryonic development - amniogenesis. Results reported in this chapter could broaden our understanding of the biology and developmental potential/competence of hPSCs, and expand the application of hPSCs into an uncharted field - implantation human embryology - that we envisage to further explore in future.

hPSCs, like many other cell types, have been found to be sensitive to microenvironmental physical factors and can change their behaviors, such as lineage differentiation, accordingly. Previous studies on the mechanobiology of hPSCs have suggested that individual biophysical cues, such as substrate softness, in the stem cell niche may be sufficient to promote uncontrolled spontaneous differentiation of hPSCs in 2D culture[89]. However, findings reported in this chapter challenged this classic view of hPSC mechanobiology, by showing that no notable amniogenic

differentiation of hPSCs occurs when only a 2D soft substrate is applied under biochemical conditions that permit hPSC self-renewal. Instead, as this work demonstrated, the integration of multiple implantation-like biophysical niche cues, including both 3D ECM and matrix softness, is required to efficiently switch hPSCs towards amniogenesis from an otherwise self-renewal state. Moreover, this work established that these biophysical niche cues are both necessary and sufficient to initiate the autonomous BMP-SMAD signaling required for amniogenesis. These findings might revises our current knowledge of the mechanobiology of hPSCs and its application in understanding developmental biomechanics and tissue engineering in future.

2.5 Conclusions

This chapter reports a biomimetic implantation-like niche for hPSCs to model human amniogenesis - a key developmental step previously not accessible to study. This chapter demonstrated that amniotic development by hPSCs is a self-organizing process that occurs in the absence of biochemical inductive cues from a maternal or extraembryonic source. Rather, physical signals from the implantation-like niche are necessary and sufficient to trigger the development of amnion-like tissue. This chapter revealed that the development of hPSC-amnion relies on an autonomously activated BMP-SMAD signaling as well as endogenous production of a unique subsets of BMP ligand. Interestingly, while the squamous hPSC-amnion reported here closely resembles human amnion tissue from morphological and transcriptomic perspectives, they do not fully recapitulate the patterned tissue morphologies of the peri-implantation human embryo, which will be addressed in the next chapter. This chapter also highlighted a previously unknown developmental potential of hPSCs and therefore opened new avenues for the application of hPSCs for human developmental modeling. In addition to advancing fundamental

understanding of human amnion development and expanding the application of hPSCs to model peri-implantation human embryogenesis, this efficient hPSC-based 3D amniogenic system could be leveraged for developing high-throughput screening assays to predict human reproductive success, examine the effect of toxins on amniotic development, or provide a therapeutic strategy for *in utero* treatment of amniotic tears. This efficient amniogenic induction system could also facilitate large-scale bio-fabrication of wound-healing-competent human amniotic cells for clinical applications.[‡]

[‡] Research presented in this chapter has received technical assistance from Dr. Kenichiro Taniguchi (cell culture), Dr. Katherine Gurdziel and Dr. Michael Czerwinski (RNA-seq data analysis), Mr. Xufeng Xue (Western blotting), Mr. Ryan F. Townshend and Dr. Koh Meng Aw Yong (qRT-PCR), and Mr. Jianming Sang (cell culture). I would also like to thank Dr. Jason R. Spence, Dr. K. Sue O'Shea, Dr. Sundeep Kalantry, Dr. Toshio Miki, Dr. William Shawlot, Dr. Allen P. Liu, Dr. Deborah L. Gumucio, and Dr. Jianping Fu for their comments on the research presented in this chapter.

CHAPTER III

Amniotic Sac Embryoid: an in vitro Model for Early Human Amniotic Sac Development

3.1 Introduction

The amniotic sac - an asymmetrically patterned epithelial cyst that encloses the amniotic cavity with squamous amnion at one pole and columnar epiblast at the other - is a key developmental structure arise from embryonic inner cell mass during the implantation of human embryo[6] (Figure 3-1). It also sets the stage for gastrulation beginning at d.p.f. 13.Despite earlier histological studies[6] and recent *in vitro* cultures of early human embryos[16,17], the development of human amniotic sac remains mysterious to date, due to a lack of *in vitro* models that can recapitulate its distinct morphogenesis and cell fate patterning during human embryogenesis from implantation to early gastrulation.

Human pluripotent stem cells (hPSCs), which share significant similarity with pluripotent

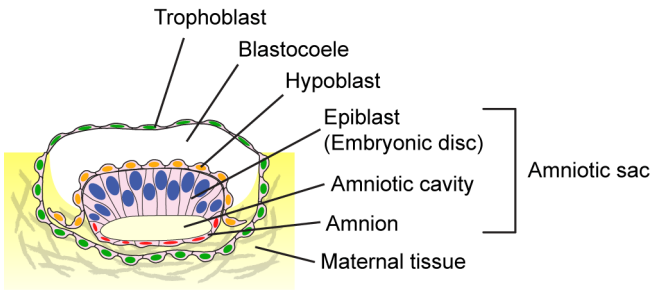

Figure 3-1 Cartoon of an implanting human embryo.

epiblast in the human embryo[9,23,90], have been successfully utilized for modeling post-gastrulation human development *in vitro*[14,25,45,49,51]. In Chapter II, in order to expand the application of hPSCs to model human development during implantation, we developed a biomimetic *in vitro* culture system that implements two implantation niche-inspired biophysical cues - an underlying soft tissue/gel bed and an overlaying three dimensional (3D) extracellular matrix (ECM). We demonstrated that even in the absence of extraembryonic tissues and exogenous biochemical inductive factors, this culture system efficiently induces spontaneous development of hPSCs to squamous epithelial cysts, which exhibit molecular characteristics of early human amnion. This chapter will further explore such an implantation-like culture system and address the question whether hPSCs can develop into a more sophisticated 3D structure modeling the development of the amniotic sac in human - including its morphogenic dynamics, cell fate partitioning, and the patterning of cell signaling - at implantation and gastrulation.[††]

3.2 Materials and Methods

3.2.1 Fabrication of Basement Membrane Matrix Gel Beds

The Geltrex™ gel bed was generated based on a "sandwich" setup developed in the last chapter. In brief, a 22 × 22 mm^2 glass coverslip ("attaching substrate") was treated with air plasma (Harrick Plasma) for 2 min, before coated with 0.1 mg ml^{-1} poly-(L-lysine) (PLL) solution (Sigma-Aldrich) for 30 min and then 1% glutaraldehyde solution (Electron Microscopy Sciences) for another 30 min. To prepare a "releasing substrate", a pre-cleaned glass slide was activated by air plasma for 2 min, and then coated with 0.1 mg ml^{-1} poly-(L-lysine)-graft-poly-

[††] The results presented in this chapter are adapted from a manuscript that we recently submitted.

(ethylene glycol) (PLL-g-PEG; SuSoS) solution for 1 h. To obtain gel beds with a nominal thickness of 100 μm, 50 μl undiluted Geltrex™ was sandwiched between the attaching and releasing substrate on ice before incubated at 37°C for 30 min. The gel bed, attached to the attaching substrate, was then peeled from the releasing substrate before submerged in DMEM/F12 medium (Thermo Fisher Scientific) and incubated at 37°C overnight before plating cells. To prepare gel beds with a nominal thickness larger than 100 μm, spacers made of polydimethylsiloxane (PDMS; Dow Corning) films were placed between the attaching and releasing substrates when preparing the gel bed sandwich. The PDMS film was generated by spin-coating liquid PDMS (mixed at a 10:1 ratio between PDMS base and curing agent) onto a petri-dish at 500 rpm for 40 s (for generating 150 μm thick PDMS film used in this study) and cured at 70°C for at least 24 h before use.

3.2.2 3D hPSC Culture

In brief, cultured hPSCs were dissociated with Accutase (Sigma-Aldrich) at 37°C for 10 min before suspended in PBS as single cells. hPSCs were centrifuged before resuspended in mTeSR1 containing 10 μM Y27632 (Tocris). hPSCs were plated as single cells at 30,000 cells cm^{-2} onto a thick gel bed with nominal thickness ≥ 100 μm. After 24 h (on day 1), culture medium was replenished with fresh mTeSR1 without Y27632, and 4% (*v*:*v*) Geltrex™ was supplemented in the medium as previously described for 3D culture[63]. Thereafter, mTeSR1 medium was replenished daily, and 4% (*v*:*v*) Geltrex™ was supplemented daily till day 5, unless otherwise noted.

3.2.3 Derivation of Anterior, Posterior, and Late Primitive Streak Cells

Anterior, posterior and late primitive streak (PS) cells, respectively, were derived from hPSCs by adapting previously published protocols[73]. In brief, hPSCs were dissociated as single

cells before plated at 25,000 cm^{-2} in Essential 8™ medium (E8; Thermo Fisher Scientific) containing 10 μM Y27632 onto glass coverslips that were thinly coated with 1% Geltrex™ solution. On day 1, the medium was replenished with fresh E8. On day 2, the medium was replaced with anterior PS, posterior PS, and late PS differentiation medium, respectively, with the following composition: (1) anterior PS differentiation medium: Essential 6™ medium (E6; Thermo Fisher Scientific) + 20 ng ml^{-1} FGF2 (Peprotech) + 10 μM LY294002 (Tocris) +25 ng ml^{-1} BMP4 (R&D Systems) + 50 ng ml^{-1} Activin A (R&D Systems); (2) posterior PS differentiation medium: E6 + 20 ng ml^{-1} FGF2 + 10 μM LY294002 + 50 ng ml^{-1} BMP4; (3) late PS differentiation medium: E6 + 20 ng ml^{-1} FGF2 + 8 μM CHIR99021 (Tocris). All differentiations were induced for 48 h before downstream analyses.

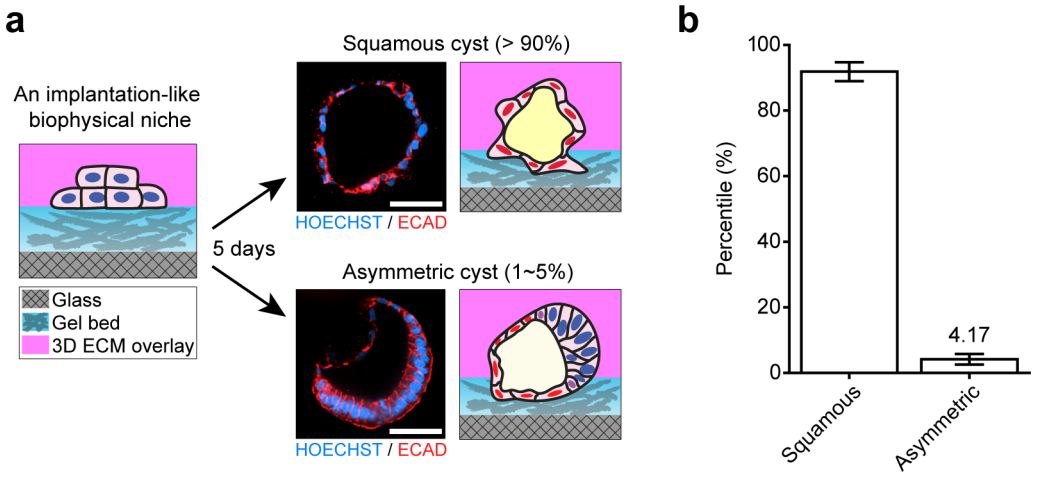

Figure 3-2 A small fraction of self-organized cysts exhibit asymmetric morphology in the biomimetic implantation-like culture. (**a**) Cartoon and confocal micrographs showing a representative squamous cyst (*top*) and a representative asymmetric cyst (*bottom*) stained for ECAD (red) and HOECHST (blue). Scale bar, 50 μm. (**b**) Bar plot showing percentages of squamous and asymmetric cysts in the 3D implantation-like culture. n = 1,728 and 78 for squamous and asymmetric cysts, respectively, out of total 1,924 cysts from 3 biological replicates. Data represent the mean ± s.e.m. The rest of 124 cysts exhibited a columnar morphology. Asymmetric cyst formation was consistently observed in n = 18 independent experiments.

3.3 Results and Discussion

3.3.1 Discovery of hPSC-derived Asymmetric Cysts in the Implantation-like Niche

In Chapter II, we demonstrated that the 3D implantation-like biophysical niche could efficiently and robustly induce amniogenic differentiation of hPSCs. Such amniogenic induction system provides the critical component - amnion - for the development of the amniotic sac. Intriguingly, on day 5, while the majority of cysts formed in the implantation-like niche have adopted squamous epithelial morphology, we consistently observed a small population of asymmetric cysts in this 3D culture system (Figure 3-2), suggesting concomitant development of a structure more complex than the simple squamous amnion cyst.

3.3.2 The Asymmetric Cyst Morphologically Resembles Peri-implantation Human Amniotic Sac

These asymmetric cysts are E-CADHERIN+/β-CATENIN+ (ECAD+/bCAT+) epithelial sacs composed of tall, columnar cells on one side, and flattened, squamous cells on the other (Figure 3-3a). They are also apico-basally polarized with EZRIN+, WGA-enriched apical surfaces facing inward (Figure 3-3b). Intriguingly, these asymmetric cysts are morphologically reminiscent of the amniotic sac in peri-implantation human embryos at Carnegie stages 5a-2, 5b, and 5c, on day past fertilization (d.p.f.) 8, 9, and 12, respectively (Figure 3-3c). Specifically, the squamous-columnar morphological transition in asymmetric cysts mirrors the amnion-epiblast partitioning in human amniotic sac, as revealed by quantitated tissue/region-specific nuclear dimension and epithelial thickness (Figure 3-3d,e). Notably, such asymmetric cyst frequently forms with the squamous side oriented towards the gel bed (Figure 3-4), reminiscent of the development of squamous amnion in proximity to the maternal tissue in implanting human embryos[6] (Figure 3-1).

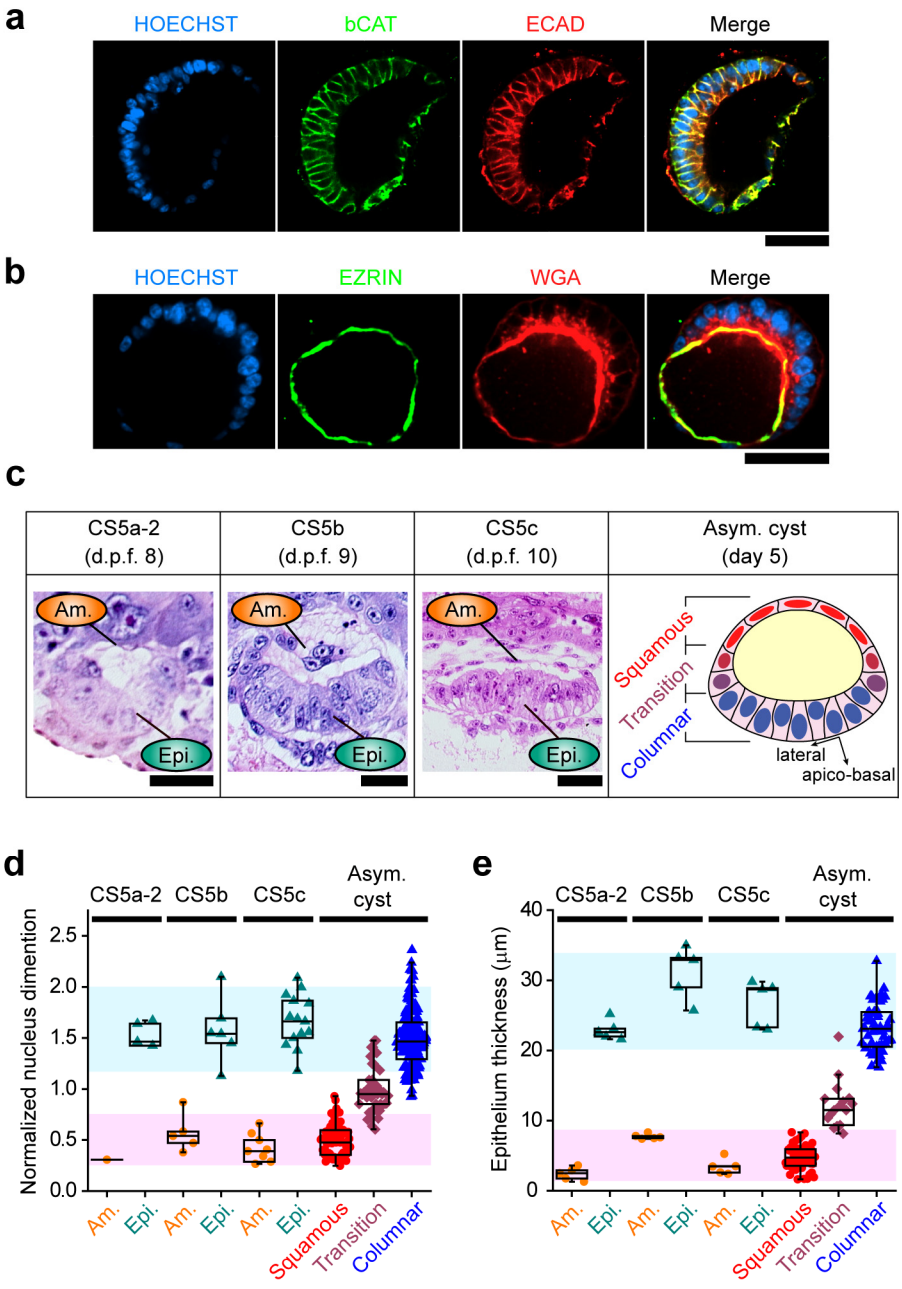

Figure 3-3 The asymmetric cyst morphologically resembles peri-implantation human amniotic sac. (**a&b**) Confocal micrographs showing an ASE on day 5, stained with indicated markers. Scale bars, 50 μm. (**c**) Comparison between the Carnegie stage embryos and the asymmetric cyst (the images are the same as shown in Figure 1-3). Scale bars, 30 μm. (**d&e**) Tissue/region-specific measurements of normalized nucleus dimension (*apico-basal* : *lateral* dimension of nuclei) (**d**) and epithelium thickness (**e**) in human embryos and in the asymmetric cyst as indicated. Box: 25-75%, bar-in-box: median, and whiskers: 1 and 99%.

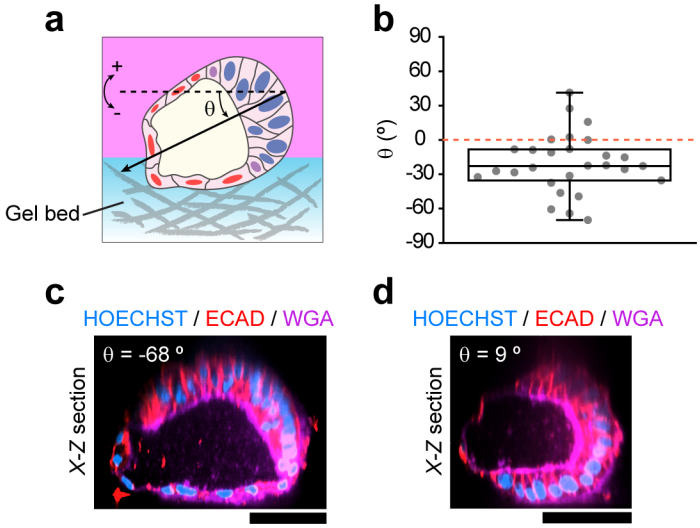

Figure 3-4 The asymmetric cyst frequently form with its squamous side oriented towards the underlying gel bed. (**a**) Schematic showing the definition of cyst orientation angle θ, which is negative when the squamous side of the cyst is closer to the gel bed. (**b**) Quantitated cyst orientation angle θ from $n = 28$ cysts. Box: 25-75%, bar-in-box: median, and whiskers: 1 and 99%. Base line of $\theta = 0°$ is drawn (red dashed line) for reference. (**c&d**) *X-Z* confocal sections showing representative cysts stained for ECAD (red) and WGA (purple), with cyst orientation angle $\theta = -68°$ (**c**) and 9° (**d**), respectively. Scale bars, 50 μm.

3.3.3 The Columnar Pole of the Asymmetric Cyst Resembles the Embryonic Disc

The columnar side of the asymmetric cyst is composed of cells that prominently retain pluripotency marker OCT4 (also known as POU5F1), which is lost in the squamous cells (Figure 3-5a). Co-staining OCT4 with other pluripotency markers - NANOG and SOX2, respectively - confirms that the columnar side of the asymmetric cyst is generally composed of undifferentiated, epiblast-like hPSCs (Figure 3-5b). Such columnar epithelial structure expressing pluripotency markers OCT4, NANOG, and SOX2 resemble the embryonic disc lining at one pole of the amniotic sac in humans and other primates[7,91] (Figure 3-3b).

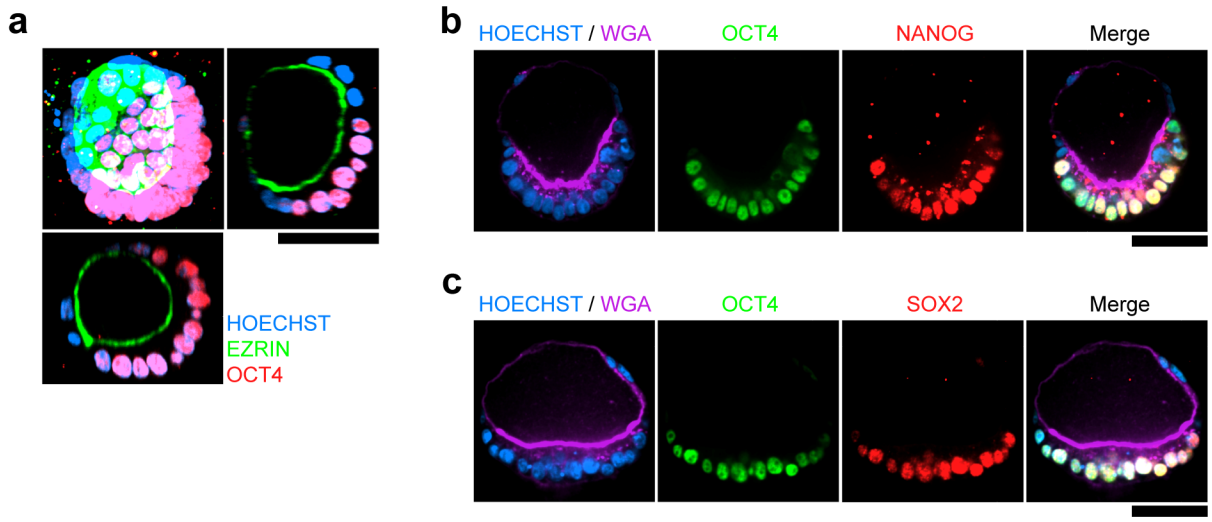

Figure 3-5 The columnar pole of the asymmetric cyst resembles the pluripotent embryonic disc. (**a**) 3D rendering of an asymmetric cyst on day 5, stained with indicated markers, flanked by *X-Z* (bottom) and *Y-Z* (right) views. Scale bar, 50 μm. (**b&c**) Confocal micrographs showing day 5 asymmetric cysts stained for OCT4 (green), NANOG (red), and WGA (purple) (**b**), and OCT4 (green), SOX2 (red), and WGA (purple) (**b**). HOECHST (blue) counterstained the nuclei. The OCT4+/NANOG+ and OCT4+/SOX2+ embryonic disc-like patterning resembles *in vivo* amniotic sac in Carnegie stage 5 human embryos as well as post-implantation primate embryos[91]. Scale bars, 50 μm.

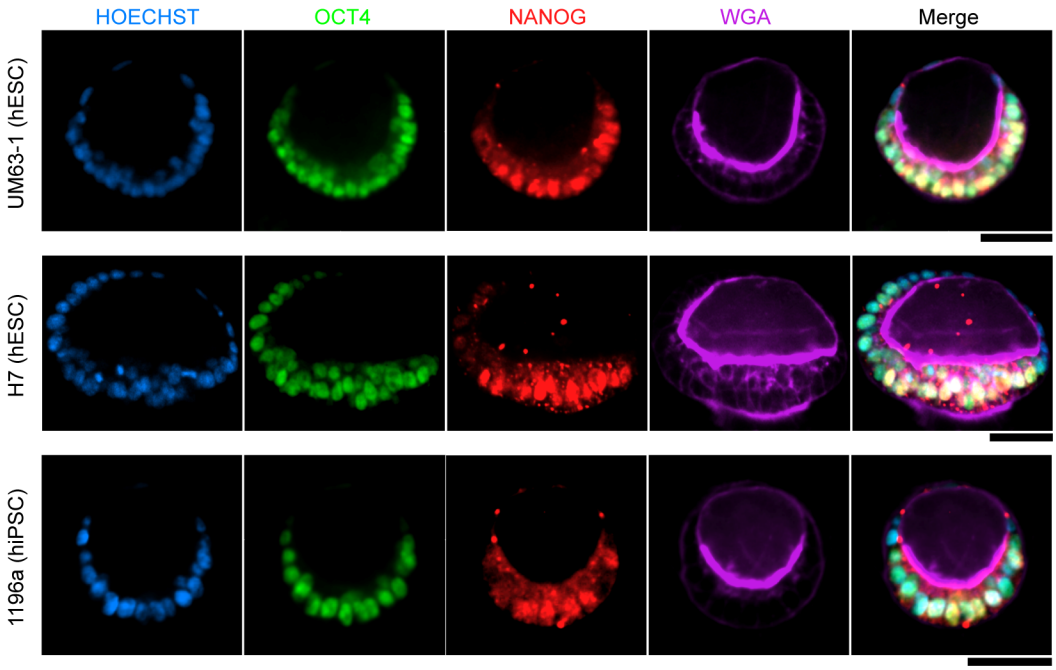

Figure 3-6 Self-organized asymmetric cysts can be successfully generated using multiple

hPSC lines. Confocal micrographs showing day 5 asymmetric cysts derived from two hESC lines (UM63-1, *top*; H7, *middle*), and one hiPSC line (1196a, *bottom*) as indicated. The cysts were stained for OCT4 (green), NANOG (red) and WGA (purple). HOECHST counterstains the nuclei. Scale bars, 50 μm.

3.3.4 The Squamous Pole of the Asymmetric Cyst Resembles the Amnion

The squamous side of the asymmetric cyst, in contrast, is composed of a flattened, differentiated epithelium that we recently identified as early human amnion-like tissue[92]. Indeed, TFAP2A and GATA3 - two markers for hPSC-derived early human amnion[92] - are expressed only in squamous cells (Figure 3-7a,b). qRT-PCR analysis shows high mRNA levels for *TFAP2A* and *GATA3* in week 16-17 human fetal amniotic epithelium, further supporting the contention that TFAP2A+/GATA3+ squamous cells molecularly resemble early human amniotic cells (Figure 3-7c). Together, these results show that hPSCs can spontaneously self-organize to form asymmetric epithelial cysts that recapitulate the peri-implantation amniotic sac in human, featuring an amniotic cavity lined by bi-polar amnion-epiblast patterning. Such hPSC-derived asymmetric cysts are thus termed amniotic sac embryoids (ASEs) henceforth (Figure 3-7d).

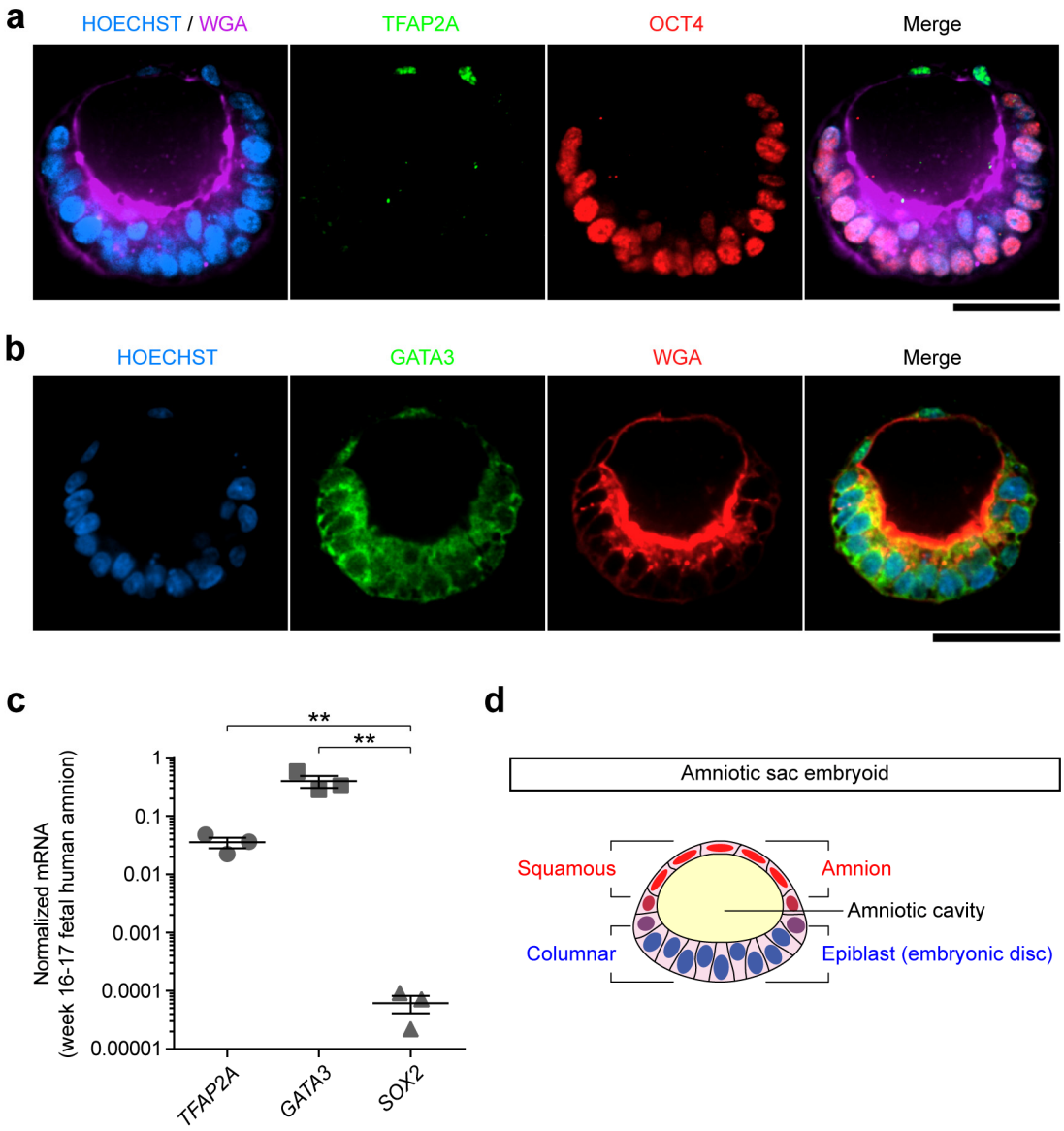

Figure 3-7 The squamous pole of the asymmetric cyst mimics the amnion. (**a**) Confocal micrographs showing an asymmetric cyst on day 5, stained with indicated markers. Scale bar, 50 µm. (**b**) Confocal micrographs showing a day 5 asymmetric cyst stained for GATA3 (green) and WGA (red), showing nuclear staining of GATA3 exclusively in the squamous cells. Scale bar, 50 µm. (**c**) qRT-PCR analysis of *TFAP2A*, *GATA3*, and *SOX2* in week 16-17 human fetal amniotic epithelial cells. Data were normalized against *GAPDH* and plotted as the mean ± s.e.m. with $n = 3$ biological replicates. *P*-values were calculated using paired, two-sided Student's *t*-test. **: $P < 0.01$. (**d**) Schematic of the asymmetric cyst. The squamous side of the cyst, which expresses early human amnion markers, resembles the amnion lining the roof of the peri-implantation human amniotic sac. The columnar side of the cyst, which expresses pluripotency markers, recapitulates the embryonic disc composed of undifferentiated epiblast cells lining the floor of the peri-implantation human amniotic sac. The cavity enclosed

by the cyst thus resembles the amniotic cavity. Together, the asymmetric cyst models the morphology and cell-fate patterning of the amniotic sac in peri-implantation human embryo. The asymmetric cyst is thus termed the amniotic sac embryoid (ASE) henceforth.

3.3.5 Amniotic Sac Embryoid Mimics the Developmental Trajectory of Human Amniotic Sac

We next examined the time course of ASE development. On day 2, most hPSCs form cysts that express both OCT4 and NANOG (Figure 3-8a). At this point, some cysts present an eccentrically positioned lumenal cavity; this represents the earliest stage of ASE development and resembles Carnegie stage 5a-1 (d.p.f. 7) embryo featuring a pro-amniotic cavity surrounded by polarized epiblast (Figure 3-8b). On day 3, two types of ASEs are present in the culture: one (type A, 20/46) exhibits slight loss of NANOG, but not OCT4, at the flattened amniotic pole, while the other (type B, 26/46) shows significant loss of both NANOG and OCT4, and a more flattened amniotic pole (Figure 3-8a). Together, day 3 ASEs exhibit the initiation and establishment of amnion-epiblast patterning *in vitro* and appear to recapitulate Carnegie stage 5a-2 (d.p.f. 8) embryo (Figure 3-8b). Notably, the initiation of squamous, amnion-like tissue development in the ASE appears to be a continuous columnar-to-squamous morphological transition occurring at the amniotic pole, and no transient opening was observed at the amniogenic site, which challenges the previous dogma proposed by Luckett[6]. From day 4-5, ASEs maintain the amnion-epiblast patterning (Figure 3-8a) and resemble the growing amniotic sac from Carnegie stage 5a-2 to 5b (d.p.f. 9) and 5c (d.p.f. 12) (Figure 3-8b). The temporal trajectory of ASE development thus closely mimics the morphogenesis and cell-fate patterning during peri-implantation human amniotic sac development (Figure 3-8c).

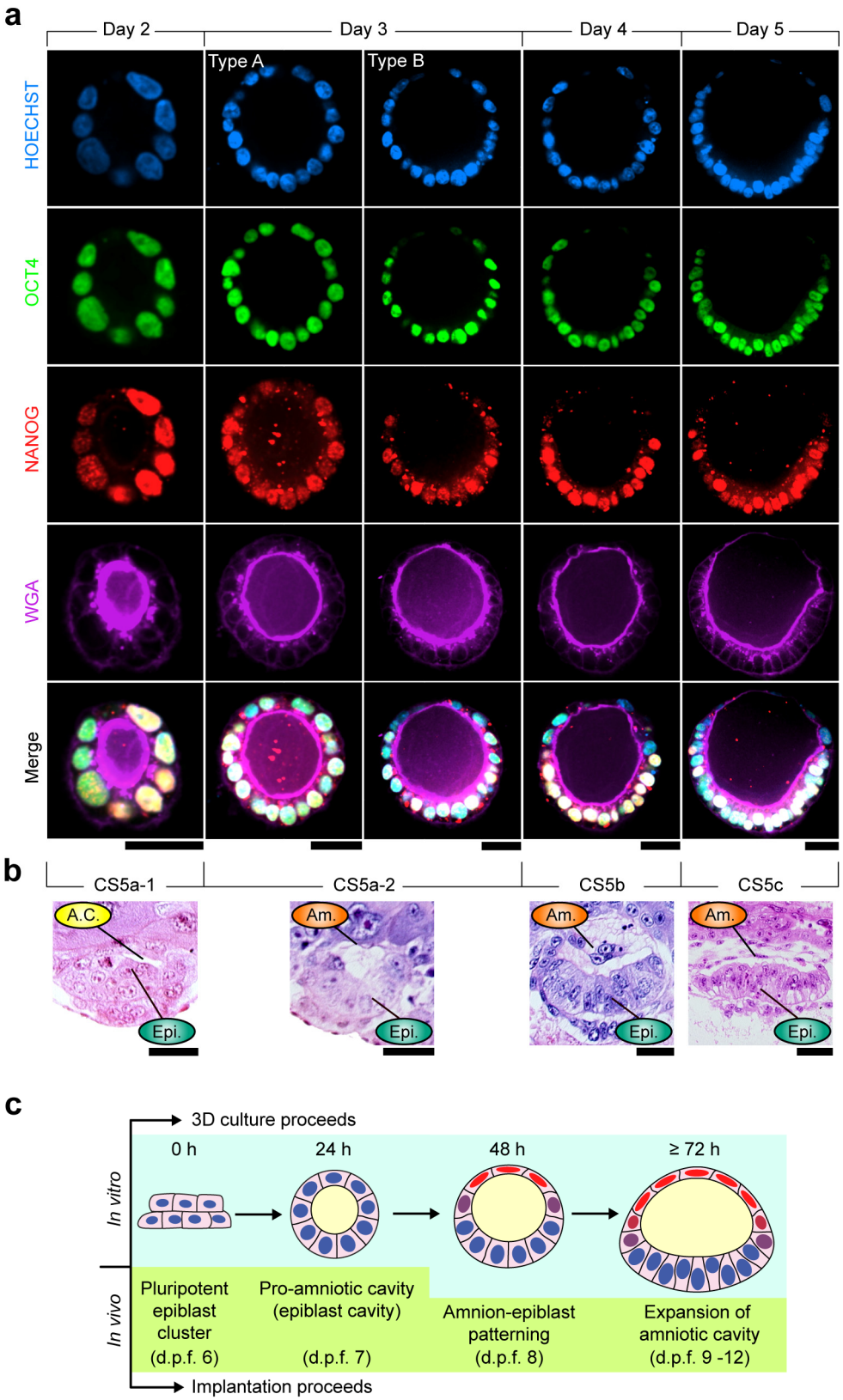
a
Day 2
Day 3
Day 4
Day 5
Type A
Type B
HOECHST
OCT4
NANOG
WGA
Merge
b
CS5a-1
CS5a-2
CS5b
CS5c
A.C.
Am.
Epi.
c
3D culture proceeds
0 h
24 h
48 h
≥ 72 h
In vitro
In vivo
Pluripotent epiblast cluster (d.p.f. 6)
Pro-amniotic cavity (epiblast cavity) (d.p.f. 7)
Amnion-epiblast patterning (d.p.f. 8)
Expansion of amniotic cavity (d.p.f. 9 -12)
Implantation proceeds

Figure 3-8 Time-dependent trajectory of ASE development *in vitro* mimics peri-implantation human amniotic sac development *in vivo*. (**a**) Confocal micrographs showing ASEs from day 2-5 stained for HOECHST (blue), OCT4 (green), NANOG (red), and WGA (purple). Since nuclear staining of NANOG typically exhibits heterogeneous intensity in cultured hPSCs, only cells in which nuclear staining of NANOG is completely absent were considered to have lost NANOG expression. (**b**) Carnegie stage (CS) 5a-1[3], 5a-2[4], 5b[3], and 5c[5] human embryos at d.p.f. 7, 8, 9, and 12, respective. Sections are obtained from the Virtual Human Embryo Project. The sections of CS5a-2, CS5b, and CS5c embryos are the same as shown in Figure 1-3. A.C.: pro-amniotic cavity; Am.: (prospective) amnion; Epi.: epiblast. Scale bars, 30 μm. (**c**) Cartoon showing the time course of ASE development *in vitro*, compared with human amniotic sac development *in vivo*.

3.3.6 ASEs Exhibit Phenotypic and Molecular Features Resembling Primitive Streak Development

Interestingly, on day 5, some ASEs (96/304) exhibit an additional phenotype, with single cells focally emigrating from, and only from, the embryonic disc lining the columnar pole (Figure 3-9a). In addition, epithelial structure and the expression of pluripotency markers OCT4 and NANOG are disrupted around the cell egression site (Figure 3-9a). It is important to note that these locally emerging cells morphologically resemble primitive streak (PS) initiation in Carnegie stage 6 embryos at early gastrulation[93] (Figure 3-9b).

To molecularly assess such gastrulation-mimicking development of ASEs, we examined the expression of BRACHYURY (BRA), a transcription factor associated with PS development[94], in day 5 ASEs. By assessing and comparing the spatial distribution of BRA staining in different ASEs, we identified three distinct patterns of BRA expression based on which we define three consecutive stages of ASE development (Figure 3-10). Stage I (59/173) depicts ASEs that exhibit no cell dissemination and no prominent nuclear BRA in the embryonic disc. Stage II (56/173) defines ASEs that express nuclear BRA in the embryonic disc, but without cell emigration. Stage III (58/173) describes ASEs that show single cells emigrating from a BRA+,

PS-like region flanked by the embryonic disc (Figure 3-10). Immunofluorescence analysis of OCT4 confirms a stage-wise loss of pluripotency that parallelizes the formation of the BRA+, PS-like region (Figure 3-10). Together, these findings implicate that Stage I - III might represent a progressive developmental process wherein PS initiates within the epiblast at the loss of pluripotency, which eventually results in the emergence of mesenchymal-looking cells emigrating from the embryonic disc.

In order to further dissect the molecular distinction between Stage II and III, other than their phenotypic discrepancies, we examined the expression of CDX2 - a marker for posterior and late PS[73] (Figure 3-11a) - in day 5 ASEs. Interestingly, CDX2 is expressed in the PS-like region in

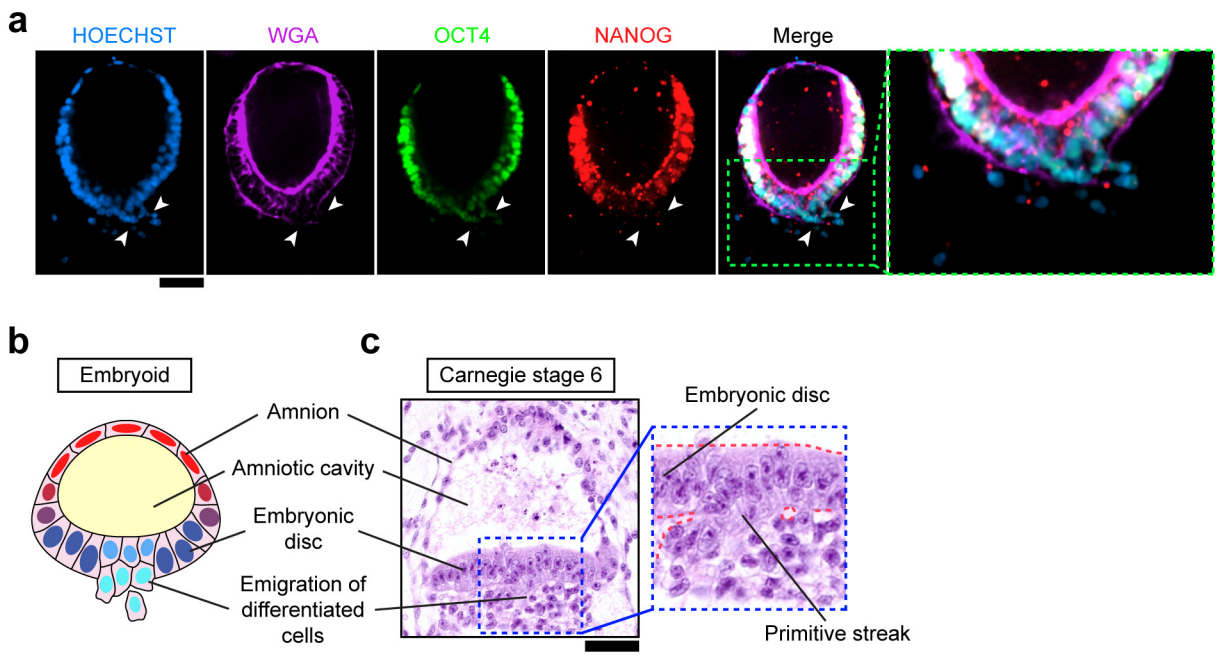

Figure 3-9 ASEs exhibit phenotype resembling primitive streak (PS) development. (**a**) Confocal micrographs showing single cells emigrating from the embryonic disc lining the columnar pole of an ASE on day 5, stained with HOECHST (blue), WGA (purple), OCT4 (green), and NANOG (red). (**b**) Cartoon showing the ASE with amnion, embryonic disc, amniotic cavity, and PS-like phenotype. ASEs with PS-like phenotype were consistently observed on day 5. n = 18 independent experiments. (**c**) Carnegie stage 6 human embryo section showing the PS. Scale bars, 50 µm.

stage III, but not stage II, ASEs (Figure 3-11b). Instead, CDX2 is only expressed at the amniotic pole of stage II ASEs (Figure 3-11b), consistent with our finding in Chapter 2 that CDX2 ss an early human amnion marker[92]. We also tested whether FOXA2 - a marker for anterior PS and endoderm[73,95] (Figure 3-11c) - was expressed in day 5 ASEs. However, FOXA2 expression was found absent in all ASEs (Figure 3-11d). Together, the molecular profile of day 5 ASEs suggests that stage I ASEs mimic peri-implantation, pre-PS amniotic sac, stage II ASEs resemble early PS organization, and stage III ASEs model posterior PS patterning.

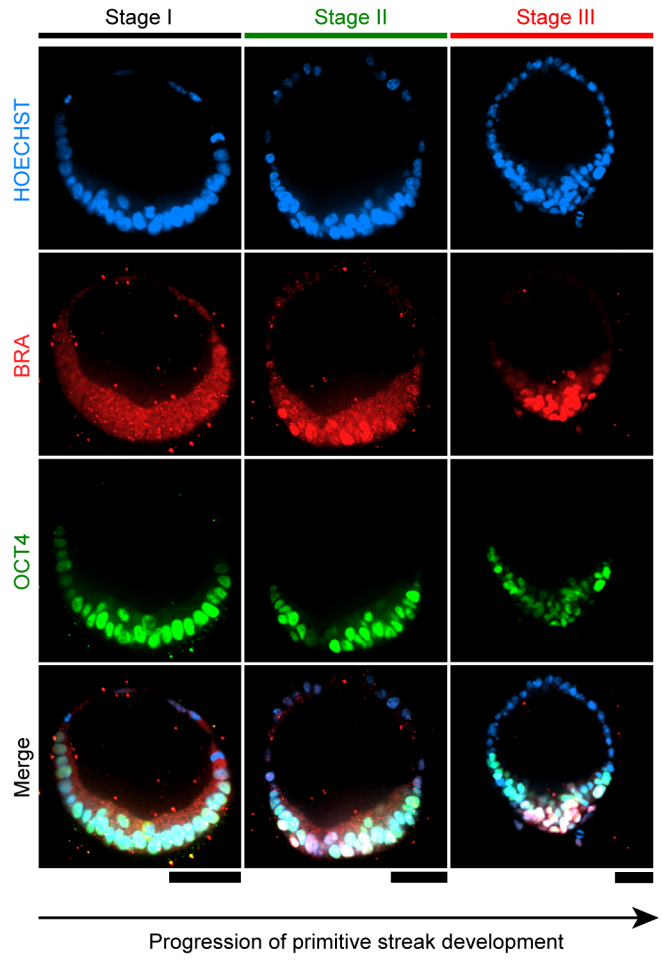

Figure 3-10 ASEs exhibit molecular signature of progressive PS development. Confocal micrographs showing ASEs with different spatial patterning of BRACHYURY (BRA; red), and OCT4 (green) on day 5. Scale bar, 50 µm.

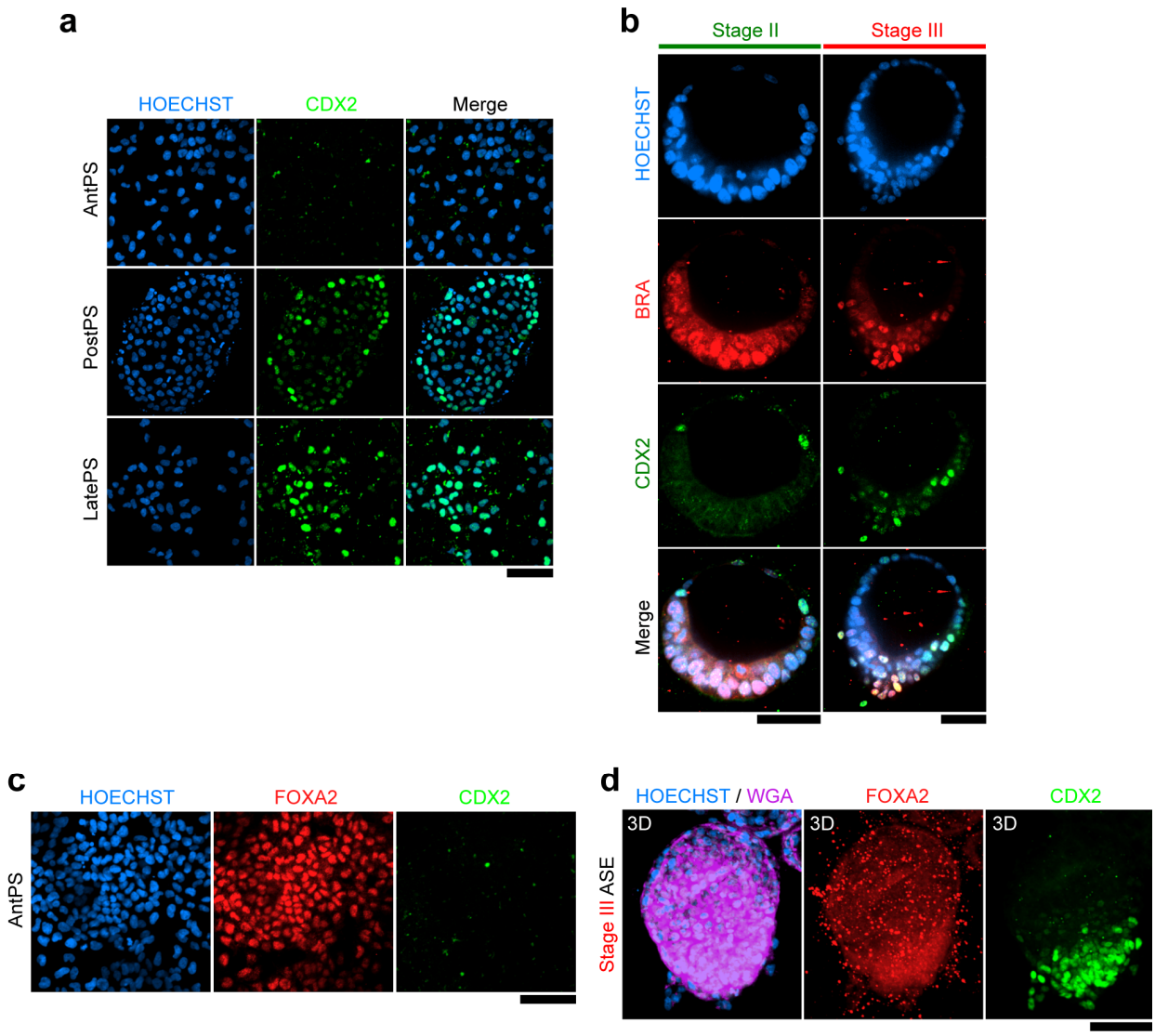

Figure 3-11 ASEs resemble the posterior PS development. (**a**) Confocal micrographs showing anterior primitive streak (AntPS), posterior primitive streak (PostPS), and late primitive streak (LatePS) cells derived from hPSCs in 2D culture, stained for CDX2 (green). HOECHST (blue) counterstains the nuclei. (**b**) Confocal micrographs showing ASEs with different spatial patterning of BRACHYURY (BRA; red), and CDX2 (green) on day 5. (**c**) Confocal micrographs showing AntPS cells, stained for FOXA2 (red), and CDX2 (green). HOECHST (blue) counterstains the nuclei. (**d**) 3D rendering of a stage III ASE, stained for WGA (purple), FOXA2 (red), and CDX2 (green). HOECHST (blue) counterstains the nuclei. Scale bars in **a**, **c**, and **d**, 100 μm; in **b**, 50 μm.

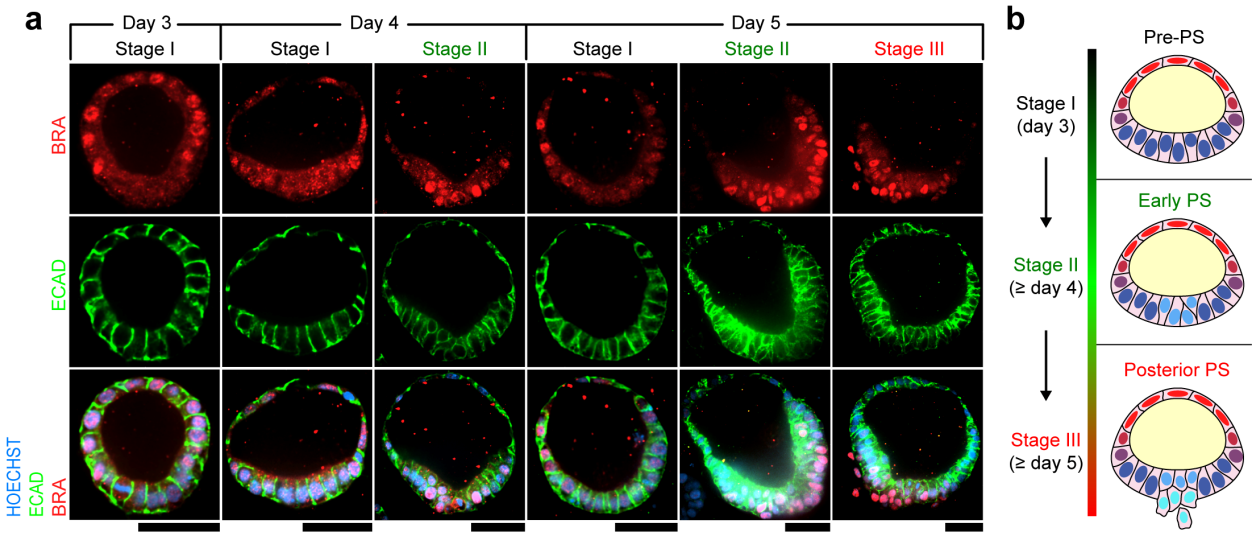

Figure 3-12 The time-course of ASE development recapitulates the sequential order of posterior PS development. (**a**) Confocal micrographs showing time-dependent, stage-wise spatial patterning of BRA (red) and ECAD (green) in ASEs from day 3-5. Scale bars, 50 µm. (**b**) Cartoon summarizing the three chronological stages of ASE development that resembles PS progression from pre-PS stage to early and then posterior PS stages.

We next traced the dynamic BRA expression during ASE development. On day 3, only stage I ASEs are observed, with nuclear BRA evident only at the flattened amniotic side (Figure 3-12a), consistent with our finding in Chapter II that BRA is an early human amnion marker, as well as another recent finding that BRA is expressed in nascent amnion in monkey embryos[19]. By day 4, nuclear BRA emerges in the embryonic disc in some, but not all (13/38), ASEs, suggesting asynchronous advances to stage II and PS initiation (Figure 3-12a). Stage III ASEs with BRA+, single emigrating cells are only evident on day 5 (Figure 3-12b). Notably, ECAD is concurrently lost in the BRA+, PS-like region of stages II and III ASEs (Figure 3-12a), consistent with a canonical EMT during PS development. Another EMT marker, SNAIL, was also expressed in cells emigrating from Stage III ASEs (data now shown). Together, these results show that ASEs can develop beyond the peri-implantation, pre-PS stage to model a progressive, posteriorizing PS development *in vitro* with *in vivo*-like sequential order (Figure 3-12b).

3.3.7 Spontaneous Patterning of BMP-SMAD Signaling in the Development of ASEs

During early embryogenesis, BMP-SMAD signaling plays a pivotal role in tissue specification and morphogenesis, as loss of Bmp2 or Smad5 results in defects in both amniotic and embryonic patterning in mice[96,97]. Recently, Sasaki *et al*. also reported the finding of BMP signaling patterning in amnion versus epiblast in post-implantation monkey embryos[19]. Thus, we next examined BMP-SMAD signaling during ASE development. Indeed, immunofluorescence analysis of phosphorylated SMAD1/5 (pSMAD1/5) - a downstream target and activator of BMP-SMAD signaling - shows prominent nuclear pSMAD1/5 only at the amniotic pole of peri-implantation (stage I) ASEs (Figure 3-13). Stage-dependent patterning of pSMAD1/5 was further observed (Figure 3-14), mirroring the progressive BRA expression patterning during ASE development (Figure 3-10, 3-12). Notably, nuclear pSMAD1/5 emerges in the embryonic disc prior to CDX2 (Figure 3-14), consistent with the recent finding that BMP-SMAD signaling activation precedes CDX2-mediated posterior PS development[95]. Importantly, BMP-SMAD signaling in the ASE is activated autonomously, as no exogenous BMP is supplemented to the culture. Together, these results provide direct evidence for autonomous, stage-dependent patterning of BMP-SMAD signaling during ASE development *in vitro* (Figure 3-15).

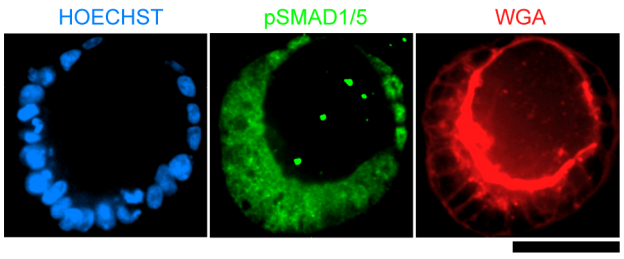

Figure 3-13 Spontaneous patterning of BMP-SMAD signaling in pre-PS ASE. Confocal micrographs showing a peri-implantation, pre-PS ASE on day 5 stained with pSMAD1/5 (green), WGA (red), and HOECHST (blue). Scale bar, 50 µm.

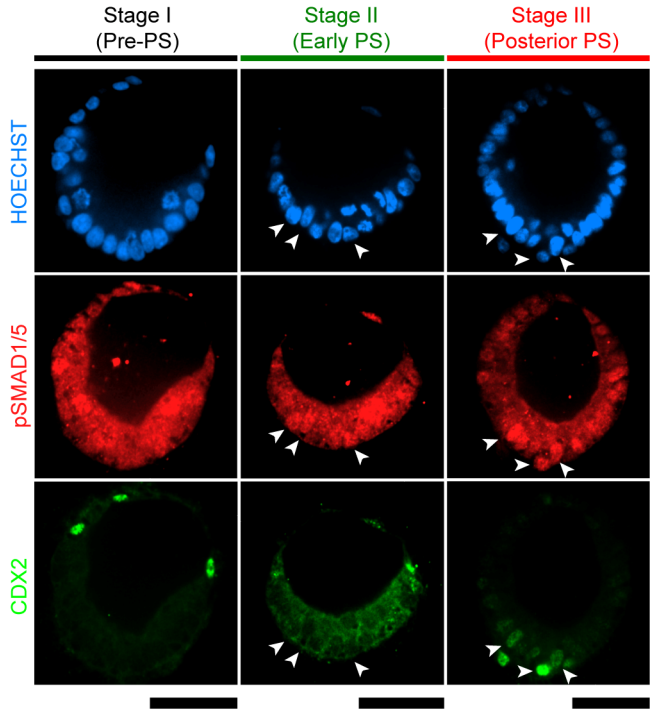

Figure 3-14 Evolution of BMP-SMAD signaling patterning at PS development of the ASE. Confocal micrographs showing stage-wise spatial patterning of pSMAD1/5 (red) and CDX2 (green) in ASEs on day 5. White arrow heads indicate pSMAD1/5+ cells in the embryonic disc of ASEs. Scale bar, 50 µm.

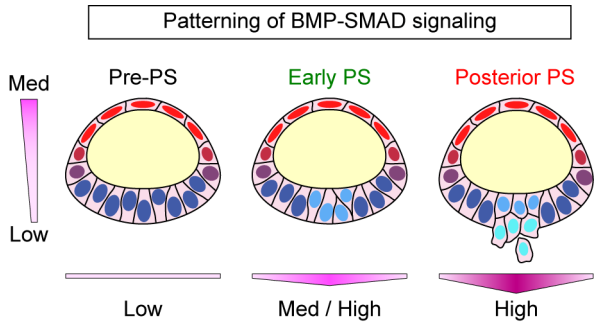

Figure 3-15 Cartoon summarizing spatial patterning of BMP-SMAD signaling in the ASE along its amnion-epiblast axis as well as along the medial-lateral axis of the embryonic disc. Color scale represents the intensity of BMP-SMAD signaling ranging from low to medium and high as indicated.

3.3.8 Discussion

Findings reported in this chapter demonstrate that hPSCs can self-organized *in vitro* and develop into a spontaneously patterned cystic structure modeling human amniotic sac development at implantation and early gastrulation. In particular, the *in vitro* model - ASE - could recapitulate the amnion-epiblast patterning and posterior PS development. However, the development of anterior PS was not observed in ASEs. Elongation of PS, which is a critical step for establishing the body axis, was not observed either. These results indicate that the current ASE can only partially model the fully complexity of human amniotic sac development. In addition, the current culture system generates ASEs only with low efficiency, which is a potential limiting factor for broader application of this *in vitro* model system. Development of more efficient and better controlled induction system for ASEs, for example, by providing an asymmetrically structured source of exogenous BMP ligand for inducing amniogenesis in only part of the cyst, would be of great interest in future studies.

So far, the canonical view in human embryology regards the amniotic sac development as a three-step process[1]: (1) epiblast polarization results in the formation of a transient cavity within the epiblast; (2) thinning of the roof of this cavity quickly opens the cavity and forms a so-called tropho-epiblastic cavity, the roof of which is formed by cytotrophoblasts and the bottom formed by the epiblast disc; (3) proliferation, differentiation, and migration of epiblast cells at the margins of the epiblast disc results in its upfolding, eventually enclosing a permanent cavity ("the amniotic cavity") with the roof made of squamous cells destined to become the amnion. However, this paradigm is entirely drawn from interpretations of images of sectioned human and primate embryos, and different observations have also been reported by others in monkey embryos[7,18].

Strikingly, results reported here clearly demonstrate that the amniotic sac develops as a continuous epithelial cyst. That is, a cavity forms in cultured epiblast-like hPSCs, and no partially opened cyst is ever observed as the cyst expands and evolves to become the amniotic sac. During its expansion, one side of the cyst undergoes a distinct morphogenic cytodifferentiation and adopts a thin, squamous epithelial morphology; these squamous cells express markers of early human amnion. The other side of the cyst organizes into a thick, columnar epithelial disc that retains pluripotency markers. The single luminal cavity in the asymmetric cyst is continuously maintained throughout such development. Therefore, our findings significantly revise, if not refute, the current theory of the human amniotic sac development, and will open doors for future fundamental investigations of early human embryogenesis at implantation and gastrulation.

3.4 Conclusions

This chapter shows that hPSCs can self-organize to model human amniotic sac development at implantation and beyond in a bio-inspired 3D culture system. Importantly, although long-established textbook dogma advocates that human amniotic sac development involves an intermediate step in which the epiblast cyst is opened to the trophoblast, forming a tropho-epiblastic cavity (d.p.f. 8)[1,6], data in this chapter suggest otherwise - human amniotic sac develops as a continuous, intact epithelial cyst that constantly encloses the (pro-)amniotic cavity throughout implantation. Intriguingly, the ASE develops in the absence of other extraembryonic tissues and autonomously activates a patterned BMP-SMAD signaling, suggesting an unforeseen self-organizing capacity of pluripotent epiblast during human amniotic sac development. Besides new understandings of human development at implantation and early gastrulation, our findings

also unveil a new developmental potential and application of hPSCs. This work provides a new model - the ASE - for investigating the fundamentals of early human embryology, complementing scarce *in vivo* studies. It is envision that the ASE can also assist in studying human pregnancy and embryo toxicology, thereby advancing the field of human reproductive medicine.[‡‡]

[‡‡] Research presented in this chapter has received technical assistance from Dr. Kenichiro Taniguchi (cell culture), Mr. Ryan F. Townshend (qRT-PCR), and Dr. Toshio Miki (RNA samples isolated from fetal human amniotic epithelial cells). I would also like to thank Dr. K. Sue O'Shea, Dr. Sundeep Kalantry, Dr. William Shawlot, Dr. Allen P. Liu, Dr. Deborah L. Gumucio, and Dr. Jianping Fu for their comments on the research presented in this chapter.

CHAPTER IV

Development of a Micro-engineered Human Amniotic Tissue Array for Reproductive Medicine

4.1 Introduction

Development of amnion is a critical step for early human embryogenesis. It patterns the rudimentary morphology of human embryos and provides a paracrine source of BMP ligands, which could serve as important embryonic induction signals for the primordial germ cells[19], epidermis[98], and potentially the primitive streak[94]. Abnormalities in amnion development or formation could result in pregnancy failure or complications such as oligohydramnios[99], premature rupture of amniotic membrane[100,101], or amniotic band syndrome[102]. In Chapter II, I reported an *in vitro* culture system that can efficiently generate early human amnion-like tissues. However, such a system lacked the control over the size and location of hPSC-amnion cysts, and the gel bed has limited compatibility with large-scale fabrication, thereby limiting the use of such system for clinically relevant translational applications where high-content screening is preferred. Development of an *in vitro* high-throughput screening platform capable of assessing the effect of a wide range of genetic mutations, pharmaceutical products, or environmental toxicants/hazards on early human amnion development could have significant implications for reproductive medicine and public health (Figure 4-1).

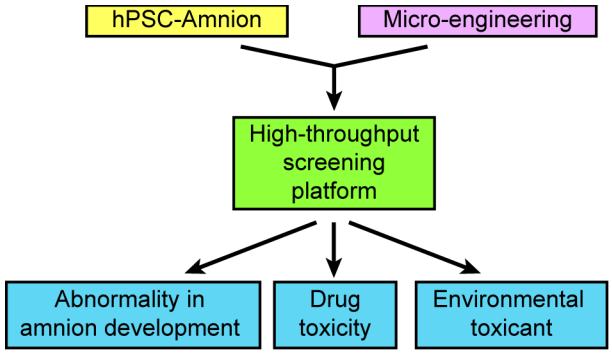

Figure 4-1 Concept of a micro-engineered human amniotic tissue array as a high-throughput screening platform for reproductive medicine.

Conventionally, pharmaceutical industry relies on massively produced high-throughput screening systems for evaluating the efficacy of products on cultured cells or other biological samples[103]. Typically, those high-throughput screening platforms come with an array format due to its compatibility with large data yield and automatable data acquisition and analysis process. Most microarray-based high-throughput screening systems are commonly fabricated *via* mass manufacturing techniques, such as electrohydrodynamic jet printing[104] or UV-mediated photo-patterning[105], on rigid substrates such as glass; while the robotic deposition of soft hydrogel materials[106] is currently more limited to pioneering lab researches. However, the method established previously in Chapter II for inducing amniogenesis from hPSCs is not compatible with rigid substrates, posing a challenge for versatile generation of high-throughput screening platforms for assessing early human amnion development.

In this chapter, therefore, our first goal is to further explore the mechano-sensitivity of hPSC-amnion development based on findings made in Chapter II. To accomplish this, we will leverage the property of integrative mechanotransduction, which will be elaborated in Section 4.3, and develop alternative strategies that can induce amniogenesis on rigid substrates that are compatible with standard, readily accessible microarray fabrication techniques. We will then

combine the new amniogenic method and a micro-engineered ECM array to demonstrate the proof of concept for a human amniotic tissue array platform that could be useful for high-throughput screening for regenerative medicine in the future.

4.2 Materials and Methods

4.2.1 3D hPSC Amniogenesis Assay

In brief, cultured hPSCs were dissociated with Accutase (Sigma-Aldrich) at 37°C for 10 min before suspended in PBS as single cells. hPSCs were centrifuged before being resuspended in mTeSR1 containing 10 μM Y27632 (Tocris). hPSCs were plated as single cells at 30,000, 20,000, 10,000, or 5,000 cells cm^{-2} onto a glass coverslip thinly coated with 1% Geltrex™ at room temperature for 1 h.

In some tests conducted on glass coverslip, culture medium was replenished at 24 h (on day 1) after cell plating with fresh mTeSR1 without Y27632, and 4% (*v*:*v*) Geltrex™ was supplemented in the medium as previously described for 3D culture. Thereafter, mTeSR1 medium was replenished daily, and 4% (*v*:*v*) Geltrex™ was supplemented daily till day 4, unless otherwise noted.

In other tests conducted on glass coverslip, the 3D ECM overlay was applied at 2 h after plating, and the culture medium was changed to fresh mTeSR1 containing 10 μM Y27632 and 4% (*v*:*v*) Geltrex™. At 24 h after plating, culture medium was replenished with mTeSR1 without Y27632, and 4% (*v*:*v*) Geltrex™ was supplemented in the medium. Thereafter, mTeSR1 medium was replenished daily, and 4% (*v*:*v*) Geltrex™ was supplemented daily till day 4.

In tests conducted on the micro-engineered ECM array, cells were plated at 40,000 cm^{-2} onto the micro-engineered ECM array in mTeSR1 containing 10 μM Y27632. The 3D ECM

overlay was applied 2 h after plating and the culture medium was changed to mTeSR1 containing 10 μM Y27632 and 4% (*v*:*v*) Geltrex™. At 24 h, culture medium was replenished with mTeSR1 without Y27632, and 4% (*v*:*v*) Geltrex™ was supplemented in the medium. Thereafter, mTeSR1 medium was replenished daily, and 4% (*v*:*v*) Geltrex™ was supplemented daily till day 3.

4.2.2 Fabrication of Micro-engineered ECM Arrays

The micro-engineered ECM array containing basement membrane matrix protein (Geltrex™) was generated using a standard micro-contact printing protocol as described elsewhere before[107]. In brief, to prepare the substrate for the ECM array, a glass coverslip was spin-coated with a thin layer of PDMS (base:curing agent ratio as 10:1) at 2,000 rpm for 40 s before being cured at 70°C for overnight. PDMS stamps containing regularly patterned circular protrusive features of area 3,600 μm^2 (diameter ~ 67 μm) were generated using standard soft lithography as described elsewhere before[71]. To "ink" the stamp with ECM proteins, 1% Geltrex™ solution was deposited onto the surface of the stamp carrying the desired patterns before being incubated in 4°C for overnight. The PDMS-coated coverslip was treated by UV Ozone for 7 min before being printed with the Geltrex™-coated stamps. The protein transfer was accomplished upon peeling off the stamp after its conformal contact with the coverslip. The printed ECM array substrate was sterilized with 70% ethanol for 1 min before being blocked for 30 min using 0.2% (*w*:*v*) Pluronic F127 to prevent cell attachment on un-printed area. The ECM array substrate was then rinsed by PBS for three times before use.

4.3 An Integrative Mechanotransduction Pathway for hPSC Amniogenesis

Cells are active "sensors" of not only their biochemical environment but also the biomechanical niche surrounding them[42,108-110]. Through past years, an important concept that I named "integrative mechanotransduction" has emerged as a general property of cells that are sensitive to microenvironmental mechanical cues[24]. Mounting experimental data obtained from various types of cells, including hPSCs[24], suggest that a wide range of upstream mechanical signals, such as matrix rigidity[111-113], substrate topography[114-116], cell/colony area and spreading[89,117,118], cell geometry/shape and local curvature[119-122], cell contractility[70], *etc.*, could eventually induce similar differentiation phenotypes from a certain cell type (Figure 4-2), *via* a shared core signaling transduction components[24], including actin cytoskeleton, SMAD, and YAP/TAZ, *etc.*, that integrates those upstream mechanical signals to elicit common downstream differentiation inductions. Herein, as an example case that supports the notion of the integrative mechanotransduction, we will first briefly review classic findings in past decade on the mechanobiology of human mesenchymal stem cells (hMSCs)[24]. We will then set to examine

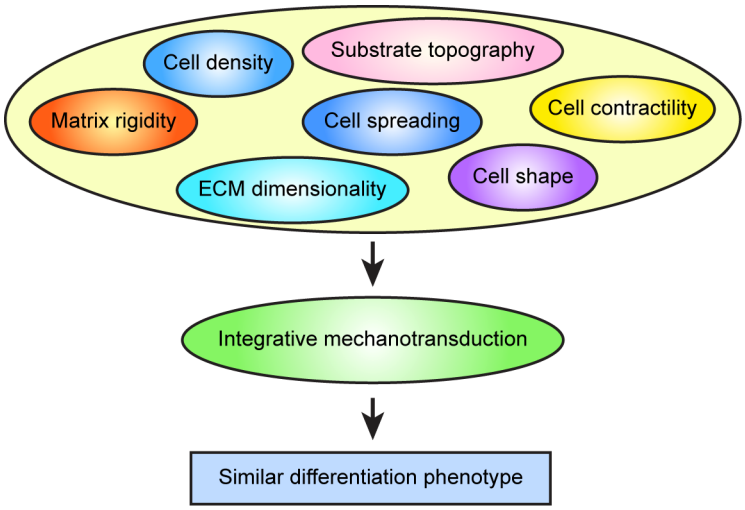

Figure 4-2 Concept of integrative mechanotransduction, which integrates multiple upstream mechanical signals to elicit similar differentiation of stem cells.

whether the amniogenesis by hPSCs can be elicited by other mechanical factors in an integrative mechanotransductive manner. Such knowledge could help develop new, versatile amniogenic methods that are compatible with a larger spectrum of substrates and bio-manufacturing systems.

4.3.1 Integrative Mechanotransduction: a Lesson from hMSCs

For over a decade, the mechanobiology and mechanotransduction of hMSCs have been extensively studied and have provided extraordinary examples and paradigms for understanding the control of stem cell fate *via* regulating extracellular insoluble biophysical signals[24,123].

As a measurement of the resistance to deformation, mechanical stiffness of the embryo varies in space and over time during development, generating a distinct pattern of tissue stiffness throughout the human body[124,125]. The interesting idea of using tissue-mimicking matrix stiffness to regulate stem cell differentiation can be originated back to the seminal work by Engler *et al.*, which demonstrated that brain-like soft polyacrylamide (PA) hydrogel substrates enhanced neurogenesis of human mesenchymal stem cells (hMSCs), while PA substrates with muscle- and bone-mimicking stiffness promoted cardiogenesis and osteogenesis, respectively[124]. Using microfabricated elastomeric polydimethylsiloxane (PDMS) micropost arrays with different post spring constants - a physical analogy of varying substrate stiffness, Fu *et al.* also demonstrated that substrate stiffness could serve as an extracellular switch to direct hMSC differentiation between osteogenesis and adipogenesis[70]. In recent studies, dynamic substrate stiffening was shown to either switch hMSCs from adipogenesis to osteogenesis[126] or promote their cardiogenic differentiation[127].

In addition, researchers have also developed different bioengineering strategies to modulate micro/nanoscale topography of cellular microenvironment, in order to control the lineage differentiation of hMSCs. A notable study by Dalby *et al.* showed that synthetic substrates with

disordered nanoscale topographical features enhanced osteogenesis of hMSCs[128]. Substrates composed of nanotubes were also applied for hMSC culture, with results demonstrating that hMSC osteogenesis was promoted on nanotubes with greater diameters[129].

Cell shape is another important cell property dynamically regulated during embryonic development and has been leveraged to regulate stem cell fate determination as well. Indeed, numerous studies have supported cell shape as a potent biophysical regulator of hMSC fate and function. In one of the earliest studies, McBeath *et al.* applied micro-contact printing to coat flat PDMS surfaces with distinct patterns of adhesive ECM islands and reported that single hMSCs confined to small ECM islands selectively underwent adipogenesis, whereas single hMSCs on large ECM islands were biased toward osteogenesis[120]. More recent studies further revealed that in addition to cell shape, cell geometry could also influence hMSC differentiation. hMSCs of elongated morphology preferred osteogenesis, whereas those with a low aspect ratio morphology were biased toward adipogenesis[121]. Similarly, Lee *et al.* observed on soft PA substrates that a confined cell shape would promote hMSC adipogenesis, whereas a spread, branching cell morphology promoted hMSC neurogenic differentiation[130].

Together, above findings clearly suggest that multiple environmental physical cues, *e.g.*, matrix rigidity, substrate topography, and cell morphology, can exert comparable regulatory effects on hMSC lineage specification towards osteogenesis, adipogenesis, or neurogenesis. However, those findings above *per se* do not clearly indicate whether different upstream physical cues are acting in parallel with each other or they are cross-talking to each other and eventually forming an "integrative" signal transduction. In other words, despite it is now evident that cells can respond to multiple environmental physical cues and translate them into similar cell fate specification instructions as schematized in Figure 4-2, it remains unclear in regard to the

identity of the cell property that truly "integrates" those signals and thereby initiates an integrative mechanotransduction.

Interestingly, those data above do manifest an emerging trend. Specifically, neurogenic environmental cues such as soft substrates and micro/nano-topographical surfaces typically induce small cell spreading area and slender, elongated cell morphology; osteogenic environmental cues such as rigid substrate and low cell confinement usually elicit large cell spreading area and plaque-like cell morphology; adipogenic environmental cues such as soft substrate and high cell confinement commonly result in limited cell spreading and small-droplet-like cell morphology. This trend implies that "cell spreading" seems to be a biological "integrator" commonly regulated by different upstream mechanical cues, suggesting a further developed view into the concept of the integrative mechanotransduction (Figure 4-3).

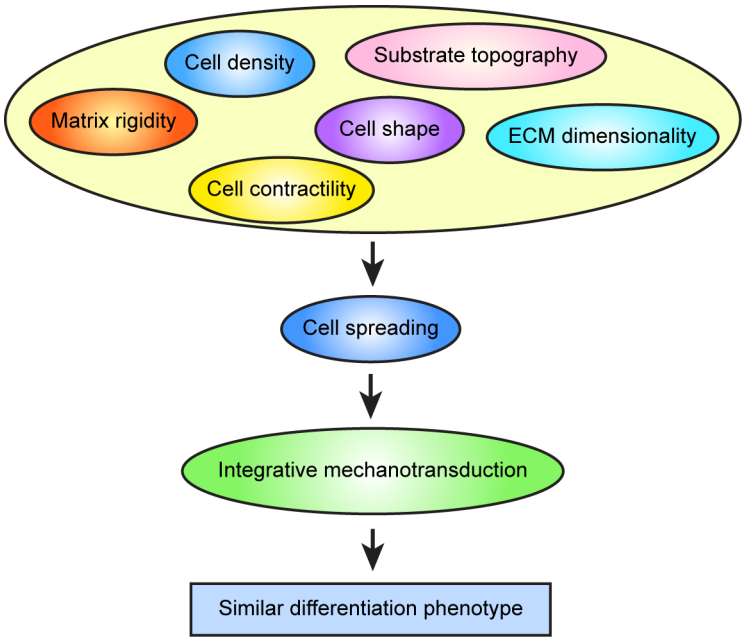

Figure 4-3 The further developed concept of integrative mechanotransduction based on previous findings from hMSCs. This schematic highlights the "integrative nature" of a mechanotransduction pathway that integrates multiple upstream mechanical signals *via* a common cell property - cell spreading - to elicit similar differentiation of stem cells.

Importantly, in order to further test whether cell spreading is the *bona fide* integrator of upstream environmental mechanical cues, researchers have developed ingenious biomaterials systems that can independently manipulate multiple extracellular and cellular mechanical properties including cell spreading. For example, Khetan *et al*. developed a 3D hyaluronic acid-based hydrogel which can be used to independently adjust the stiffness and degradability of the matrix environment surrounding the encapsulated hMSCs[118]. Interestingly, they found that by rendering a soft hydrogel degradable by cell-surface-localized matrix proteases, cultured hMSCs exhibited spread morphology and were predisposed towards osteogenesis instead of adipogenesis; in contrast, a non-degradable hydrogel, regardless of its stiffness, confines hMSCs and limits cell spreading, eventually resulting in adipogenesis rather than osteogenesis even when a stiff hydrogel was used. These results, together the other results discussed earlier, suggest that fully deployed cell spreading, instead of high matrix rigidity, is the common cell property that promotes hMSC osteogenesis; while confined cell spreading, rather than low matrix rigidity, is the common cell property that induces hMSC adipogenesis. These data support the concept that I herein developed for the "integrative mechanotransduction" (Figure 4-3), which has not yet been explored in hPSCs[24]. Further understanding of the integrative mechanotransduction in hPSCs could enable more versatile bioengineering strategies for inducing desired cell fates.

4.3.2 Substrate Rigidity, Cell Cluster Size, and Cell Spreading Share an Integrative Mechanotransduction Pathway for hPSC Amniogenesis

Inspired by the concept of the integrative mechanotransduction, we next set to explore whether other mechanical factors, such as cell spreading/area, can induce amniogenesis from hPSCs on rigid substrates to a level that is comparable to that in the Gel-3D culture system. Indeed, when cultured on rigid substrate (glass) and soft substrate (thick gel bed), respectively,

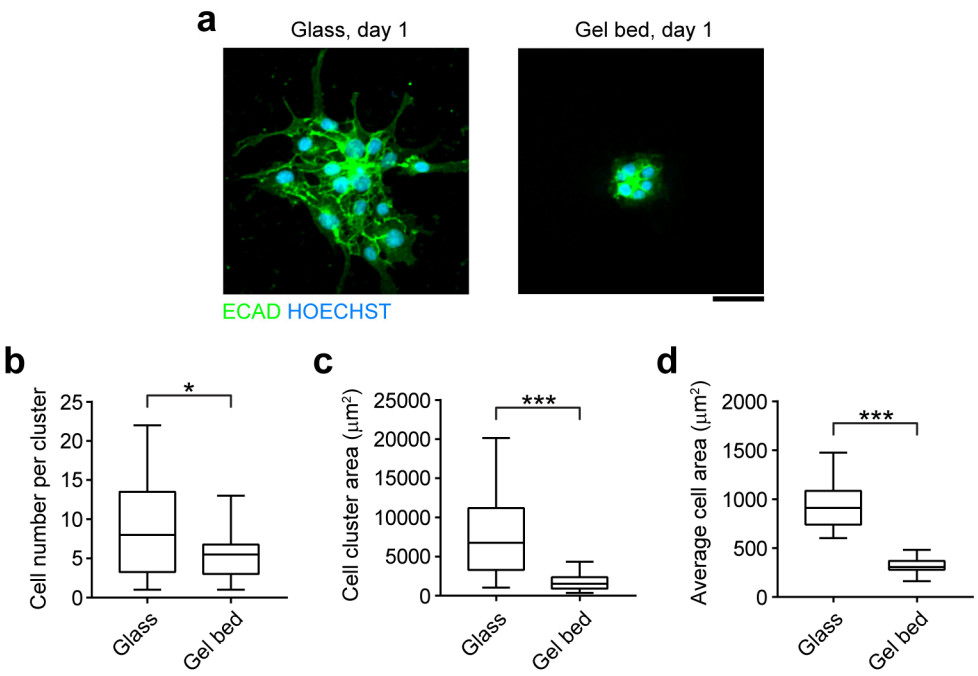

Figure 4-4 Soft gel bed restricts the size of cell clusters as well as individual cells. (**a**) Confocal micrographs showing the immunostaining of ECAD (green) and HOECHST (blue) in hPSCs cultured on glass coverslip (*left*) and gel bed (*right*) 24 h after plating. Scale bar, 50 μm. (**b-d**) Statistical results of cell number in each cluster (**b**), cell cluster size (**c**), and average cell size (*cell cluster size* / *cell number per cluster*) (**d**) for hPSCs cultured on glass and gel bed, respectively. Box charts: box, 25-75%; line-in-box: median; wiskers: 1-99%. *P*-values were calculated using unpaired, two-sided Student's *t*-test. *: $P < 0.05$; **: $P < 0.01$; ***: $P < 0.001$.

for just 24 h without adding 3D ECM overlay, hPSC clusters exhibit significantly different sizes. Specifically, hPSCs clusters on rigid substrate contain larger number of cells and also appear to be significantly larger in size/projected area (Figure 4-4a,b,c). Individual cells within the cluster on a rigid substrate also adopt more spread morphology and larger area (Figure 4-4a,d). In contrast, hPSC clusters formed on soft gel bed are smaller in size/projected area and also contain fewer cells per cluster (Figure 4-4a,b,c). The average area for individual cells is also notably smaller on the gel bed (Figure 4-4a,d). Together, these results suggest that the softness of Gel-3D amniogenic niche exerts concurrent restriction on cell cluster size, cell size, and cell spreading.

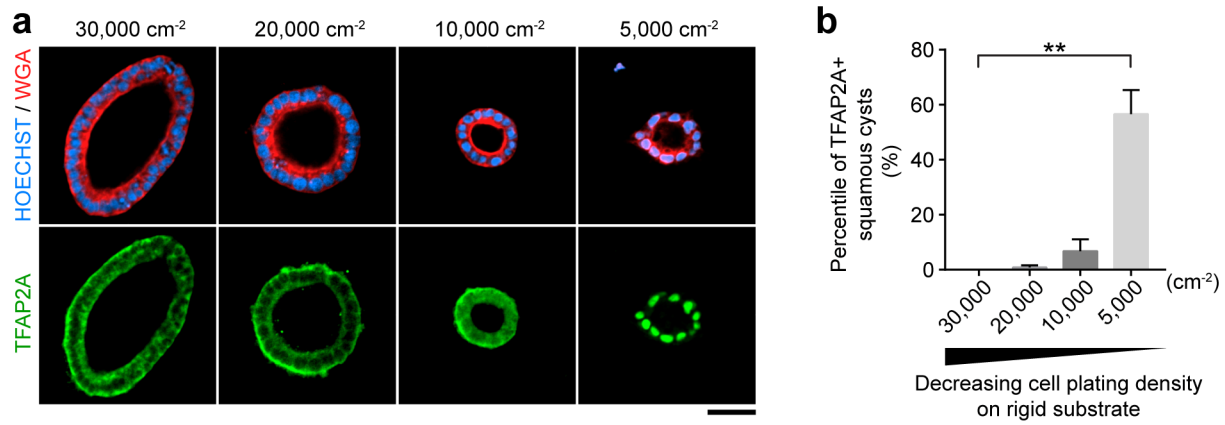

Figure 4-5 Reducing cell plating density in Glass-3D condition modestly increases the hPSC-amnion development. (**a**) Confocal micrographs showing immunostaining of HOECHST (blue), WGA (red), and amniotic marker TFAP2A (green) in hPSCs cultured in Glass-3D condition under different cell plating density as indicated at day 3. Scale bar, 50 µm. (**b**) Statistical results showing the percentage of TFAP2A+ squamous cysts under each condition as indicated. Data were plotted as mean ± s.e.m. *P*-values were calculated using unpaired, two-sided Student's *t*-test. **: $P < 0.01$.

We next set to examine whether decrease in cell plating density, which effectively reduces the size of hPSC clusters in culture, could enhance the development of amniotic tissue from hPSCs on rigid glass substrate (Glass-3D condition). Specifically, the cell plating density was reduced from previously 30,000 cm^{-2} to 20,000, 10,000, and 5,000 cm^{-2}, respectively. Interestingly, modest differentiation of TFAP2A+, squamous, amnion-like cysts was observed in Glass-3D condition when the cell plating density, and thereby the cell cluster size, is at the lower end (Figure 4-5). This result suggests that it is indeed possible to elicit hPSC amniogenesis on a rigid substrate by mimicking the restricting effect of soft gel bed on cell cluster sizes, consistent with the idea of integrative mechanotransduction. Specifically, above results indicate that cell cluster size/projected area and cell-cell interaction, both of which are affected by the cell plating density, might be involved in the integrative mechanotransduction for hPSC amniogenesis.

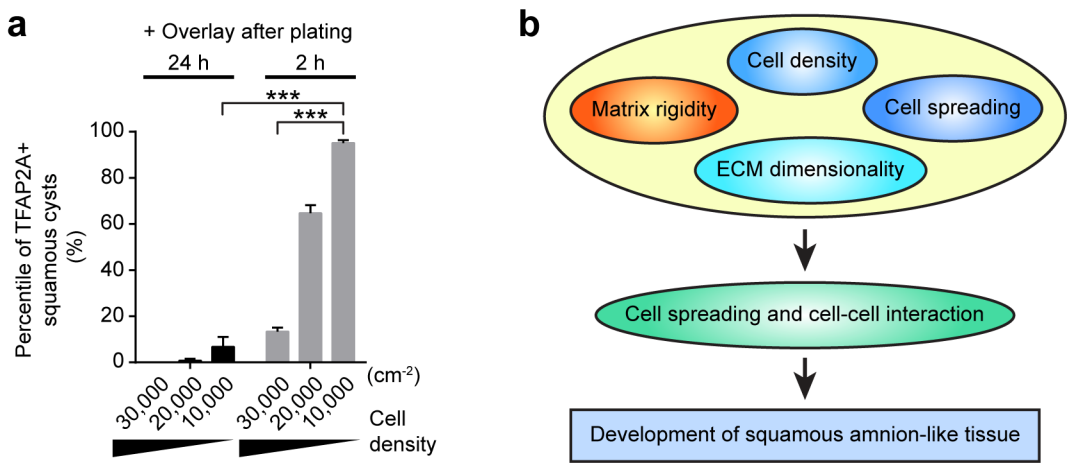

Figure 4-6 Introducing 3D ECM overlay shortly after cell attachment, before full deployment of cell spreading, significantly increases the development of amnion-like cysts. (**a**) Statistical results showing the percentage of TFAP2A+ squamous cysts under different conditions as indicated at day 3. 3D ECM overlay was applied either at 24 h or at 2 h after plating. When it was applied 2 h after plating, 10 μM Y27632 was also supplemented in the medium and remained till the next change of medium at 24 h. (**b**) Schematic illustrating the concept of the integrative mechanotransduction in the development of squamous amnion-like tissue from hPSCs.

Results shown in Figure 4-4a&d also suggest that in Gel-3D condition, soft gel bed restricts cell spreading and cell area, which, together with 3D ECM environment, might further induce amniogenesis from hPSCs. In order to test whether restricted cell spreading, in combination with 3D culture, is sufficient to mimic the amniogenic property of Gel-3D condition on a rigid substrate, we plated hPSCs on glass substrate and supplemented the 3D ECM overlay 2 h after plating, before cell spreading was fully deployed. Compared with previous tests under Glass-3D conditions, wherein the ECM overlay was provided 24 h after cell plating, supplementation of 3D ECM overlay shortly after cell plating significantly increases the development of TFAP2A+, squamous amnion-like cysts under all conditions tested (Figure 4-6a). This result demonstrates that the combination of 3D ECM environment and limited cell spreading is sufficient to induce efficient hPSC amniogenesis on a rigid substrate, likely due to the recapitulation of the effect of

Gel-3D niche on constraining cell spreading by substrate softness. Above findings also support the existence of an integrative mechanotransduction pathway that controls the development of amnion-like tissues from hPSCs *via* integrating multiple upstream mechanical signals including matrix rigidity, cell density, ECM dimensionality, and cell spreading to make a common fate decision, with cell spreading and cell-cell interaction probably acting as the "integrator" (Figure 4-6b). In complementary to the Gel-3D culture developed in Chapter II, results reported in this chapter have established an alternative method that can be applied on rigid substrates to induce amniogenic differentiation from hPSCs.

4.4 Development of a Micro-engineered Human Amniotic Tissue Array

As a standard and easily accessible bioengineering technique for micro-scale patterning, micro-contact printing has enabled rapid prototyping of microarray-based experimental platforms. By leveraging micron-contact printing, we can conveniently create large-scale arrays

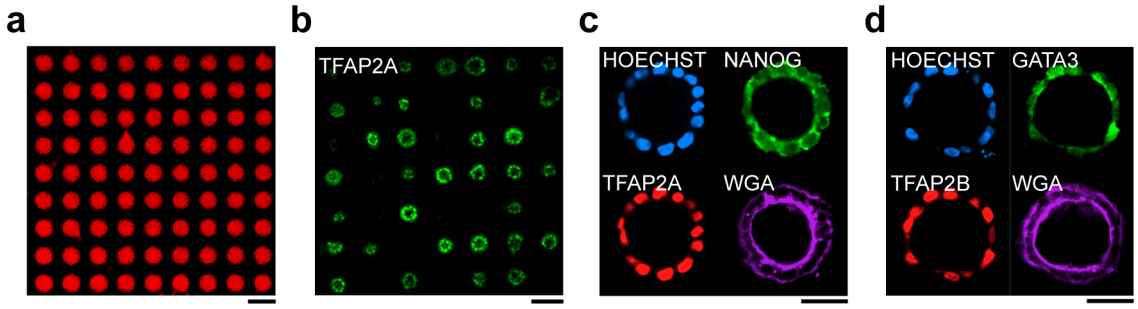

Figure 4-7 Micro-engineered human amniotic tissue array from hPSCs. (**a**) Confocal micrograph showing the staining of LAMININ (red) in the micro-contact printed array of Geltrex™. Scale bar, 100 µm. (**b**) Confocal micrograph showing the staining of amniotic marker TFAP2A (green) in the cysts formed on the Geltrex™ ECM array. Scale bar, 100 µm. (**c**) Confocal micrographs showing the staining of HOECHT (blue), NANOG (green), TFAP2A (red), and WGA (purple) in a representative cyst cultured on the micro-engineered ECM array at day 3. Scale bar, 30 µm. (**d**) Confocal micrographs showing the staining of HOECHT (blue), GATA3 (green), TFAP2B (red), and WGA (purple) in a representative cyst cultured on the micro-engineered ECM array at day 3. Scale bar, 30 µm.

of ECM proteins, herein 1% Geltrex^{TM} (Figure 4-7a), on a glass coverslip pre-coated with a thin layer of PDMS.

By using the modified Glass-3D culture condition, wherein 3D ECM overlay was supplemented shortly after cell plating, we have conducted hPSC amniogenesis assay on the micro-contact printed ECM arrays and successfully induced the development of squamous cystic structures expressing TFAP2A (Figure 4-7b), an early human amniotic marker we identified in Chapter II. As expected, those cysts only grew on the pre-defined microarrays (Figure 4-7b), which is a prerequisite for this system to be used as a high-throughput screening system in future . Those cystic structures also showed expression of TFAP2B and GATA3, which are additional hPSC-amnion markers; expression of pluripotency marker NANOG was lost (Figure 4-7c,d) in those squamous cysts. These results demonstrated the proof of concept for the development of a human amniotic tissue array *in vitro*.

4.5 Conclusions

In conclusion, this chapter has expanded our previous understanding of the mechanosensitive nature of hPSC-amnion development and leveraged such new knowledge to demonstrate the proof of concept for a micro-engineered human amniotic tissue array that is derived from cultured hPSCs *in vitro*. Specifically, findings reported in this chapter indicated an integrative mechanotransduction pathway that integrates diverse upstream mechanical signals, *e.g.*, matrix rigidity, cell density, and cell spreading/area, to induce hPSC-amnion development. Such notion could enable the application of a wider spectrum of substrates and culture conditions in the bio-manufacturing of hPSC-amnion in future. It also achieves the successful combination of micro-engineered ECM array with hPSC-amnion development, thereby generating a human

amniotic tissue array that can potentially be applied for reproductive medicine in the future. At this moment, the work described in this chapter is still preliminary for the translational application it aims at. The molecular basis for the newly found integrative mechanotransduction underlying hPSC amniogenesis also needs to be studied in the future. The outlook of this work will be discussed in Chapter 5.[‡‡‡]

‡‡‡ Research presented in this chapter has received technical assistance from Ms. Sajedeh Nasr Esfahani (cell culture, ECM microarray fabrication), Mr. Xufeng Xue, Mr. Zida Li, and Mr. Jianming Sang (silicon mold fabrication). I would also like to thank Dr. K. Sue O'Shea, Dr. Allen P. Liu, Dr. Deborah L. Gumucio, and Dr. Jianping Fu for their comments on the research presented in this chapter.

CHAPTER V

Conclusions and Future Work

5.1 Summary

Implantation is a critical process that initiates the intrauterine development of a human embryo. Abnormalities during implantation could potentially cause pregnancy failure or birth defects. A better understanding of peri-implantation human embryogenesis is of fundamental and clinical importance, but has been hindered by the inaccessibility to *in vivo* samples and the lack of *in vitro* methods. In this dissertation, I endeavored to fill this gap in knowledge and technology about early human embryonic development, by developing hPSC-derived *in vitro* culture models that mimic peri-implantation development of the human amnion and amniotic sac. These *in vitro* models will provide researchers with easily accessible, scalable, and malleable tools for studying peri-implantation human developmental events that were barely approachable before.

By using an hPSC-based *in vitro* model, we unveiled the previously unrecognized ability of hPSCs to respond to extracellular mechanical cues to recapitulate the morphological and cell fate characteristics of early human amnion development during implantation. In particular, we demonstrate that human amnion-like tissue can develop from hPSCs in the absence of additional inductive signals from maternal and other extraembryonic tissues, thereby challenging traditional

dogma about the requirement of maternal/trophoblastic paracrine signals for amniogenesis. Interestingly, this dissertation identified a unique sensitivity of hPSC amniogenesis to the physical property of the matrix. By simply modulating the thickness of the matrix bed, which tunes it apparent mechanical stiffness, it can toggle hPSCs between amniogenic differentiation and self-renewing expansion. This finding indicates that physical cues in the peri-implantation niche might play an important role in eliciting amniogenesis from an otherwise continuously self-renewing population of epiblast.

The work in this dissertation also demonstrated a self-sustaining mechanism underlying human amniogenesis, which occurs *via* autocrine BMP-SMAD signaling. Specifically, the amniogenic differentiation of hPSCs activates endogenous BMP ligand production, which is in turn required for sustaining the progression of amniogenesis. This finding suggests that the amnion might serve as a source of BMP ligands and a paracrine BMP signaling center for the induction of additional extraembryonic tissues in the early human embryo. Indeed, such notion is supported by recent finding in cynomolgus monkey embryos, which highlighted a potential role of nascent amnion in inducing PGC differentiation *via* paracrine BMP signaling[19].

By demonstrating the hPSC-derived asymmetric cystic structure that resembles early human amniotic sac, the data in this dissertation highlighted a previously unappreciated self-patterning nature of human amniotic sac development. In particular, we showed that bipolar amnion-epiblast patterning can be established within an intact lumenal cyst *via* concurrent differential morphogenic cytodifferentiation, which suggests a developmental paradigm different from the long-established textbook dogma put forward by Luckett[6] in 1975. Indeed, under no circumstances did we observe opening of and re-sealing of the cyst as required in the Luckett model. The patterning of amnion-epiblast axis is also demonstrated to be correlated with a

similarly patterned BMP-SMAD signaling, indicating an important role of intrinsic signal patterning/gradient for the development of human amniotic sac. Indeed, such bipolar patterning of BMP signaling along the amnion-epiblast axis was recently confirmed in post-implantation cynomolgus monkey embryos[19].

As a final aim, I also endeavored to extend our newly developed *in vitro* model for peri-implantation human amniogenesis to a translationally applicable format that is compatible with large-scale screening for reproductive medicine. To achieve this goal, we first examined cellular properties that are possibly required for the amniogenic differentiation from hPSCs. Importantly, we identified cell spreading and cell density-dependent cell-cell interactions as two possible integrators of an integrative mechanotransduction pathway that underlies the amnion-like tissue development from hPSCs. This finding significantly broadened the scope of bioengineering strategies that can be used to induce hPSC amniogenesis. Leveraging such findings, we demonstrated the proof of concept for a micro-engineered hPSC-based human amniotic tissue array, which could potentially open new avenues for reproductive medicine in the future.

In conclusion, I describe in this dissertation the first hPSC-derived *in vitro* models for studying and understanding important peri-implantation human developmental events. The findings reported in this dissertation provide new insights into early human developmental biology and bring opportunities for future exploration of an uncharted territory - peri-implantation human embryology.

5.2 Future Work and Perspectives

5.2.1 Developmental Biology of hPSC-Amnion Development and Human Amniogenesis

Serving as an efficient *in vitro* model, hPSC-amnion can be utilized in the future for studying the developmental biology of human amniogenesis. Although in this dissertation we have extensively demonstrated the molecular similarity between hPSC-amnion *in vitro* and early human amniotic tissue *in vivo*, we were limited by currently available human amniotic tissue transcriptome data sets which were acquired only for later pregnancy. An important future goal is therefore to compare the molecular profile of hPSC-amnion to that of peri-implantation non-human primate amnion, since human amniotic tissues at corresponding stage are likely not available for ethical reasons. Despite the fact that such primate data sets do not exist in publicly available database at this moment, recent studies by the Saitou group suggest that it might be possible, although technically challenging, to isolate peri-/post-implantation monkey amniotic cells and subject them to single-cell RNA-seq analysis in the near future[19]. By comparing the *in vitro* hPSC-amnion model with *in vivo* data set, it could not only ultimately and definitively validate the legitimacy of our *in vitro* model, but also reveal more information on the spatiotemporal connection between hPSC-amnion development and the *in vivo* human amniogenesis. For example, by comparing the transcriptome of hPSC-amnion at different time points along the 5-day developmental course with that of monkey amniotic cells at different developmental stages, *e.g.* from E11 - E15, we might be able to match the *in vitro* hPSC-amnion development with distinct stages during *in vivo* amnion development.

In addition, our RNA-seq data indicate an enrichment of *HOX* genes, *e.g.*, *HOXB2* and *HOXB3*, in hPSC-amnion. Given the well-established role of *HOX* genes in the specification of posterior embryonic patterning[131,132], this result suggests that hPSC-amnion might have adopted

a posterior amniotic fate. Therefore, if it becomes technically feasible in the future to isolate monkey amniotic cells from anterior and posterior regions, respectively, and then subject them to single-cell RNA-seq analysis, it will be of importance to investigate whether the hPSC-amnion *in vitro* is more similar to anterior or posterior amniotic cells *in vivo*, thereby providing new insights regarding whether hPSC-amnion has already undergone regional specification in the current culture system.

Extending from the above rationale, it will also be of importance to examine whether the composition of the currently used culture medium - mTeSR1 - might have certain effects on specifying the regional identity of hPSC-amnion generated *in vitro*. In fact, mTeSR1 contains lithium chloride (LiCl)[133], a chemical that inhibits GSK3β and thereby could indirectly activate β-CATENIN/WNT signaling pathway that is known to be involved in certain posteriorizing embryonic patterning events[134]. In light of this consideration, it is tempting to speculate that the existence of LiCl in the current culture system might be a reason that causes the appearance of *HOX* genes in hPSC-amnion. In order to test whether certain components of mTeSR1 medium have important roles in the morphogenesis, differentiation, and/or possibly regionalization of hPSC-amnion, I plan to take advantage of a different medium called Essential 8 (E8)[135], which is a formula simplified from mTeSR1 and contains only 8 essential factors of mTeSR1. The E8 medium provides an easily accessible chemical platform from which I could reconstruct a "reduced" formula of mTeSR1, which can be designed to lack certain factors, for example LiCl, that are seen in standard mTeSR1. By using such a defined and "reduced" formula, I will examine whether withdrawing certain factors from standard mTeSR1 could cause a significant change in hPSC-amnion's molecular or morphological identities. This work could potentially shed light on the biochemical signaling that controls hPSC-amnion fate and morphology. If

successful, this work could also yield sufficient knowledge so that we can compose customized cell culture medium for inducing amnion-like tissues of possibly different regional identities. Generation of potentially regionalized human amniotic tissues will not only help advance our understanding of early human amniogenesis, but also could provide a novel platform for studying the developmental origin of other embryonic and extraembryonic tissues that are related to amnion. For example, Sasaki *et al*. recently found that PGCs, the precursors of germ cells that develop in the embryo proper, originate from posterior amniotic epithelium in cynomolgus monkey embryos[19]. Therefore, I am interested in exploring the possibility to derive human PGC-like cells from hPSC-derived posterior amnion-like tissues in the future.

Nevertheless, there are also other possible explanations for the enrichment of posteriorization-associated *HOX* genes in hPSC-amnion. For example, given that BMP signaling has also been known involved in posterior embryonic regionalization in mice[136], and that endogenous BMP signaling has been found as a prominent inductive signal during hPSC-amnion development in this dissertation, it is possible that the appearance of those *HOX* genes is attributed to such BMP signaling, instead of the existence of LiCl in the culture medium. Indeed, in the recent study by Sasaki *et al*., BMP4 is found first expressed throughout the entire early monkey amnion and then becomes more restricted at the posterior amniotic epithelium during further development[19]. This observation implies that the BMP4 signaling *per se* might have certain inductive effect for posterior tissue specification. Therefore, it is also worthy of studying in the future whether BMP signaling is truly the driving force for posterior amniotic tissue specification, or it is just a concurrent signaling that supports, but does not necessarily causes, the posteriorization of early primate amnion.

Notably, the hPSC-amnion described in this dissertation likely represents only the early stage of human amnion development. Considering that human amniotic membrane will later on recruit extraembryonic mesenchymal cells during further development, and that it will eventually fuse with the chorion, it will be of interest in the future to attempt to generate more matured and sophisticated human amnion-like tissues *in vitro*, by either modifying the culture medium or supplementing mesenchymal cells into the current culture system to build a co-culture platform. These efforts could lead to broader understanding of amniotic tissue development in humans.

5.2.2 Cell Biology of the hPSC-Amnion

Besides examining the developmental biology of hPSC-amnion, I am also interested in investigating the unique cell biological properties of hPSC-amnion. Notably, hPSC-amnion as well as *in vivo* human amnion adopt a unique squamous epithelial morphology, which is drastically different from the columnar epithelial morphology seen in undifferentiated hPSCs and *in vivo* epiblast cells. The biological meaning of such a squamous morphology is an intriguing fundamental question that needs to be answer in the future.

Specifically, considering that amnion, but not epiblast, is the main source for amniotic fluid and is responsible for regulating the volume and pressure inside the amniotic cavity/sac as well as other physiochemical parameters like the ion concentration, pH value, *etc*. in the amniotic fluid, it is tempting to speculate that such differences in functions between amnion and epiblast might root in their differences in epithelial cell characteristics. For example, claudins - a family of proteins localized at tight-junctions that seal an epithelial sheet - are known to have important roles in controlling ion/fluid transportation during embryonic epithelial structure morphogenesis (*e.g.*, gut lumen formation in zebrafish[137]). Interestingly, the RNA-seq data set reported in this dissertation demonstrated that compared with undifferentiated hPSCs, hPSC-amnion

significantly up-regulates the mRNA levels for *CLDN4* and *CLDN10* - transcripts encoding two distinct members of the CLAUDIN family, suggesting a remodeled tight-junction protein community in hPSC-amnion. The next step is to study whether there is a functional connection between CLDN4, CLDN10 and amnion-specific functions such as ion/fluid transportation. Furthermore, by using the RNA-seq data set provided in this dissertation, a comprehensive transcriptomic and functional ontology analysis in regard to cell polarity-associated functional terms for hPSC-amnion might provide deeper insights into the regulatory mechanisms underlying amnion-specific epithelial functions.

During embryonic development, cells constantly "talk" to each other through secreted molecules and elements. Given that the amnion and epiblast enclose the same single fluid-filled cavity - the amniotic cavity, they are poised for constant cross-talk *via* paracrine signaling. Therefore, it is tempting to ask how amnion and epiblast cross-talk to each other, and to speculate whether the amnion and epiblast have different cell secretion and whether such a difference could play an important role in dictating or sustaining the bipolar amnion-epiblast patterning, possibly through unknown feedback signaling loops. Following this line of thinking, it is important to study in the future the secretome of both hPSC-amnion and undifferentiated hPSCs. Such a study could deepen our understanding of the specific and possibly distinct roles played by amnion and epiblast, respectively, in the amniotic sac morphogenesis, lending us the answer to the question - "amnion and epiblast, are they friends or foes?".

In addition, it will also be of interest to investigate the molecular determinants of the squamous epithelial morphology of amnion. In this dissertation, we found that hPSC-amnion activates a unique subset of EMT-related transcription factors (EMT-TFs), namely BRA, SLUG, but not SNAIL, while undergoing a columnar-to-squamous epithelial morphological transition

(Figures 2-10, 2-11, and 2-12). Such co-existence of ECAD+ epithelial phenotype and EMT-TFs in the squamous amnion-like tissue appears paradoxical, because EMT-TFs such as BRA and SLUG have been demonstrated as transcriptional repressors of ECAD[138]; nevertheless, no down-regulation of ECAD at either mRNA or protein level did we observe in the hPSC-amnion development. In contrast, expressions of BRA, SLUG, as well as SNAIL were observed in PS-cell development, with concurrent transformation from hPSC-associated epithelial phenotype to PS-cell-associated mesenchymal phenotype. Taken together, these observations suggest that EMT-TFs might have more complicated interactions with epithelial tissue regulation than that is conventionally regarded. Specifically, each EMT-TFs might have its distinct role in regulating the epithelial phenotype. Therefore, it will be of importance in the future to dissect the specific role of EMT-TFs like SLUG and SNAIL, respectively, in hPSC-amnion development. By leveraging CRISPR/CAS9[139,140] - an efficient gene-editing system that has been rapidly adapted among life science research community, we can generate genetically modified hPSC lines in which SLUG or SNAIL is deleted. Using these knockout hPSC lines, we can examine the role of each of those EMT-TFs in hPSC-amnion morphogenesis.

In this dissertation, our data demonstrated significant up-regulation of a cohort of transcription factors during the development of hPSC-amnion. This cohort of transcription factors include quite a few well-known targets of BMP signaling, *e.g.*, HAND1/2, MSX1/2, DLX5/6. However, it remains unclear whether these transcription factors are *bona fide* molecular determinants of the amniotic cell fate or they are merely mediators of a more fundamental regulatory circuitry that specifies the amniogenesis. Given the broad implication of these BMP targets in a variety of developmental processes such as neural crest development[141] and heart development[142], it is tempting to speculate that they might not be the direct determinants for the

amniotic cell fate. Therefore, it remains an important question to study that whether other transcription factors (*e.g.*, TFAP2A, TFAP2B) that are not direct downstream targets of BMP signaling could be the determinants of the amniotic fate. In the end, it will be of interest to identify a minimal set of transcription factors that are capable of reprogramming the transcriptional circuitry of adult human somatic cells to that of amniotic cells; these induced or directly reprogrammed human amniotic cells will no longer require hPSCs as source cells and eliminate the need of a 3D matrix environment for derivation, thereby greatly simplifying the bio-fabrication process and facilitate their clinical applications.

5.2.3 Mechanobiology of hPSC-Amnion Development

In this dissertation, we clearly demonstrated that the development of hPSC-amnion is regulated by microenvironmental physical factors - namely, the matrix rigidity and ECM dimensionality - in a biochemical context permissive for hPSC self-renewal. This finding reveals a previously unrecognized mechano-sensitive nature of hPSCs and suggests a potential important role of mechanotransduction for early human embryonic inductions. To further explore the scope of the mechano-sensitivity of hPSC-amnion development, we examined the effect of other physical factors and demonstrated an integrative mechanotransduction pathway that allow cells to integrate matrix rigidity, ECM dimensionality, cell density, and cell spreading to induce hPSC amniogenesis. These findings have not only broadened the bioengineering strategies for generating hPSC-amnion *in vitro*, but also provided new insights into the mechanobiology and mechanotransduction underlying the amniotic cell fate specification.

Notably, the prominent sensitivity of hPSC-amnion development to matrix rigidity suggests a potential role for cell-matrix adhesions in the amniogenic mechanotransduction. Interestingly, our RNA-seq analysis results indicated a significant increase in *ITGA8* and *ITGB6* in hPSC-

amnion, putting integrins - a transmembrane protein family that plays a pivotal role in meditating cell-ECM adhesions - under my focus. Integrins have long been known for its capability of responding to extracellular mechanical cues and thus being at the very upstream of cellular mechanotransduction[143]. I will briefly review our current understanding of integrin-mediated mechanotransduction in the next a few paragraphs[144].

Integrins are heterodimeric transmembrane proteins composed of an α and a β subunit. Currently, there are 24 known integrin heterodimers constituted by different combinations of 18 α and 8 β subunits[145-148]. hESCs express a broad range of integrins including α_1, α_2, α_3, α_5, α_6, α_7, α_{11}, α_V, α_E, and β_1, β_2, β_3, β_5, β_6 integrins. hiPSCs are also reported to express mainly α_5, α_6, α_V, β_1, and β_5 integrins, with variations among different hiPSC lines[149-151]. The first step adherent

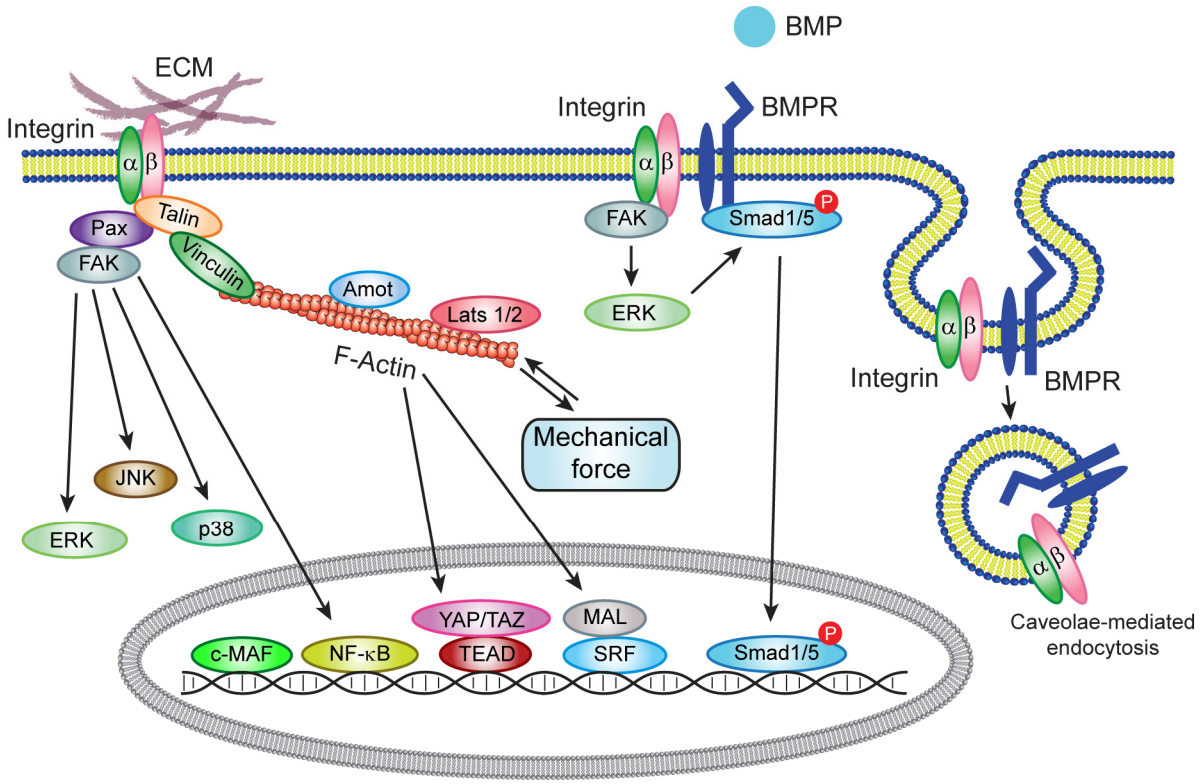

Figure 5-1 Schematic summarizing a few hypothetical mechanotransduction pathways underlying the mechano-sensitive hPSC amniogenesis.

cells take to probe the surrounding ECM is mediated by the "inside-out" and "outside-in" bidirectional regulation of integrin-ligand binding[152-154]. Specifically, initial binding of integrin to adhesive molecules initiates clustering of intracellular adaptor proteins including talin, which in turn binds the cytoplasmic domain of integrin, resulting in a conformational change of integrin's extracellular domain and its heightened affinity to corresponding ECM ligands. Firm binding of integrin to ECM ligand in turn activates clustering of integrins through their intracellular domains and further recruits adaptor and signaling proteins to adhesion sites. Key molecular players in the early stage of integrin-mediated cell-ECM adhesion (also known as "focal adhesion", or FA) include adaptor proteins talin, vinculin, and paxillin as well as tyrosine kinases such as focal adhesion kinase (FAK) and Src family kinases[155,156] (Figure 5-1).

Through adaptor proteins such as talin and vinculin[157], FAs physically connect to actin cytoskeleton (CSK) which is interwoven with myosin family motor proteins such as non-muscle myosin II[158]. Due to its intricate actomyosin contractile machinery, actin CSK can generate mechanical forces that pull on the associated FA proteins as well as the ECM linked to the integrins[158]. Such mechanical contractile force, in feedback, will dictate the dynamics of integrin recruitment and FA assembly/disassembly[158-161]. This ECM-integrin-actin CSK mechanical linkage constitutes a main mechanism that allows the cell to "sense" the rigidity of the ECM[143] (Figure 5-1). Because of its compositional and structural complexity, FAs can potentially relay its force-sensitive dynamics to elicit down-stream mechanotransductive signaling *via* two major paradigms.

An important signaling axis downstream of integrin-mediated FA is the FAK-Src pathway[155,162,163] (Figure 5-1), which is dominated by kinase-driven phosphorylation. Activated by integrin ligation, FAK is recruited to FA by binding integrin, which in turn activates FAK

through autophosphorylation on Y397. Further phosphorylation of FAK is completed by binding of FAK to Src family proteins. Together, FAK and Src form a signaling complex to relay signals from integrin to control downstream signaling such as the MAPK pathways including the FAK/Ras/Raf/MEK/ERK signaling, Fyn/Shc/Grb2/SOS/Ras signaling, p38 MAPK signaling, and JNK signaling[164-168], as well as the nuclear factor κB (NF-κB) signaling (Figure 5-1). Previous studies have demonstrated that mechanical tension as well as rigid substrate can activate the FAK-MAPK signaling axis[169,170]. The activation of MAPK pathways could further increase or decrease transcriptional activities of a myriad of factors. For example, the Ras/ERK signaling has been demonstrated as an inhibitory signal for transcription factor c-MAF[171] (Figure 5-1). Interesting, our RNA-seq analysis results indicates that *MAF*, the gene that encodes the transcription factor c-MAF, is up-regulated in hPSC-amnion cultured on soft gel bed. This observation appears to be consistent with the hypothesized low FAK-ERK signaling and thereby high c-MAF signaling on soft substrate in hPSC-amnion. Nevertheless, a deeper study on the role of mechanosensitive integrin-FAK-MAPK signaling pathway on hPSC-amnion development is needed in the future.

Another important signaling axis downstream of integrin and FA is through regulating the actin CSK (Figure 5-1). As an intracellular structure physically anchored to FA and also an effector downstream of substrate rigidity and cell shape/area, the actin CSK and its integrity may serve as an integrator of a multitude of extracellular mechanical signals[172]. Supporting this view, recent reports have demonstrated disorganized F-actin CSK and compromised CSK contractility in adherent cells cultured on soft substrates[173] or under high geometric confinement[174]. Herein I briefly discuss the current understanding of the role of the actin CSK in mechanotransduction.

Recently, the Hippo-YAP/TAZ pathway, which is important for organ size control and cancer[175,176], has been identified as a downstream effector of the quality, dynamics as well as the intrinsic contractility of the F-actin CSK[174,177-182] (Figure 5-1). Interestingly, experimental evidence that has been accumulated in past years implicates an emerging pattern of mechanical regulation of the Hippo-YAP/TAZ pathway: extracellular mechanical cues (*e.g.*, rigid substrate, external stretch, large cell size) resulting in prominent F-actin CSK formation can promote a high nuclear YAP/TAZ activity, while those cues (*e.g.*, soft substrate and small cell size) that compromise the integrity of F-actin CSK lead to a low YAP/TAZ activity[177,178]. Specifically, by forming prominent F-actin CSK on rigid substrate, it substantiates YAP/TAZ signaling by secluding YAP/TAZ inhibitory regulators Lats1/2 and Angiomotin (Amot) to F-actin, thereby preventing the association between YAP/TAZ and their inhibitor proteins (Figure 5-1). Such a role of the F-actin CSK as a potent mechanical signal integrator has been supported by recent studies in both 2D and 3D contexts on a myriad of cellular behaviors and functions[178]. Furthermore, signaling through the F-actin CSK to suppress YAP activity has also been shown involved in regulating mechanosensitive motor neuronal differentiation of hESCs[183].

In addition, the integrity and polymerization of actin CSK have also been implicated in regulating SRF (serum response factor) signaling[184,185] (Figure 5-1). Specifically, enhanced polymerization of cytoplasmic actin monomers (G-actin) releases MAL, a transcription co-factor, from its association with G-actin, resulting in MAL nuclear translocation and thus elevated SRF signaling. Following this mechanism, large cell area with elevated cytoplasmic G-actin level has been found to inhibit SRF signaling and differentiation of epidermal stem cells[184]. Taken together, the F-actin CSK has been well-established as a mechano-sensor and integrator during cellular mechanotransduction.

Despite that it is still unclear whether YAP/TAZ or SRF/MAL signaling is related to amniogenic fate specification, given the prevalence of matrix rigidity and cell spreading area in regulating hPSC amniogenesis, as well as the generally observed connection between actin CSK integrity and matrix rigidity or cell spreading, it is worthy of studying in the future whether the F-actin CSK could be a key signaling component of the integrative amniogenic mechanotransduction.

Moreover, since the work in this dissertation has highlighted the necessity and prominence of BMP-SMAD signaling in hPSC-amnion development, I am interested in examining possible mechanistic connections between integrin-mediated cell-ECM adhesions and BMP-SMAD signaling regulation during the mechano-sensitive amniogenic differentiation (Figure 5-1). In an interesting recent study, Zhou *et al*. demonstrated in endothelial cells that $\alpha_V\beta_3$ integrins can physically associate with BMP receptor IB (BMPRIB) under oscillatory shear flow stimulation[186]. This study further demonstrated that such integrin-BMPRIB association results in non-canonical SMAD1/5 activation through FAK-ERK pathway-mediated phosphorylation. As shown in Figure 5-1, since this non-canonical integrin-BMPR-SMAD1/5 activation paradigm is directly related to a critical amniogenic signaling pathway and does not seem require externally supplied BMP ligands,, which is consistent with our observations in this dissertation, I am interested in examining the possibility of this signaling pathway in the context of hPSC amniogenesis in the future. As a starter, anti-integrin α_V or anti-integrin β_3 antibodies can be used to treat hPSCs cultured under the Gel-3D condition, in order to assess whether $\alpha_V\beta_3$ integrins are required for hPSC-amnion development. In another interesting study on hMSCs, Du *et al*. found that soft substrate could promote caveolae-mediated endocytosis of β_1 integrin along with the BMPRIA that is associated with it[187] (Figure 5-1). This finding identified a mechano-sensitive

regulatory mechanism for controlling the amount of BMPR on cell surface, thereby adding another level of complexity to integrin-mediated regulation of BMP signaling. However, this study implies a decreased level of cell-surface BMPR and thus a lower level of BMP signaling on soft substrate, which is not consistent with our observation that soft matrix bed activates endogenous BMP signaling during hPSC amniogenesis. Taken together, the non-canonical integrin-BMPR-SMAD1/5 signaling axis mediated by FAK-ERK pathway seems more promising and will be the top candidate hypothesis to be examined in the future.

5.2.4 Physiology and Regenerative Functions of hPSC-Amnion

hPSC-amnion also provides an opportunity to study and apply human amnion physiology in the future. For example, for over a century, human amnion has been used as a substitute for skin graft for facilitating wound healing in various contexts[62,188-191]. Such a beneficial effect has been largely attributed to the anti-inflammatory physiological function of amnion. Therefore, it will be of interest to examine whether hPSC-amnion has a similar anti-inflammatory function and if it has a potent capacity for stimulating wound-healing and promoting epithelial tissue regeneration in clinically relevant context. If effective, given the scalability of its derivation, hPSC-amnion might provide a substitute bioactive material to replace the cryopreserved human amnion tissues currently used in clinics for treating chronic non-healing wounds in patient suffered from such as diabetic ulcers.

5.2.5 Morphogenic Patterning in Early Human Amniotic Sac Development

In this dissertation, we demonstrated a novel *in vitro* model, the ASE, for early human amniotic sac development. However, the ASE-derivation efficiency using the current culture system is low, probably because of its high-efficiency in inducing amniogenic differentiation. Indeed, I observed in previous experiments that some asymmetric cysts appearing at earlier days

(*e.g.*, day 3) eventually completely differentiated to squamous cysts at later days (*e.g.*, day 5), suggesting strong pro-amniogenesis property of the current culture system. Therefore, to promote the application of the *in vitro* amniotic sac model in fundamental and translational studies, it will be of great importance to develop a more efficient system for inducing the asymmetric cysts, or ASEs.

Since now that BMP signaling is shown to be involved in the development of amnion, one might develop an efficient ASE induction system by engineering asymmetric induction of BMP signaling (Figure 5-2). For example, one might culture hPSCs first under an anti-amniogenic condition, *e.g.*, Gel-2D, and then apply asymmetric amniogenic induction by treating cells with BMP only at one side (Figure 5-2). Such an asymmetric induction system can be achieved, in principle, by leveraging microfluidic gradient-generating devices[192]. Furthermore, it is also possible to apply additional inductive signals for gastrulation only to the columnar side of the cyst (Figure 5-2) once the squamous amnion takes its form. By doing so, we could potentially

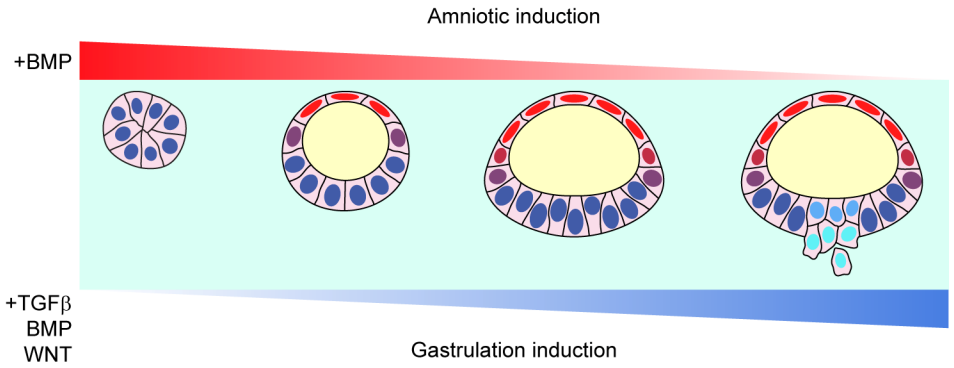

Figure 5-2 Schematic showing the concept of a defined ASE induction system. In this system, exogenous differentiating factors are added in an asymmetric manner to cultured hPSC clusters/cysts *in vitro*. Specifically, BMP ligand is provided to one side of the cyst at decreasing concentration over the time course to induce the development of the squamous, amnion-like tissue (red); in the meantime, growth factors known to be involved in primitive streak development, such as TGFβ, BMP4, and WNT, are introduced to the columnar/embryonic disc (blue) side of the cyst at increasing concentration over the time course to induce the development of gastrulating cells (cyan).

achieve modeling early human embryonic development at both implantation and gastrulation in a defined and controlled manner *in vitro*.

The ASE reported in this dissertation provides an important tool for studying the morphogenesis, especially the bipolar amnion-epiblast patterning, during human amniotic sac development. It will be of significant interest to study the cellular and molecular mechanisms underlying such patterning - at both cellular and tissue scale - in the future to deepen our understanding of human amniotic sac development. For example, the cellular process *via* which early epiblast cells organize and form the amniotic cavity (the lumen) remains unknown and can be studied using the ASE system with the help of high-resolution live-cell imaging and hPSCs that have forced expression of fluorescently tagged apical proteins like EZRIN or PODXL. The mechanism underlying the formation of a tissue boundary between the squamous amnion and the columnar epiblast is also an intriguing yet still mysterious question, which can be studied in future by leveraging the ASE system. In particular, the cell-cell cross-talk between amnion/epiblast at the site where the boundary forms would be interesting to investigate. The spontaneous patterning of BMP-SMAD signaling in ASEs, which implies the existence of a BMP signaling gradient - also merits deeper studies in the future; this goal could be achieved using hPSCs expressing and secreting fluorescently tagged functional BMP4 proteins. In addition, the emergence of PS-like development from the ASE is another interesting observation of self-patterning phenomenon in this dissertation. However, the mechanism for the spontaneous initiation and subsequent ingression/egression of PS-like cells in the ASE remains to be studied in future. For example, by leveraging the CRISPR/CAS9 genome editing tool, we can potentially screen a variety of EMT-TFs, *e.g.*, SNAIL, SLUG, TWIST1/2, ZEB1, for their role in either the initiation of PS or the subsequent dissemination of gastrulating cells.

5.2.6 Micro-engineered High-Throughput Screening System for Reproductive Medicine

In this dissertation, we demonstrated the proof of concept for a micro-engineered platform containing hPSC-derived amnion-like tissue arrays. However, the application of this system remains to be demonstrated in future. Specifically, experiments need to be conducted to test the compatibility of such a micro-tissue array system with high-throughput screening process. In addition, it will be of interest to apply this system to screen the effect of a library of drugs or small molecule inhibitors on the development of hPSC-amnion. It is also of importance to use this system to test the toxicity of various environmental toxicants, such as lead and mercury, as well as other public health hazards, to early amnion development. It is also possible to use this system as a supplementary test to predict the reproductive success in clinics if using hiPSCs derived from patients with reproductive health concerns.

In all, it is envisioned that the findings reported in this dissertation will lead to new trends at both the fundamental and the clinical fronts of scientific research in bioengineering, biomaterial sciences, stem cell biology, and developmental biology in the future.

APPENDICES

APPENDIX A. General Cell Biology Assays

Cell lines

This dissertation used hPSC lines that included H9 (WA09, P50, WiCell; NIH registration number: 0062), H7 (WA07, P52, WiCell; NIH registration number: 0061), UM63-1 (P25, provided by Dr. Gary D. Smith at the University of Michigan MStem Cell Laboratories; NIH registration number: 0277), and 1196a (an iPSC line, P42, from the University of Michigan Pluripotent Stem Cell Core1). All protocols for the use of hPSC lines were approved by the Human Pluripotent Stem Cell Research Oversight Committee at the University of Michigan. All hPSC lines have been authenticated by the original sources and also authenticated in-house by immunostaining for pluripotency markers and successful differentiation to three germ layer cells. All hPSC lines were maintained in a feeder-free system for at least 10 passages and authenticated as karyotypically normal at the indicated passage number. Karyotype analysis was performed by Cell Line Genetics (Madison, USA). All hPSC lines were tested negative for mycoplasma contamination (LookOut Mycoplasma PCR Detection Kit, Sigma-Aldrich).

Cell culture

hPSCs were maintained in a standard feeder-free culture system using mTeSR1 medium (STEMCELL Technologies) and lactate dehydrogenase-elevating virus (LDEV)-free hESC-qualified reduced growth factor basement membrane matrix GeltrexTM (Thermo Fisher

Scientific; derived from Engelbreth-Holm-Swarm tumors similarly as Matrigel®) per the manufacturers' instructions. All cultures were visually examined during every passage to ensure the absence of spontaneously differentiated, mesenchymal-like cells in the culture. All hPSCs were used before reaching P70.

Cell fixation and immunocytochemistry (also known as immunofluorescence analysis)

hPSCs were fixed in 4% paraformaldehyde (buffered in 1 × PBS) for 30 min, and permeabilized in 0.1% SDS (sodium dodecyl sulfate, dissolved in PBS) solution for another 30 min. Samples were first incubated in 2% goat serum solution (Thermo Fisher Scientific) at 4°C for 24 h, and then with primary antibody solution prepared in 2% goat serum at 4°C for another 24 h. Samples were then labeled with goat-raised secondary antibodies (1:500) at 4°C for 24 h. HOECHST 33342 (Thermo Fisher Scientific) was used for counterstaining the cell nucleus. Alexa-fluor dye-conjugated wheat germ agglutinin (WGA; Thermo Fisher Scientific) was used as a pan-cell membrane marker. All primary antibodies, their sources, and dilutions are listed in Table B-1.

Confocal microscopy and image analysis

Images were acquired on an Olympus 1X81 fluorescence microscope equipped with a CSU-X1 spinning-disc unit (YOKOGAWA) or a Nikon-A1 laser scanning confocal microscope (Nikon). Fluorescence images acquired from confocal microscopy were reconstructed in 3D using Imaris8.2 (Bitplane).

Cell and cyst morphology characterization

Measurements of cell nucleus dimensions, cyst epithelial thickness, and cell cluster size were performed manually using the Measurement tool in ImageJ (NIH)11. The normalized nucleus dimension, defined as the ratio of nucleus dimension along the apico-basal direction to that along the lateral direction, was then calculated. Distance between the apical and basal surfaces (both stained by WGA) of the epithelium was measured at 5 different positions evenly distributed along the circumference of the cyst. The average of these 5 measurements was used as the representative epithelial thickness for a cyst.

Western blotting

Whole cell lysates were prepared from cells and homogenized by sonication. Proteins in lysates were separated via SDS-polyacrylamide gel electrophoresis (SDS-PAGE) before transferring to PVDF membranes. PVDF membranes were then incubated with blocking buffer (Li-Cor) for 1 h and then with primary antibodies (Table B-1) at 4°C overnight with gentle shaking. Blots were then incubated with IRDye secondary antibodies (Li-Cor) for 1 h before imaging using the Li-Cor Odyssey Sa Infrared Imaging System (Li-Cor). The investigator who performed the Western blotting was blinded to the test condition allocation during the experiment.

Total RNA isolation

Samples were collected and prepared for RNA isolation following a protocol commonly used for processing *in vivo* tissues. In brief, samples were washed with DMEM/F12 to remove ECM overlay. Cysts (ca. 5,000 or more per sample) were then scraped from the culture substrate,

before being spun down at 1,000 rpm for 3 min in a conical tube. RNA was isolated from the cell pellet using an RNeasy Micro Kit (QIAGEN) following the manufacturer's instruction.

The total RNA from fetal human amniotic epithelial cells was provided by Dr. Toshio Miki (University of South California). The RNA isolation was conducted by following the protocol below. Fetal placentae were obtained from the Allegheny Reproductive Health Center under the approval of the University of Pittsburgh's Internal Review Board and prior written consents of the donors[193]. Any patient tested positive for human immunodeficiency virus, hepatitis B virus, hepatitis C virus, tuberculosis, chlamydia trachomatis, neisseria gonorrhoeae, syphilis or any placenta showing macroscopic abnormality were excluded. Human amniotic epithelial (AE) cells were enzymatically isolated from the amniotic membrane as previously described[194]. In brief, the amnion layer was mechanically separated from the chorion layer and washed several times with phosphate buffered saline (PBS) without calcium and magnesium to remove blood. To dissociate AE cells, the amniotic membrane was incubated at 37°C with 0.05% trypsin containing 0.53mM EDTA-4Na (Life Technologies). Digest from the first 10 min of trypsin digestion was discarded to exclude debris. Cells from the second and third 40 min digests were pooled and washed three times with PBS and immediately cryopreserved with embryonic stem cell-qualified fetal bovine serum containing 10% DMSO. Total RNA was isolated from the cryopreserved samples by using Trizol and DNA-Free RNA Kit (Zymo Research).

Quantitative reverse transcription polymerase chain reaction (qRT-PCR) analysis

RNA quality and quantity were determined using a NanoDrop 1000 spectrophotometer (Thermo Scientific). Reverse transcription was performed using the iScript™ cDNA synthesis Kit (Bio-Rad). qRT-PCR analysis was performed using Quantitect Sybr Green MasterMix

(QIAGEN) and specific primers (as listed in Table C-1) on a CFX Connect™ Real-Time System (Bio-Rad). qRT-PCR result was considered as "not detected" when no signal was observed within 40 cycles. Human *GAPDH* was used as an internal control for quantifying relative gene expression by using the $2^{-\Delta Ct}$ method[195]. All analyses were performed with 2 - 3 technical replicates and ≥ 3 biological replicates as described in figure captions.

RNA-sequencing and data analysis

mRNA-sequencing was performed by the University of Michigan DNA Sequencing Core following Illumina guideline. RNA samples were sequenced on an Illumina HiSeq-2500 High-Output system generating 50 cycle single reads. Samples were barcoded and run on a single lane. Publically available RNA-seq data (GSE66302) were downloaded from GEO. Reads were mapped to the human reference genome (Build hg19) using STAR[196] and tabulated using HTSeq[197]. Differential RNA expression was determined using edgeR[198]. Normalized levels of gene expression and the color scale were determined by scaling raw reads for each gene to account for different total read counts across samples before values were log2 transformed. Raw and processed RNA-seq data files used in this dissertation have been deposited in Gene Expression Omnibus (GEO, accession number GSE89479).

Cluster analysis

Hierarchical clustering analysis of transcript expression data was performed within Cluster 3.0 using uncentered correlation with average linkage[199]. Java Treeview was used for visualizing the clustered data[200].

Gene ontology (GO) enrichment analysis

Quality check of the data was conducted using the Trinity toolkit (https://github.com/trinityrnaseq/trinityrnaseq/wiki/QC-Samples-and-Replicates)[201]. Differential expression analysis was carried out for hPSC-amnion, 9-week human amnion, human chorion, and human placenta, respectively, relative to hPSCs, with the DESeq2 package (https://www.bioconductor.org/packages/release/bioc/html/DESeq2.html)[202]. The output (.DE_results) were converted to an Excel format, sorted by log2 fold change and used as a unified set for GO enrichment analysis by DAVID, v6.8 (https://david.ncifcrf.gov).

Gene set enrichment analysis (GSEA)

Genes were ranked by fold change in expression level relative to hPSCs. The entire ranked data set (i.e., genes enriched and depleted in amnion-like cysts) was queried for 35 genes of the ALK-pathway-related gene set, BIOCARTA_ALK_PATHWAY, using the GSEA software (http://www.broad.mit.edu/gsea/) and the Molecular Signature Database (MSigDB)[203].

APPENDIX B. List of Primary Antibodies

Table B-1 List of primary antibodies used for the immunocytochemistry (ICC) and western blotting (WB).

Protein	Species	Application	Catalog No.	Vendor
EZRIN	Mouse	1:2000 (ICC)	E8897	Sigma-Aldrich
E-CADHERIN	Mouse	1:500 (ICC) 1:1000 (WB)	610181	BD Biosciences
NANOG	Rabbit	1:500 (ICC) 1:2000 (WB)	4903S	Cell Signaling Technology
OCT4	Mouse	1:200 (ICC) 1:500 (WB)	SC-5279	Santa-Cruz Biotechnology
SOX2	Rabbit	1:1000 (ICC) 1:1000 (WB)	09-0024	Stemgent
GAPDH	Rabbit	1:1000 (WB)	SC-25778	Santa-Cruz Biotechnology
BRACHYURY	Rabbit	1:100 (ICC)	SC-20109	Santa-Cruz Biotechnology
SNAIL	Rabbit	1:100 (ICC)	SC-28199	Santa-Cruz Biotechnology
SLUG	Rabbit	1:400 (ICC)	9585	Cell Signaling Technology
N-CADHERIN	Rat	1:500 (ICC)	MNCD2-c	Developmental Studies Hybridoma Bank
FOXA2	Rabbit	1:500 (ICC)	WRAB-1200	Seven Hills Bioreagents
pSMAD1/5	Rabbit	1:100 (ICC) 1:1000 (WB)	9516S	Cell Signaling Technology
SMAD1/5/8	Rabbit	1:1000 (WB)	SC-6031-R	Santa-Cruz Biotechnology
CDX2	Mouse	1:500 (ICC)	CDX2-88	Biogenex
GATA3	Mouse	1:100 (ICC)	SC-268	Santa-Cruz Biotechnology
SSEA-4	Mouse	1:500 (ICC)	MAB4304	EMD Millipore
BMP4	Mouse	1:1000 (WB)	4680	Cell Signaling Technology
E-CADHERIN	Rabbit	1:100 (ICC)	ab15148	Abcam
β-CATENIN	Mouse	1:200 (ICC)	610153	BD Biosciences
OCT4	Rabbit	1:500 (ICC)	2750	Cell Signaling Technology

APPENDIX C. List of qRT-PCR Primers

Table C-1 List of primers used for the qRT-PCR analysis.

Gene	Primer Sequences (5' -> 3')	Reference
NANOG	*Forward:* GATTTGTGGGCCTGAAGAAA	*NA*
	Reverse: ATGGAGGAGGGAAGAGGAGA	*NA*
OCT4	*Forward:* GTGGAGGAAGCTGACAACAA	*NA*
	Reverse: GGTTCTCGATACTGGTTCGC	*NA*
SOX2	*Forward:* GCTTAGCCTCGTCGATGAAC	*NA*
	Reverse: AACCCCAAGATGCACAACTC	*NA*
GAPDH	*Forward:* CTCTGCTCCTCCTGTTCGAC	*NA*
	Reverse: TTAAAAGCAGCCCTGGTGAC	*NA*
CDH1	*Forward:* TCTTCAATCCCACCACGTACA	*NA*
	Reverse: TGCCATCGTTGTTCACTGGA	*NA*
CDH2	*Forward:* ATCAACCCCATACACCAGCC	*NA*
	Reverse: GTCGATTGGTTTGACCACGG	*NA*
CLDN6	*Forward:* TGTTCGGCTTGCTGGTCTAC	PrimerBank[204]
	Reverse: CGGGGATTAGCGTCAGGAC	PrimerBank
BRACHYURY	*Forward:* TGCTGCAATCCCATGACA	PrimerBank
	Reverse: CGTTGCTCACAGACCACA	PrimerBank
SNAI1	*Forward:* TCGGAAGCCTAACTACAGCGA	PrimerBank
	Reverse: AGATGAGCATTGGCAGCGAG	PrimerBank
SNAI2	*Forward:* CGAACTGGACACACATACAGTG	PrimerBank
	Reverse: CTGAGGATCTCTGGTTGTGGT	PrimerBank
FOXA2	*Forward:* CGACTGGAGCAGCTACTATGC	*NA*
	Reverse: TACGTGTTCATGCCGTTCAT	*NA*
GATA2	*Forward:* CAGCAAGGCTCGTTCCTGTT	PrimerBank
	Reverse: GGCTTGATGAGTGGTCGGT	PrimerBank
GATA3	*Forward:* GCCCCTCATTAAGCCCAAG	PrimerBank
	Reverse: TTGTGGTGGTCTGACAGTTCG	PrimerBank
CDX2	*Forward:* GACGTGAGCATGTACCCTAGC	PrimerBank

	Reverse: GCGTAGCCATTCCAGTCCT	PrimerBank
TP63	*Forward:* CTGGAAAACAATGCCCAGA	Li *et al.*[78]
	Reverse: AGAGAGCATCGAAGGTGGAG	Li *et al.*[78]
GATA4	*Forward:* CGACACCCCAATCTCGATATG	PrimerBank
	Reverse: GTTGCACAGATAGTGACCCGT	PrimerBank
GATA6	*Forward:* CTCAGTTCCTACGCTTCGCAT	PrimerBank
	Reverse: GTCGAGGTCAGTGAACAGCA	PrimerBank
KRT7	*Forward:* AGGATGTGGATGCTGCCTAC	Li *et al.*[78]
	Reverse: CACCACAGATGTGTCGGAGA	Li *et al.*[78]
CGA	*Forward:* CACTCCACTAAGGTCCAAGAAGA	PrimerBank
	Reverse: CCGTGTGGTTCTCCACTTTGA	PrimerBank
HLA-G	*Forward:* GAGGAGACACGGAACACCAAG	PrimerBank
	Reverse: GTCGCAGCCAATCATCCACT	PrimerBank
ITGB6	*Forward:* CTCAACACAATAAAGGAGCTGGG	PrimerBank
	Reverse: AAAGGGGATACAGGTTTTTCCAC	PrimerBank
VTCN1	*Forward:* TCTGGGCATCCCAAGTTGAC	PrimerBank
	Reverse: TCCGCCTTTTGATCTCCGATT	PrimerBank
GABRP	*Forward:* TTTCTCAGGCCCAATTTTGGT	PrimerBank
	Reverse: GCTGTCGGAGGTATATGGTGG	PrimerBank
MUC16	*Forward:* GGAGCACACGCTAGTTCAGAA	PrimerBank
	Reverse: GGTCTCTATTGAGGGGAAGGT	PrimerBank
HAND1	*Forward:* CCAAGGATGCACAGTCTGG	PrimerBank
	Reverse: AGGAGGAAAACCTTCGTGCTG	PrimerBank
POSTN	*Forward:* GAAAGGGAGTAAGCAAGGGAG	Dobreva *et al.*[83]
	Reverse: ATAATGTCCAGTCTCCAGGTTG	Dobreva *et al.*[83]
TFAP2A	*Forward:* GCATATCCGTTCACGCCGAT	Tadeu *et al.*[205]
	Reverse: GGGAGATTGACCTACAGTGCC	Tadeu *et al.*[205]
TFAP2B	*Forward:* AGCAAATGTCACGTTACTCACC	PrimerBank
	Reverse: TGTGCTGCCGGTTCAAATACT	PrimerBank
KRT17	*Forward:* AAGATCCGTGACTGGTACCAGAGG	Sankar *et al.*[206]
	Reverse: GATGTCGGCCTCCACACTCAGG	Sankar *et al.*[206]
KRT18	*Forward:* TCGCAAATACTGTGGACAATGC	PrimerBank
	Reverse: GCAGTCGTGTGATATTGGTGT	PrimerBank
BMP2	*Forward:* ACTACCAGAAACGAGTGGGAA	PrimerBank
	Reverse: GCATCTGTTCTCGGAAAACCT	PrimerBank
BMP4	*Forward:* TCCACAGCACTGGTCTTGAG	Xu *et al.*[207]
	Reverse: GGGATGTTCTCCAGATGTTCTT	Xu *et al.*[207]

BMP6	*Forward:* AGCGACACCACAAAGAGTTCA	PrimerBank
	Reverse: GCTGATGCTCCTGTAAGACTTGA	PrimerBank
BMP7	*Forward:* TCGGCACCCATGTTCATGC	PrimerBank
	Reverse: GAGGAAATGGCTATCTTGCAGG	PrimerBank

NA: not applicable.

APPENDIX D. List of 108 putative pluripotency genes

Table D-1 List of 108 putative pluripotency genes detected in hPSCs and hPSC-amnion in RNA-seq. Genes[86] are consecutively listed as plotted, from left to right, in Figure 2-17.

1	*CUZD1*	**28**	*SCLY*	**55**	*TOMM40*	**82**	*RLIM*
2	*CER1*	**29**	*TXLNG*	**56**	*SEPHS1*	**83**	*RC3H2*
3	*CCL26*	**30**	*JMJD1C*	**57**	*SLIRP*	**84**	*PINX1*
4	*LEFTY2*	**31**	*EIF2AK4*	**58**	*EMG1*	**85**	*RPRM*
5	*GDF3*	**32**	*TARS*	**59**	*DDX18*	**86**	*GRPR*
6	*ADD2*	**33**	*SNURF*	**60**	*MTAP*	**87**	*GNPTAB*
7	*DDX21*	**34**	*RRP15*	**61**	*TFAM*	**88**	*FGF2*
8	*PNO1*	**35**	*USP45*	**62**	*NIP7*	**89**	*MYO1E*
9	*DPPA4*	**36**	*SHISA9*	**63**	*HSPD1*	**90**	*LARP7*
10	*RRAS2*	**37**	*NANOG*	**64**	*TIMM8A*	**91**	*CACHD1*
11	*GABRB3*	**38**	*CCRN4L*	**65**	*POU5F1*	**92**	*PHC1*
12	*RPL22L1*	**39**	*C10orf76*	**66**	*POU5F1P3*	**93**	*VRTN*
13	*MDN1*	**40**	*EXOC2*	**67**	*DDX6*	**94**	*TERF1*
14	*GAL*	**41**	*G3BP2*	**68**	*CENPN*	**95**	*CHAC2*
15	*PMAIP1*	**42**	*PHAX*	**69**	*TUBB2B*	**96**	*TDGF1*
16	*BICD1*	**43**	*CDC25A*	**70**	*DENR*	**97**	*SLC25A21*
17	*AKIRIN1*	**44**	*MTHFD1L*	**71**	*CASP3*	**98**	*USP44*
18	*FGD6*	**45**	*RNASEH1*	**72**	*SKP2*	**99**	*LEFTY1*
19	*MRS2*	**46**	*L1TD1*	**73**	*MKKS*	**100**	*NODAL*
20	*BPTF*	**47**	*LRR1*	**74**	*NUDT15*	**101**	*RRM2*
21	*KIF13A*	**48**	*MRPS30*	**75**	*FKBP4*	**102**	*GLB1L3*
22	*RAC3*	**49**	*PSME3*	**76**	*NUP160*	**103**	*C21orf88*
23	*C9orf85*	**50**	*MSH2*	**77**	*TMPO*	**104**	*SMPDL3B*
24	*DNAH14*	**51**	*EEF1E1*	**78**	*MMS22L*	**105**	*UNC5D*
25	*METTL21A*	**52**	*NLN*	**79**	*ESRP1*	**106**	*LECT1*
26	*METTL8*	**53**	*LOC100506054*	**80**	*SKIL*	**107**	*ZIC3*
27	*BCAT1*	**54**	*NOLC1*	**81**	*SNX5*	**108**	*RTP1*

APPENDIX E. Differentially regulated genes in hPSC-amnion

Table E-1 List of 50 most up-regulated genes (UP-50) and 50 most down-regulated genes (DOWN-50) in hPSC-amnion compared with hPSCs. Genes are consecutively ranked as plotted, from left to right, in Figure 2-17.

UP-50 genes				DOWN-50 genes			
Rank	Gene	**Rank**	Gene	**Rank**	Gene	**Rank**	Gene
1	*HAND1*	**26**	*PLSCR5*	**1**	*CUZD1*	**26**	*VTN*
2	*TFAP2B*	**27**	*HOXC13*	**2**	*CH25H*	**27**	*IFITM5*
3	*ISL1*	**28**	*MEIS1*	**3**	*PTGFR*	**28**	*MIRLET7BHG*
4	*LUM*	**29**	*WNT6*	**4**	*TMPRSS3*	**29**	*LOC399829*
5	*C8orf4*	**30**	*NR2F2*	**5**	*JAKMIP2-AS1*	**30**	*XIST*
6	*EVX1*	**31**	*MSX2*	**6**	*ANKRD22*	**31**	*KCNJ1*
7	*DLX5*	**32**	*CCR1*	**7**	*ISL2*	**32**	*UCP1*
8	*TBX3*	**33**	*CYSLTR2*	**8**	*RXFP1*	**33**	*TNFAIP6*
9	*HOXB2*	**34**	*EPAS1*	**9**	*PCDHB1*	**34**	*C3orf72*
10	*ERP27*	**35**	*KRT23*	**10**	*OLIG3*	**35**	*SEZ6*
11	*COL3A1*	**36**	*TP63*	**11**	*WDR49*	**36**	*CBLN4*
12	*GATA3*	**37**	*MEIS1-AS3*	**12**	*AQP7*	**37**	*LOC100127888*
13	*GUCY1A3*	**38**	*BARX2*	**13**	*NLRP10*	**38**	*FREM3*
14	*P2RY6*	**39**	*HMX1*	**14**	*NPTX1*	**39**	*TMEM114*
15	*TNFSF8*	**40**	*HOXC6*	**15**	*LOC100507387*	**40**	*DRD1*
16	*TFAP2A*	**41**	*HOXB-AS1*	**16**	*TAC1*	**41**	*DSG3*
17	*DCN*	**42**	*IGFBP7*	**17**	*GABRA1*	**42**	*PRSS56*
18	*VGLL1*	**43**	*DIO3*	**18**	*FOXE1*	**43**	*CCR9*
19	*HOXB9*	**44**	*HOXB3*	**19**	*NXF4*	**44**	*GPR17*
20	*GATA3-AS1*	**45**	*LOC642366*	**20**	*TPH2*	**45**	*PAPLN*
21	*CDX2*	**46**	*ITGA8*	**21**	*RUFY4*	**46**	*COL20A1*
22	*PGLYRP4*	**47**	*C1orf105*	**22**	*HTR1A*	**47**	*HMX2*
23	*SLC40A1*	**48**	*ANKRD1*	**23**	*SERPINB4*	**48**	*LOC100507244*
24	*CHI3L2*	**49**	*LCP1*	**24**	*NEUROG3*	**49**	*TPSB2*
25	*HAND2*	**50**	*DLX6*	**25**	*CDH19*	**50**	*MPO*

APPENDIX F. Tabulated Gene Set Enrichment Analysis Results

Table F-1 Tabulated gene set enrichment analysis results. The data set (hPSC-amnion versus hPSCs) was queried using the gene set, BIOCARTA_ALK_PATHWAY, a collection of 35 genes related to BMP signaling.

Gene set			**BIOCARTA_ALK_PATHWAY**			
Enrichment score (ES)			0.7473358			
Normalized enrichment score (NES)			2.1402795			
Nominal p-value			0			
FDR q-value			0			
FWER p-value			0			
	PROBE	GENE SYMBOL	RANK IN GENE LIST	RANK METRIC SCORE	RUNNING ES	CORE ENRICHMENT
1	BMP4	BMP4	123	6.028	0.1195	Yes
2	NOG	NOG	224	4.789	0.2144	Yes
3	TGFB2	TGFB2	328	3.962	0.2919	Yes
4	SMAD6	SMAD6	348	3.879	0.3714	Yes
5	BMP5	BMP5	434	3.509	0.4404	Yes
6	FZD1	FZD1	618	2.794	0.4904	Yes
7	NKX2-5	NKX2-5	754	2.632	0.5391	Yes
8	NPPB	NPPB	1070	1.929	0.5654	Yes
9	BMP10	BMP10	1088	1.924	0.6045	Yes
10	BMP2	BMP2	1517	1.479	0.6166	Yes
11	NPPA	NPPA	1598	1.408	0.6424	Yes
12	TGFB1	TGFB1	1638	1.381	0.6693	Yes
13	GATA4	GATA4	1660	1.356	0.6964	Yes
14	CHRD	CHRD	1747	1.294	0.7195	Yes
15	BMPR2	BMPR2	2175	1.04	0.7226	Yes
16	BMP7	BMP7	2468	0.935	0.7294	Yes
17	GSK3B	GSK3B	2661	0.885	0.7394	Yes
18	CTNNB1	CTNNB1	2873	0.824	0.7473	Yes
19	SMAD1	SMAD1	4004	0.62	0.7114	No
20	BMPR1A	BMPR1A	4196	0.593	0.7154	No

21	SMAD5	SMAD5	5296	0.452	0.6773	No
22	MEF2C	MEF2C	5496	0.428	0.6776	No
23	MAP3K7	MAP3K7	6985	0.268	0.6188	No
24	HNF1A		7505	0.217	0.6009	No
25	ATF2	ATF2	9280	0.063	0.5256	No
26	SMAD4	SMAD4	9814	0.005	0.5027	No
27	RFC1	RFC1	12640	-0.02	0.3811	No
28	ACVR1	ACVR1	13433	-0.105	0.349	No
29	TGFBR2	TGFBR2	13945	-0.164	0.3304	No
30	AXIN1	AXIN1	14035	-0.175	0.3301	No
31	DVL1	DVL1	14975	-0.301	0.2958	No
32	TGFB3	TGFB3	15146	-0.327	0.2953	No
33	APC	APC	15186	-0.333	0.3005	No
34	TGFBR1	TGFBR1	15434	-0.371	0.2975	No
35	MYL2	MYL2	20846	-1.802	0.1011	No
35	MYL2	MYL2	20846	-1.802	0.1011	No

BIBLIOGRAPHY

1. Schoenwolf, G. C., Bleyl, S. B., Brauer, P. R. and Francis-West, P. H. *Larsen's Human Embryology*. Churchill Livingstone/Elsevier, 576 (2014).

2. Niakan, K. K., Han, J., Pedersen, R. A., Simon, C. and Pera, R. A. Human pre-implantation embryo development. *Development* **139**, 829-841 (2012).

3. Hertig, A. T. and Rock, J. *Two human ova of the pre-villous stage, having a development age of about eight and nine days respectively. Contributions to Embryology* Carnegie Institution of Washington, **33**, (1945).

4. Hertig, A. T. and Rock, J. *Two human ova of the pre-villous stage, having a development age of about seven and nine days respectively*. *Contributions to Embryology* Carnegie Institution of Washington, **31**, (1949).

5. Hertig, A. T. and Rock, J. *Two human ova of the pre-villous stage, having an ovulation age of about eleven and twelve days respectively*. *Contributions to Embryology* Carnegie Institution of Washington, **29**, (1941).

6. Luckett, W. P. The development of primordial and definitive amniotic cavities in early Rhesus monkey and human embryos. *Am. J. Anat.* **144**, 149-167 (1975).

7. Enders, A. C., Schlafke, S. and Hendrickx, A. G. Differentiation of the embryonic disc, amnion, and yolk sac in the rhesus monkey. *Am. J. Anat.* **177**, 161-185 (1986).

8. Nakamura, T., Okamoto, I., Sasaki, K., Yabuta, Y., Iwatani, C., Tsuchiya, H., Seita, Y., Nakamura, S., Yamamoto, T. and Saitou, M. A developmental coordinate of pluripotency among mice, monkeys and humans. *Nature* **537**, 57-62 (2016).

9. Yan, L., Yang, M., Guo, H., Yang, L., Wu, J., Li, R., Liu, P., Lian, Y., Zheng, X., Yan, J., Huang, J., Li, M., Wu, X., Wen, L., Lao, K., Li, R., Qiao, J. and Tang, F. Single-cell RNA-Seq profiling of human preimplantation embryos and embryonic stem cells. *Nat. Struct. Mol. Biol.* **20**, 1131-1139 (2013).

10. Blakeley, P., Fogarty, N. M., del Valle, I., Wamaitha, S. E., Hu, T. X., Elder, K., Snell, P., Christie, L., Robson, P. and Niakan, K. K. Defining the three cell lineages of the human blastocyst by single-cell RNA-seq. *Development* **142**, 3151-3165 (2015).

11. Petropoulos, S., Edsgard, D., Reinius, B., Deng, Q., Panula, S. P., Codeluppi, S., Plaza Reyes, A., Linnarsson, S., Sandberg, R. and Lanner, F. Single-Cell RNA-Seq Reveals Lineage and X Chromosome Dynamics in Human Preimplantation Embryos. *Cell* **165**, 1012-1026 (2016).

12. Smith, Z. D., Chan, M. M., Humm, K. C., Karnik, R., Mekhoubad, S., Regev, A., Eggan, K. and Meissner, A. DNA methylation dynamics of the human preimplantation embryo. *Nature* **511**, 611-615 (2014).

13. Grow, E. J., Flynn, R. A., Chavez, S. L., Bayless, N. L., Wossidlo, M., Wesche, D. J., Martin, L., Ware, C. B., Blish, C. A., Chang, H. Y., Pera, R. A. and Wysocka, J. Intrinsic retroviral reactivation in human preimplantation embryos and pluripotent cells. *Nature* **522**, 221-225 (2015).

14. Warmflash, A., Sorre, B., Etoc, F., Siggia, E. D. and Brivanlou, A. H. A method to recapitulate early embryonic spatial patterning in human embryonic stem cells. *Nat. Methods* **11**, 847-854 (2014).

15. Etoc, F., Metzger, J., Ruzo, A., Kirst, C., Yoney, A., Ozair, M. Z., Brivanlou, A. H. and Siggia, E. D. A Balance between Secreted Inhibitors and Edge Sensing Controls Gastruloid Self-Organization. *Dev. Cell* **39**, 1-14 (2016).

16. Deglincerti, A., Croft, G. F., Pietila, L. N., Zernicka-Goetz, M., Siggia, E. D. and Brivanlou, A. H. Self-organization of the in vitro attached human embryo. *Nature* **533**, 251-254 (2016).

17. Shahbazi, M. N., Jedrusik, A., Vuoristo, S., Recher, G., Hupalowska, A., Bolton, V., Fogarty, N. M., Campbell, A., Devito, L. G., Ilic, D., Khalaf, Y., Niakan, K. K., Fishel, S. and Zernicka-Goetz, M. Self-organization of the human embryo in the absence of maternal tissues. *Nat. Cell Biol.* **18**, 700-708 (2016).

18. Dobreva, M. P., Pereira, P. N., Deprest, J. and Zwijsen, A. On the origin of amniotic stem cells: of mice and men. *Int. J. Dev. Biol.* **54**, 761-777 (2010).

19. Sasaki, K., Nakamura, T., Okamoto, I., Yabuta, Y., Iwatani, C., Tsuchiya, H., Seita, Y., Nakamura, S., Shiraki, N., Takakuwa, T., Yamamoto, T. and Saitou, M. The germ cell fate of cynomolgus monkeys is specified in the nascent amnion. *Dev. Cell* **39**, 169-185 (2016).

20. Ferner, K. and Mess, A. Evolution and development of fetal membranes and placentation in amniote vertebrates. *Respir. Physiol. Neurobiol.* **178**, 39-50 (2011).

21. de Melo Bernardo, A. and Chuva de Sousa Lopes, S. M. The involvement of the proamnion in the development of the anterior amnion fold in the chicken. *PLoS One* **9**, e92672 (2014).

22. Wu, J. and Izpisua Belmonte, J. C. Stem Cells: A Renaissance in Human Biology Research. *Cell* **165**, 1572-1585 (2016).

23. O'Leary, T., Heindryckx, B., Lierman, S., van Bruggen, D., Goeman, J. J., Vandewoestyne, M., Deforce, D., de Sousa Lopes, S. M. and De Sutter, P. Tracking the progression of the human inner cell mass during embryonic stem cell derivation. *Nat. Biotechnol.* **30**, 278-282 (2012).

24. Shao, Y., Sang, J. and Fu, J. On human pluripotent stem cell control: The rise of 3D bioengineering and mechanobiology. *Biomaterials* **52**, 26-43 (2015).

25. Fatehullah, A., Tan, S. H. and Barker, N. Organoids as an in vitro model of human development and disease. *Nat. Cell Biol.* **18**, 246-254 (2016).

26. Shamir, E. and Ewald, A. Three-dimensional organotypic culture: experimental models of mammalian biology and disease. *Nat. Rev. Mol. Cell Biol.* **15**, 647-664 (2014).

27. Lancaster, M. and Knoblich, J. Organogenesis in a dish: modeling development and disease using organoid technologies. *Science* **345**, 1247125 (2014).

28. Sasai, Y. Next-generation regenerative medicine: organogenesis from stem cells in 3D culture. *Cell Stem Cell* **12**, 520-530 (2013).

29. Thomson, J. A., Itskovitz-Eldor, J., Shapiro, S. S., Waknitz, M. A., Swiergiel, J. J., Marshall, V. S. and Jones, J. M. Embryonic stem cell lines derived from human blastocysts. *Science* **282**, 1145-1147 (1998).

30. Takahashi, K., Tanabe, K., Ohnuki, M., Narita, M., Ichisaka, T., Tomoda, K. and Yamanaka, S. Induction of pluripotent stem cells from adult human fibroblasts by defined factors. *Cell* **131**, 861-872 (2007).

31. Staerk, J., Dawlaty, M. M., Gao, Q., Maetzel, D., Hanna, J., Sommer, C. A., Mostoslavsky, G. and Jaenisch, R. Reprogramming of human peripheral blood cells to induced pluripotent stem cells. *Cell Stem Cell* **7**, 20-24 (2010).

32. Rodda, D. J., Chew, J. L., Lim, L. H., Loh, Y. H., Wang, B., Ng, H. H. and Robson, P. Transcriptional regulation of NANOG by OCT4 and SOX2. *J. Biol. Chem.* **280**, 24731-24737 (2005).

33. Chin, M. H., Mason, M. J., Xie, W., Volinia, S., Singer, M., Peterson, C., Ambartsumyan, G., Aimiuwu, O., Richter, L., Zhang, J., Khvorostov, I., Ott, V., Grunstein, M., Lavon, N., Benvenisty, N., Croce, C. M., Clark, A. T., Baxter, T., Pyle, A. D., Teitell, M. A., Pelegrini, M., Plath, K. and Lowry, W. E. Induced pluripotent stem cells and embryonic stem cells are distinguished by gene expression signatures. *Cell Stem Cell* **5**, 111-123 (2009).

34. Narsinh, K. H., Plews, J. and Wu, J. C. Comparison of human induced pluripotent and embryonic stem cells: fraternal or identical twins? *Mol. Ther.* **19**, 635-638 (2011).

35. Sasaki, K., Yokobayashi, S., Nakamura, T., Okamoto, I., Yabuta, Y., Kurimoto, K., Ohta, H., Moritoki, Y., Iwatani, C., Tsuchiya, H., Nakamura, S., Sekiguchi, K., Sakuma, T., Yamamoto, T., Mori, T., Woltjen, K., Nakagawa, M., Yamamoto, T., Takahashi, K., Yamanaka, S. and Saitou, M. Robust In Vitro Induction of Human Germ Cell Fate from Pluripotent Stem Cells. *Cell Stem Cell* **17**, 178-194 (2015).

36. Easley, C. A., Phillips, B. T., McGuire, M. M., Barringer, J. M., Valli, H., Hermann, B. P., Simerly, C. R., Rajkovic, A., Miki, T., Orwig, K. E. and Schatten, G. P. Direct Differentiation of Human Pluripotent Stem Cells into Haploid Spermatogenic Cells. *Cell Reports* **2**, 440-446 (2012).

37. Sperber, H., Mathieu, J., Wang, Y., Ferreccio, A., Hesson, J., Xu, Z., Fischer, K. A., Devi, A., Detraux, D., Gu, H., Battle, S. L., Showalter, M., Valensisi, C., Bielas, J. H., Ericson, N. G., Margaretha, L., Robitaille, A. M., Margineantu, D., Fiehn, O., Hockenbery, D., Blau, C. A., Raftery, D., Margolin, A. A., Hawkins, R. D., Moon, R. T., Ware, C. B. and Ruohola-Baker, H. The metabolome regulates the epigenetic landscape during naive-to-primed human embryonic stem cell transition. *Nat. Cell Biol.* **17**, 1523-1535 (2015).

38. Vallier, L., Alexander, M. and Pedersen, R. A. Activin/Nodal and FGF pathways cooperate to maintain pluripotency of human embryonic stem cells. *J. Cell Sci.* **118**, 4495-4509 (2005).

39. Takashima, Y., Guo, G., Loos, R., Nichols, J., Ficz, G., Krueger, F., Oxley, D., Santos, F., Clarke, J., Mansfield, W., Reik, W., Bertone, P. and Smith, A. Resetting transcription factor control circuitry toward ground-state pluripotency in human. *Cell* **158**, 1254-1269 (2014).

40. Guo, G., von Meyenn, F., Santos, F., Chen, Y., Reik, W., Bertone, P., Smith, A. and Nichols, J. Naive Pluripotent Stem Cells Derived Directly from Isolated Cells of the Human Inner Cell Mass. *Stem Cell Rep.* **6**, 437-446 (2016).

41. Wu, J., Okamura, D., Li, M., Suzuki, K., Luo, C., Ma, L., He, Y., Li, Z., Benner, C., Tamura, I., Krause, M. N., Nery, J. R., Du, T., Zhang, Z., Hishida, T., Takahashi, Y., Aizawa, E., Kim, N. Y., Lajara, J., Guillen, P., Campistol, J. M., Esteban, C. R., Ross, P. J., Saghatelian, A., Ren, B., Ecker, J. R. and Izpisua Belmonte, J. C. An alternative pluripotent state confers interspecies chimaeric competency. *Nature* **521**, 316-321 (2015).

42. Discher, D. E., Mooney, D. J. and Zandstra, P. W. Growth Factors, Matrices, and Forces Combine and Control Stem Cells. *Science* **324**, 1673-1677 (2009).

43. Miller, C. and Davidson, L. The interplay between cell signalling and mechanics in developmental processes. *Nat. Rev. Genet.* **14**, 733-744 (2013).

44. Ranga, A., Gjorevski, N. and Lutolf, M. P. Drug discovery through stem cell-based organoid models. *Adv. Drug Deliver. Rev* **69**, 19-28 (2014).

45. Nakano, T., Ando, S., Takata, N., Kawada, M., Muguruma, K., Sekiguchi, K., Saito, K., Yonemura, S., Eiraku, M. and Sasai, Y. Self-formation of optic cups and storable stratified neural retina from human ESCs. *Cell Stem Cell* **10**, 771-785 (2012).

46. Eiraku, M., Watanabe, K., Matsuo-Takasaki, M., Kawada, M., Yonemura, S., Matsumura, M., Wataya, T., Nishiyama, A., Muguruma, K. and Sasai, Y. Self-organized formation of polarized cortical tissues from ESCs and its active manipulation by extrinsic signals. *Cell Stem Cell* **3**, 519-532 (2008).

47. Mariani, J., Simonini, M., Palejev, D., Tomasini, L., Coppola, G., Szekely, A., Horvath, T. and Vaccarino, F. Modeling human cortical development in vitro using induced pluripotent stem cells. *Proc. Natl. Acad. Sci. U. S. A.* **109**, 12770-12775 (2012).

48. Ozone, C., Suga, H., Eiraku, M., Kadoshima, T., Yonemura, S., Takata, N., Oiso, Y., Tsuji, T. and Sasai, Y. Functional anterior pituitary generated in self-organizing culture of human embryonic stem cells. *Nat. Commun.* **7**, 10351 (2016).

49. Lancaster, M., Renner, M., Martin, C.-A., Wenzel, D., Bicknell, L., Hurles, M., Homfray, T., Penninger, J., Jackson, A. and Knoblich, J. Cerebral organoids model human brain development and microcephaly. *Nature* **501**, 373-379 (2013).

50. Takasato, M., Er, P. X., Becroft, M., Vanslambrouck, J. M., Stanley, E. G., Elefanty, A. G. and Little, M. H. Directing human embryonic stem cell differentiation towards a renal lineage generates a self-organizing kidney. *Nat. Cell Biol.* **16**, 118-126 (2014).

51. Takasato, M., Er, P. X., Chiu, H. S., Maier, B., Baillie, G. J., Ferguson, C., Parton, R. G., Wolvetang, E. J., Roost, M. S., Chuva de Sousa Lopes, S. M. and Little, M. H. Kidney organoids from human iPS cells contain multiple lineages and model human nephrogenesis. *Nature* **526**, 564-568 (2015).

52. Kusuma, S., Shen, Y. I., Hanjaya-Putra, D., Mali, P., Cheng, L. and Gerecht, S. Self-organized vascular networks from human pluripotent stem cells in a synthetic matrix. *Proc. Natl. Acad. Sci. U. S. A.* **110**, 12601-12606 (2013).

53. Samuel, R., Daheron, L., Liao, S., Vardam, T., Kamoun, W., Batista, A., Buecker, C., Schäfer, R., Han, X., Au, P., Scadden, D., Duda, D., Fukumura, D. and Jain, R. Generation of functionally competent and durable engineered blood vessels from human induced pluripotent stem cells. *Proc. Natl. Acad. Sci. U. S. A.* (2013).

54. Spence, J. R., Mayhew, C. N., Rankin, S. A., Kuhar, M. F., Vallance, J. E., Tolle, K., Hoskins, E. E., Kalinichenko, V. V., Wells, S. I., Zorn, A. M., Shroyer, N. F. and Wells, J. M. Directed differentiation of human pluripotent stem cells into intestinal tissue in vitro. *Nature* **470**, 105-109 (2011).

55. Watson, C., Mahe, M., Múnera, J., Howell, J., Sundaram, N., Poling, H., Schweitzer, J., Vallance, J., Mayhew, C., Sun, Y., Grabowski, G., Finkbeiner, S., Spence, J., Shroyer, N., Wells, J. and Helmrath, M. An in vivo model of human small intestine using pluripotent stem cells. *Nat. Med.* **In press**, (2014).

56. McCracken, K. W., Cata, E. M., Crawford, C. M., Sinagoga, K. L., Schumacher, M., Rockich, B. E., Tsai, Y. H., Mayhew, C. N., Spence, J. R., Zavros, Y. and Wells, J. M.

Modelling human development and disease in pluripotent stem-cell-derived gastric organoids. *Nature* **516**, 400-404 (2014).

57. Takebe, T., Sekine, K., Enomura, M., Koike, H., Kimura, M., Ogaeri, T., Zhang, R. R., Ueno, Y., Zheng, Y. W., Koike, N., Aoyama, S., Adachi, Y. and Taniguchi, H. Vascularized and functional human liver from an iPSC-derived organ bud transplant. *Nature* **499**, 481-484 (2013).

58. Huang, L., Holtzinger, A., Jagan, I., BeGora, M., Lohse, I., Ngai, N., Nostro, C., Wang, R., Muthuswamy, L. B., Crawford, H. C., Arrowsmith, C., Kalloger, S. E., Renouf, D. J., Connor, A. A., Cleary, S., Schaeffer, D. F., Roehrl, M., Tsao, M. S., Gallinger, S., Keller, G. and Muthuswamy, S. K. Ductal pancreatic cancer modeling and drug screening using human pluripotent stem cell- and patient-derived tumor organoids. *Nat. Med.* **21**, 1364-1371 (2015).

59. Dye, B. R., Hill, D. R., Ferguson, M. A., Tsai, Y. H., Nagy, M. S., Dyal, R., Wells, J. M., Mayhew, C. N., Nattiv, R., Klein, O. D., White, E. S., Deutsch, G. H. and Spence, J. R. In vitro generation of human pluripotent stem cell derived lung organoids. *Elife* **4**, e05098 (2015).

60. Dye, B. R., Dedhia, P. H., Miller, A. J., Nagy, M. S., White, E. S., Shea, L. D. and Spence, J. R. A bioengineered niche promotes in vivo engraftment and maturation of pluripotent stem cell derived human lung organoids. *Elife* **5**, e19732 (2016).

61. Huang, L., Holtzinger, A., Jagan, I., BeGora, M., Lohse, I., Ngai, N., Nostro, C., Wang, R., Muthuswamy, L. B., Crawford, H. C., Arrowsmith, C., Kalloger, S. E., Renouf, D. J., Connor, A. A., Cleary, S., Schaeffer, D. F., Roehrl, M., Tsao, M. S., Gallinger, S., Keller, G. and Muthuswamy, S. K. Ductal pancreatic cancer modeling and drug screening using human pluripotent stem cell- and patient-derived tumor organoids. *Nat. Med.* **21**, 1364-1371 (2015).

62. Zheng, Y., Ji, S., Wu, H., Tian, S., Zhang, Y., Wang, L., Fang, H., Luo, P., Wang, X., Hu, X., Xiao, S. and Xia, Z. Topical administration of cryopreserved living micronized amnion accelerates wound healing in diabetic mice by modulating local microenvironment. *Biomaterials* **113**, 56-67 (2016).

63. Taniguchi, K., Shao, Y., Townshend, R. F., Tsai, Y. H., DeLong, C. J., Lopez, S. A., Gayen, S., Freddo, A. M., Chue, D. J., Thomas, D. J., Spence, J. R., Margolis, B., Kalantry, S., Fu, J. P., O'Shea, K. S. and Gumucio, D. L. Lumen formation is an intrinsic property of isolated human pluripotent stem cells. *Stem Cell Rep.* **5**, 954-962 (2015).

64. Chaudhuri, O., Koshy, S. T., Branco da Cunha, C., Shin, J. W., Verbeke, C. S., Allison, K. H. and Mooney, D. J. Extracellular matrix stiffness and composition jointly regulate the induction of malignant phenotypes in mammary epithelium. *Nature Mater.* **13**, 970-978 (2014).

65. Watanabe, K., Ueno, M., Kamiya, D., Nishiyama, A., Matsumura, M., Wataya, T., Takahashi, J. B., Nishikawa, S., Nishikawa, S., Muguruma, K. and Sasai, Y. A ROCK

inhibitor permits survival of dissociated human embryonic stem cells. *Nat. Biotechnol.* **25**, 681-686 (2007).

66. Tse, J. and Engler, A. Preparation of hydrogel substrates with tunable mechanical properties. *Current Protocols in Cell Biology* **Ch. 10**, (2010).

67. Fischer, R., Myers, K., Gardel, M. and Waterman, C. Stiffness-controlled three-dimensional extracellular matrices for high-resolution imaging of cell behavior. *Nat. Protoc.* **7**, 2056-2066 (2012).

68. Buxboim, A., Rajagopal, K., Brown, A. E. X. and Discher, D. E. How deeply cells feel: Methods for thin gels. *J. Phys.: Condens. Mat.* **22**, 194116 (2010).

69. Koschwanez, J. H., Carlson, R. H. and Meldrum, D. R. Thin PDMS films using long spin times or Tert-Butyl Alcohol as a solvent. *PLoS One* **4**, e4572 (2009).

70. Fu, J., Wang, Y.-K., Yang, M., Desai, R., Yu, X., Liu, Z. and Chen, C. Mechanical regulation of cell function with geometrically modulated elastomeric substrates. *Nat. Methods* **7**, 733-736 (2010).

71. Shao, Y., Mann, J. M., Chen, W. Q. and Fu, J. P. Global architecture of the F-actin cytoskeleton regulates cell shape-dependent endothelial mechanotransduction. *Integr. Biol.* **6**, 300-311 (2014).

72. Weng, S. and Fu, J. Synergistic regulation of cell function by matrix rigidity and adhesive pattern. *Biomaterials* **32**, 9584-9593 (2011).

73. Mendjan, S., Mascetti, V. L., Ortmann, D., Ortiz, M., Karjosukarso, D. W., Ng, Y., Moreau, T. and Pedersen, R. A. NANOG and CDX2 pattern distinct subtypes of human mesoderm during exit from pluripotency. *Cell Stem Cell* **15**, 310-325 (2014).

74. Ben-David, U., Nudel, N. and Benvenisty, N. Immunologic and chemical targeting of the tight-junction protein Claudin-6 eliminates tumorigenic human pluripotent stem cells. *Nat. Commun.* **4**, 1992 (2013).

75. Buxboim, A., Ivanovska, I. and Discher, D. Matrix elasticity, cytoskeletal forces and physics of the nucleus: how deeply do cells 'feel' outside and in? *J. Cell Sci.* **123**, 297-308 (2010).

76. Thiery, J., Acloque, H., Huang, R. and Nieto, M. Epithelial-mesenchymal transitions in development and disease. *Cell* **139**, 871-890 (2009).

77. Zhang, X. Q., Huang, C. T., Chen, J., Pankratz, M. T., Xi, J. J., Li, J., Yang, Y., LaVaute, T. M., Li, X. J., Ayala, M., Bondarenko, G. I., Du, Z. W., Jin, Y., Golos, T. G. and Zhang, S. C. Pax6 Is a human neuroectoderm cell fate determinant. *Cell Stem Cell* **7**, 90-100 (2010).

78. Li, Y. C., Moretto-Zita, M., Soncin, F., Wakeland, A., Wolfe, L., Leon-Garcia, S., Pandian, R., Pizzo, D., Cui, L., Nazor, K., Loring, J. F., Crum, C. P., Laurent, L. C. and Parast, M. M.

BMP4-directed trophoblast differentiation of human embryonic stem cells is mediated through Delta Np63(+) cytotrophoblast stem cell state. *Development* **140**, 3965-3976 (2013).

79. Lee, C. Q. E., Gardner, L., Turco, M., Zhao, N., Murray, M. J., Coleman, N., Rossant, J., Hemberger, M. and Moffett, A. What is trophoblast? A combination of criteria define human first-trimester trophoblast. *Stem Cell Rep.* **6**, 257-272 (2016).

80. Henderson, J. K., Draper, J. S., Baillie, H. S., Fishel, S., Thomson, J. A., Moore, H. and Andrews, P. W. Preimplantation human embryos and embryonic stem cells show comparable expression of stage-specific embryonic antigens. *Stem Cells* **20**, 329-337 (2002).

81. Roost, M. S., van Iperen, L., Ariyurek, Y., Buermans, H. P., Arindrarto, W., Devalla, H. D., Passier, R., Mummery, C. L., Carlotti, F., de Koning, E. J. P., van Zwet, E. W., Goeman, J. J. and Lopes, S. M. C. D. KeyGenes, a tool to probe tissue differentiation using a human fetal transcriptional atlas. *Stem Cell Rep.* **4**, 1112-1124 (2015).

82. Miki, T. and Strom, S. C. Amnion-derived pluripotent/multipotent stem cells. *Stem Cell Rev.* **2**, 133-141 (2006).

83. Dobreva, M. P., Lhoest, L., Pereira, P. N. G., Umans, L., Lopes, S. M. C. D. and Zwijsen, A. Periostin as a biomarker of the amniotic membrane. *Stem Cells Int.* **2012**, 987185 (2012).

84. Slieker, R. C., Roost, M. S., van Iperen, L., Suchiman, H. E. D., Tobi, E. W., Carlotti, F., de Koning, E. J. P., Slagboom, P. E., Heijmans, B. T. and Lopes, S. M. C. D. DNA methylation landscapes of human fetal development. *Plos Genetics* **11**, e1005583 (2015).

85. Regauer, S., Franke, W. W. and Virtanen, I. Intermediate filament cytoskeleton of amnion epithelium and cultured amnion epithelial-cells - expression of epidermal cytokeratins in cells of a simple epithelium. *J. Cell Biol.* **100**, 997-1009 (1985).

86. Mallon, B. S., Chenoweth, J. G., Johnson, K. R., Hamilton, R. S., Tesar, P. J., Yavatkar, A. S., Tyson, L. J., Park, K., Chen, K. G., Fann, Y. C. and McKay, R. D. G. StemCellDB: The human pluripotent stem cell database at the National Institutes of Health. *Stem Cell Res.* **10**, 57-66 (2013).

87. Graham, S. J. L., Wicher, K. B., Jedrusik, A., Guo, G. J., Herath, W., Robson, P. and Zernicka-Goetz, M. BMP signalling regulates the pre-implantation development of extra-embryonic cell lineages in the mouse embryo. *Nat. Commun.* **5**, 5667 (2014).

88. Pereira, P. N., Dobreva, M. P., Graham, L., Huylebroeck, D., Lawson, K. A. and Zwijsen, A. N. Amnion formation in the mouse embryo: the single amniochorionic fold model. *BMC Dev. Biol.* **11**, 48 (2011).

89. Sun, Y., Villa-Diaz, L., Lam, R., Chen, W., Krebsbach, P. and Fu, J. Mechanics regulates fate decisions of human embryonic stem cells. *PLoS One* **7**, (2012).

90. Tesar, P. J., Chenoweth, J. G., Brook, F. A., Davies, T. J., Evans, E. P., Mack, D. L., Gardner, R. L. and McKay, R. D. New cell lines from mouse epiblast share defining features with human embryonic stem cells. *Nature* **448**, 196-199 (2007).

91. Tomonori Nakamura, Ikuhiro Okamoto, Sasaki, K., Yabuta, Y., Chizuru Iwatani, Hideaki Tsuchiya, Seita, Y., Shinichiro Nakamura, Yamamoto, T. and Saitou, M. A developmental coordinate of pluripotency among mice, monkeys and humans. *Nature* **In press**, (2016).

92. Shao, Y., Taniguchi, K., Gurdziel, K., Townshend, R. F., Xue, X., Yong, K. M. A., Sang, J., Spence, J. R., Gumucio, D. L. and Fu, J. Self-organized amniogenesis by human pluripotent stem cells in a biomimetic implantation-like niche. *Nature Mater.* **In press**, Published online on Dec. 12th, DOI: 10.1038/NMAT4829 (2016).

93. Heuser, C. H., Rock, J. and Hertig, A. T. *Two human embryos showing early stages of the definitive yolk sac*. *Contributions to Embryology* Carnegie Institution of Washington, **31**, (1945).

94. Bernardo, A. S., Faial, T., Gardner, L., Niakan, K. K., Ortmann, D., Senner, C. E., Callery, E. M., Trotter, M. W., Hemberger, M., Smith, J. C., Bardwell, L., Moffett, A. and Pedersen, R. A. BRACHYURY and CDX2 mediate BMP-induced differentiation of human and mouse pluripotent stem cells into embryonic and extraembryonic lineages. *Cell Stem Cell* **9**, 144-155 (2011).

95. Faial, T., Bernardo, A. S., Mendjan, S., Diamanti, E., Ortmann, D., Gentsch, G. E., Mascetti, V. L., Trotter, M. W. B., Smith, J. C. and Pedersen, R. A. Brachyury and SMAD signalling collaboratively orchestrate distinct mesoderm and endoderm gene regulatory networks in differentiating human embryonic stem cells. *Development* **142**, 2121-2135 (2015).

96. Zhang, H. B. and Bradley, A. Mice deficient for BMP2 are nonviable and have defects in amnion chorion and cardiac development. *Development* **122**, 2977-2986 (1996).

97. Chang, H., Huylebroeck, D., Verschueren, K., Guo, Q. X., Matzuk, M. M. and Zwijsen, A. Smad5 knockout mice die at mid-gestation due to multiple embryonic and extraembryonic defects. *Development* **126**, 1631-1642 (1999).

98. Metallo, C. M., Ji, L., de Pablo, J. J. and Palecek, S. P. Retinoic acid and bone morphogenetic protein signaling synergize to efficiently direct epithelial differentiation of human embryonic stem cells. *Stem Cells* **26**, 372-380 (2008).

99. Sarno, A. P., Jr., Ahn, M. O. and Phelan, J. P. Intrapartum amniotic fluid volume at term. Association of ruptured membranes, oligohydramnios and increased fetal risk. *J. Reprod. Med.* **35**, 719-723 (1990).

100. Ananth, C. V., Oyelese, Y., Srinivas, N., Yeo, L. and Vintzileos, A. M. Preterm premature rupture of membranes, intrauterine infection, and oligohydramnios: risk factors for placental abruption. *Obstet. Gynecol.* **104**, 71-77 (2004).

101. Thibeault, D. W., Beatty, E. C., Jr., Hall, R. T., Bowen, S. K. and O'Neill, D. H. Neonatal pulmonary hypoplasia with premature rupture of fetal membranes and oligohydramnios. *J. Pediatr.* **107**, 273-277 (1985).

102. Seeds, J. W., Cefalo, R. C. and Herbert, W. N. Amniotic band syndrome. *Am. J. Obstet. Gynecol.* **144**, 243-248 (1982).

103. Macarron, R., Banks, M. N., Bojanic, D., Burns, D. J., Cirovic, D. A., Garyantes, T., Green, D. V., Hertzberg, R. P., Janzen, W. P., Paslay, J. W., Schopfer, U. and Sittampalam, G. S. Impact of high-throughput screening in biomedical research. *Nat. Rev. Drug Discov.* **10**, 188-195 (2011).

104. Park, J. U., Hardy, M., Kang, S. J., Barton, K., Adair, K., Mukhopadhyay, D. K., Lee, C. Y., Strano, M. S., Alleyne, A. G., Georgiadis, J. G., Ferreira, P. M. and Rogers, J. A. High-resolution electrohydrodynamic jet printing. *Nature Mater.* **6**, 782-789 (2007).

105. Azioune, A., Carpi, N., Tseng, Q., Théry, M. and Piel, M. Protein micropatterns: A direct printing protocol using deep UVs. *Method. Cell Biol.* **97**, 133-146 (2010).

106. Gobaa, S., Hoehnel, S., Roccio, M., Negro, A., Kobel, S. and Lutolf, M. Artificial niche microarrays for probing single stem cell fate in high throughput. *Nat. Methods* **8**, 949-955 (2011).

107. Qin, D., Xia, Y. and Whitesides, G. Soft lithography for micro- and nanoscale patterning. *Nat. Protoc.* **5**, 491-502 (2010).

108. Higuchi, A., Ling, Q.-D., Chang, Y., Hsu, S.-T. and Umezawa, A. Physical cues of biomaterials guide stem cell differentiation fate. *Chem. Rev.* **113**, 3297-3328 (2013).

109. Sun, Y. B., Chen, C. S. and Fu, J. P. Forcing Stem Cells to Behave: A Biophysical Perspective of the Cellular Microenvironment. *Annu. Rev. Biophys.* **41**, 519-542 (2012).

110. Eyckmans, J., Boudou, T., Yu, X. and Chen, C. A hitchhiker's guide to mechanobiology. *Dev. Cell* **21**, 35-47 (2011).

111. Sun, Y. B., Villa-Diaz, L. G., Lam, R. H. W., Chen, W. Q., Krebsbach, P. H. and Fu, J. P. Mechanics Regulates Fate Decisions of Human Embryonic Stem Cells. *PLoS One* **7**, e37178 (2012).

112. Musah, S., Morin, S. A., Wrighton, P. J., Zwick, D. B., Jin, S. and Kiessling, L. L. Glycosaminoglycan-Binding Hydrogels Enable Mechanical Control of Human Pluripotent Stem Cell Self-Renewal. *ACS Nano* **6**, 10168-10177 (2012).

113. Sun, Y. B., Aw Yong, K. M., Villa-Diaz, L. G., Zhang, X. L., Chen, W. Q., Philson, R., Weng, S. N., Xu, H. X., Krebsbach, P. H. and Fu, J. P. Hippo/YAP-mediated rigidity-dependent motor neuron differentiation of human pluripotent stem cells. *Nature Mater.* **13**, 599-604 (2014).

114. Chen, W., Villa-Diaz, L., Sun, Y., Weng, S., Kim, J., Lam, R., Han, L., Fan, R., Krebsbach, P. and Fu, J. Nanotopography influences adhesion, spreading, and self-renewal of human embryonic stem cells. *ACS Nano* **6**, 4094-4103 (2012).

115. Ross, A., Jiang, Z., Bastmeyer, M. and Lahann, J. Physical aspects of cell culture substrates: topography, roughness, and elasticity. *Small* **8**, 336-355 (2012).

116. Kim, D.-H., Provenzano, P., Smith, C. and Levchenko, A. Matrix nanotopography as a regulator of cell function. *J. Cell Biol.* **197**, 351-360 (2012).

117. Nazareth, E. J. P., Ostblom, J. E. E., Lucker, P. B., Shukla, S., Alvarez, M. M., Oh, S. K. W., Yin, T. and Zandstra, P. W. High-throughput fingerprinting of human pluripotent stem cell fate responses and lineage bias. *Nat. Methods* **10**, 1225-+ (2013).

118. Khetan, S., Guvendiren, M., Legant, W., Cohen, D., Chen, C. and Burdick, J. Degradation-mediated cellular traction directs stem cell fate in covalently crosslinked three-dimensional hydrogels. *Nature Mater.* **12**, 458-465 (2013).

119. Minc, N., Burgess, D. and Chang, F. Influence of cell geometry on division-plane positioning. *Cell* **144**, 414-426 (2011).

120. McBeath, R., Pirone, D. M., Nelson, C. M., Bhadriraju, K. and Chen, C. S. Cell shape, cytoskeletal tension, and RhoA regulate stem cell lineage commitment. *Dev. Cell* **6**, 483-495 (2004).

121. Kilian, K., Bugarija, B., Lahn, B. and Mrksich, M. Geometric cues for directing the differentiation of mesenchymal stem cells. *Proc. Natl. Acad. Sci. U. S. A.* **107**, 4872-4877 (2010).

122. Lee, J., Abdeen, A. A., Wycislo, K. L., Fan, T. M. and Kilian, K. A. Interfacial geometry dictates cancer cell tumorigenicity. *Nat Mater* **15**, 856-862 (2016).

123. Dave, P. C., Dingal, P. and Discher, D. E. Combining insoluble and soluble factors to steer stem cell fate. *Nature Mater.* **13**, 532-537 (2014).

124. Engler, A., Sen, S., Sweeney, H. and Discher, D. Matrix elasticity directs stem cell lineage specification. *Cell* **126**, 677-689 (2006).

125. Zhou, J. A., Kim, H. Y., Wang, J. H. C. and Davidson, L. A. Macroscopic stiffening of embryonic tissues via microtubules, RhoGEF and the assembly of contractile bundles of actomyosin. *Development* **137**, 2785-2794 (2010).

126. Guvendiren, M. and Burdick, J. Stiffening hydrogels to probe short- and long-term cellular responses to dynamic mechanics. *Nat. Commun.* **3**, 792 (2012).

127. Young, J. L. and Engler, A. J. Hydrogels with time-dependent material properties enhance cardiomyocyte differentiation in vitro. *Biomaterials* **32**, 1002-1009 (2011).

128. Dalby, M., Gadegaard, N., Tare, R., Andar, A., Riehle, M., Herzyk, P., Wilkinson, C. and Oreffo, R. The control of human mesenchymal cell differentiation using nanoscale symmetry and disorder. *Nature Mater.* **6**, 997-1003 (2007).

129. Oh, S., Brammer, K., Li, Y., Teng, D., Engler, A., Chien, S. and Jin, S. Stem cell fate dictated solely by altered nanotube dimension. *Proc. Natl. Acad. Sci. U. S. A.* **106**, 2130-2135 (2009).

130. Lee, J., Abdeen, A. A., Zhang, D. and Kilian, K. A. Directing stem cell fate on hydrogel substrates by controlling cell geometry, matrix mechanics and adhesion ligand composition. *Biomaterials* **34**, 8140-8148 (2013).

131. Krumlauf, R. Hox genes in vertebrate development. *Cell* **78**, 191-201 (1994).

132. Pearson, J. C., Lemons, D. and McGinnis, W. Modulating Hox gene functions during animal body patterning. *Nat. Rev. Genet.* **6**, 893-904 (2005).

133. Ludwig, T. E., Levenstein, M. E., Jones, J. M., Berggren, W. T., Mitchen, E. R., Frane, J. L., Crandall, L. J., Daigh, C. A., Conard, K. R., Piekarczyk, M. S., Llanas, R. A. and Thomson, J. A. Derivation of human embryonic stem cells in defined conditions. *Nat. Biotechnol.* **24**, 185-187 (2006).

134. Yamaguchi, T. P. Heads or tails: Wnts and anterior-posterior patterning. *Curr. Biol.* **11**, R713-724 (2001).

135. Chen, G., Hou, Z., Gulbranson, D. and Thomson, J. Actin-myosin contractility is responsible for the reduced viability of dissociated human embryonic stem cells. *Cell stem cell* **7**, 240-248 (2010).

136. Arnold, S. J. and Robertson, E. J. Making a commitment: cell lineage allocation and axis patterning in the early mouse embryo. *Nat. Rev. Mol. Cell Biol.* **10**, 91-103 (2009).

137. Bagnat, M., Cheung, I. D., Mostov, K. E. and Stainier, D. Y. Genetic control of single lumen formation in the zebrafish gut. *Nat. Cell Biol.* **9**, 954-960 (2007).

138. Bolos, V., Peinado, H., Perez-Moreno, M. A., Fraga, M. F., Esteller, M. and Cano, A. The transcription factor Slug represses E-cadherin expression and induces epithelial to mesenchymal transitions: a comparison with Snail and E47 repressors. *J. Cell Sci.* **116**, 499-511 (2003).

139. Sander, J. D. and Joung, J. K. CRISPR-Cas systems for editing, regulating and targeting genomes. *Nat. Biotechnol.* **32**, 347-355 (2014).

140. Hsu, P. D., Lander, E. S. and Zhang, F. Development and applications of CRISPR-Cas9 for genome engineering. *Cell* **157**, 1262-1278 (2014).

141. Liem, K. F., Jr., Tremml, G., Roelink, H. and Jessell, T. M. Dorsal differentiation of neural plate cells induced by BMP-mediated signals from epidermal ectoderm. *Cell* **82**, 969-979 (1995).

142. van Wijk, B., Moorman, A. F. and van den Hoff, M. J. Role of bone morphogenetic proteins in cardiac differentiation. *Cardiovasc. Res.* **74**, 244-255 (2007).

143. Humphrey, J. D., Dufresne, E. R. and Schwartz, M. A. Mechanotransduction and extracellular matrix homeostasis. *Nat. Rev. Mol. Cell Biol.* **15**, 802-812 (2014).

144. Chen, W., Shao, Y., Li, X., Zhao, G. and Fu, J. Nanotopographical Surfaces for Stem Cell Fate Control: Engineering Mechanobiology from the Bottom. *Nano Today* **9**, 759-784 (2014).

145. Schwartz, Martin, Ginsberg and Mark. Networks and crosstalk: integrin signalling spreads. *Nat. Cell Biol.* **4**, E65-E68 (2002).

146. Arnaout, M., Goodman, S. and Xiong, J.-P. Structure and mechanics of integrin-based cell adhesion. *Curr. Opin. Cell Biol.* **19**, 495-507 (2007).

147. Rossier, O., Octeau, V., Sibarita, J.-B., Leduc, C., Tessier, B., Nair, D., Gatterdam, V., Destaing, O., Albigès-Rizo, C., Tampé, R., Cognet, L., Choquet, D., Lounis, B. and Giannone, G. Integrins β1 and β3 exhibit distinct dynamic nanoscale organizations inside focal adhesions. *Nat. Cell Biol.* **14**, 1057-1067 (2012).

148. Schiller, H., Hermann, M.-R., Polleux, J., Vignaud, T., Zanivan, S., Friedel, C., Sun, Z., Raducanu, A., Gottschalk, K.-E., Théry, M., Mann, M. and Fässler, R. β1- and αv-class integrins cooperate to regulate myosin II during rigidity sensing of fibronectin-based microenvironments. *Nat. Cell Biol.* **15**, 625-636 (2013).

149. Li, L., Bennett, S. A. L. and Wang, L. S. Role of E-cadherin and other cell adhesion molecules in survival and differentiation of human pluripotent stem cells. *Cell Adhesion & Migration* **6**, 59-70 (2012).

150. Meng, Y., Eshghi, S., Li, Y. J., Schmidt, R., Schaffer, D. V. and Healy, K. E. Characterization of integrin engagement during defined human embryonic stem cell culture. *FASEB J.* **24**, 1056-1065 (2010).

151. Rowland, T. J., Miller, L. M., Blaschke, A. J., Doss, E. L., Bonham, A. J., Hikita, S. T., Johnson, L. V. and Clegg, D. O. Roles of Integrins in Human Induced Pluripotent Stem Cell Growth on Matrigel and Vitronectin. *Stem Cells and Development* **19**, 1231-1240 (2010).

152. Hynes, R. Integrins: bidirectional, allosteric signaling machines. *Cell* (2002).

153. Qin, J., Vinogradova, O. and Plow, E. Integrin bidirectional signaling: a molecular view. *PLoS Biol.* **2**, (2004).

154. Askari, J. A., Buckley, P. A., Mould, A. P. and Humphries, M. J. Linking integrin conformation to function. *J. Cell Sci.* **122**, 165-170 (2009).

155. Geiger, B., Spatz, J. and Bershadsky, A. Environmental sensing through focal adhesions. *Nat. Rev. Mol. Cell Biol.* **10**, 21-33 (2009).

156. Zaidel-Bar, R. and Geiger, B. The switchable integrin adhesome. *J. Cell Sci.* **123**, 1385-1388 (2010).

157. Kanchanawong, P., Shtengel, G., Pasapera, A., Ramko, E., Davidson, M., Hess, H. and Waterman, C. Nanoscale architecture of integrin-based cell adhesions. *Nature* **468**, 580-584 (2010).

158. Chen, C. S. Mechanotransduction - a field pulling together? *J. Cell Sci.* **121**, 3285-3292 (2008).

159. Wolfenson, H., Bershadsky, A., Henis, Y. and Geiger, B. Actomyosin-generated tension controls the molecular kinetics of focal adhesions. *J. Cell Sci.* **124**, 1425-1432 (2011).

160. Balaban, N., Schwarz, U., Riveline, D., Goichberg, P., Tzur, G., Sabanay, I., Mahalu, D., Safran, S., Bershadsky, A., Addadi, L. and Geiger, B. Force and focal adhesion assembly: a close relationship studied using elastic micropatterned substrates. *Nat. Cell Biol.* **3**, 466-472 (2001).

161. Weng, S., Shao, Y., Chen, W. and Fu, J. Mechanosensitive subcellular rheostasis drives emergent single-cell mechanical homeostasis. *Nature Mater.* **15**, 961-967 (2016).

162. Mitra, S., Hanson, D. and Schlaepfer, D. Focal adhesion kinase: in command and control of cell motility. *Nat. Rev. Mol. Cell Biol.* **6**, 56-68 (2005).

163. Seong, J., Tajik, A., Sun, J., Guan, J. L., Humphries, M. J., Craig, S. E., Shekaran, A., Garcia, A. J., Lu, S. Y., Lin, M. Z., Wang, N. and Wang, Y. X. Distinct biophysical mechanisms of focal adhesion kinase mechanoactivation by different extracellular matrix proteins. *Proc. Natl. Acad. Sci. U. S. A.* **110**, 19372-19377 (2013).

164. Schlaepfer, D. D., Hanks, S. K., Hunter, T. and Vandergeer, P. Integrin-Mediated Signal-Transduction Linked to Ras Pathway by Grb2 Binding to Focal Adhesion Kinase. *Nature* **372**, 786-791 (1994).

165. Hong, S. Y., Jeon, Y. M., Lee, H. J., Kim, J. G., Baek, J. A. and Lee, J. C. Activation of RhoA and FAK induces ERK-mediated osteopontin expression in mechanical force-subjected periodontal ligament fibroblasts. *Mol. Cell Biochem.* **335**, 263-272 (2010).

166. Wary, K. K., Mariotti, A., Zurzolo, C. and Giancotti, F. G. A requirement for caveolin-1 and associated kinase Fyn in integrin signaling and anchorage-dependent cell growth. *Cell* **94**, 625-634 (1998).

167. Aikawa, R., Nagai, T., Kudoh, S., Zou, Y. Z., Tanaka, M., Tamura, M., Akazawa, H., Takano, H., Nagai, R. and Komuro, I. Integrins play a critical role in mechanical stress-induced p38 MAPK activation. *Hypertension* **39**, 233-238 (2002).

168. Oktay, M., Wary, K. K., Dans, M., Birge, R. B. and Giancotti, F. G. Integrin-mediated activation of focal adhesion kinase is required for signaling to Jun NH2-terminal kinase and progression through the G1 phase of the cell cycle. *J. Cell Biol.* **145**, 1461-1469 (1999).

169. Guilluy, C., Swaminathan, V., Garcia-Mata, R., O'Brien, E. T., Superfine, R. and Burridge, K. The Rho GEFs LARG and GEF-H1 regulate the mechanical response to force on integrins. *Nat. Cell Biol.* **13**, 722-727 (2011).

170. Shih, Y. R., Tseng, K. F., Lai, H. Y., Lin, C. H. and Lee, O. K. Matrix stiffness regulation of integrin-mediated mechanotransduction during osteogenic differentiation of human mesenchymal stem cells. *J. Bone Miner. Res.* **26**, 730-738 (2011).

171. Brundage, M. E., Tandon, P., Eaves, D. W., Williams, J. P., Miller, S. J., Hennigan, R. H., Jegga, A., Cripe, T. P. and Ratner, N. MAF mediates crosstalk between Ras-MAPK and mTOR signaling in NF1. *Oncogene* **33**, 5626-5636 (2014).

172. DuFort, C., Paszek, M. and Weaver, V. Balancing forces: architectural control of mechanotransduction. *Nat. Rev. Mol. Cell Biol.* **12**, 308-319 (2011).

173. Yeung, T., Georges, P., Flanagan, L., Marg, B., Ortiz, M., Funaki, M., Zahir, N., Ming, W., Weaver, V. and Janmey, P. Effects of substrate stiffness on cell morphology, cytoskeletal structure, and adhesion. *Cell Motil. Cytoskel.* **60**, 24-34 (2005).

174. Wada, K. I., Itoga, K., Okano, T., Yonemura, S. and Sasaki, H. Hippo pathway regulation by cell morphology and stress fibers. *Development.* **138**, 3907-3914 (2011).

175. Mo, J. S., Park, H. W. and Guan, K. L. The Hippo signaling pathway in stem cell biology and cancer. *EMBO Rep.* **15**, 642-656 (2014).

176. Dong, J. X., Feldmann, G., Huang, J. B., Wu, S., Zhang, N. L., Comerford, S. A., Gayyed, M. F., Anders, R. A., Maitra, A. and Pan, D. J. Elucidation of a universal size-control mechanism in Drosophila and mammals. *Cell* **130**, 1120-1133 (2007).

177. Dupont, S., Morsut, L., Aragona, M., Enzo, E., Giulitti, S., Cordenonsi, M., Zanconato, F., Le Digabel, J., Forcato, M., Bicciato, S., Elvassore, N. and Piccolo, S. Role of YAP/TAZ in mechanotransduction. *Nature* **474**, 179-183 (2011).

178. Aragona, M., Panciera, T., Manfrin, A., Giulitti, S., Michielin, F., Elvassore, N., Dupont, S. and Piccolo, S. A Mechanical Checkpoint Controls Multicellular Growth through YAP/TAZ Regulation by Actin-Processing Factors. *Cell* **154**, 1047-1059 (2013).

179. Fernandez, B. G., Gaspar, P., Bras-Pereira, C., Jezowska, B., Rebelo, S. R. and Janody, F. Actin-Capping Protein and the Hippo pathway regulate F-actin and tissue growth in Drosophila. *Development* **138**, 2337-2346 (2011).

180. Mo, J. S., Park, H. W. and Guan, K. L. The Hippo signaling pathway in stem cell biology and cancer. *EMBO Rep.* **In Press**, (2014).

181. Sansores-Garcia, L., Bossuyt, W., Wada, K. I., Yonemura, S., Tao, C. Y., Sasaki, H. and Halder, G. Modulating F-actin organization induces organ growth by affecting the Hippo pathway. *EMBO. J.* **30**, 2325-2335 (2011).

182. Yang, C., Tibbitt, M. W., Basta, L. and Anseth, K. S. Mechanical memory and dosing influence stem cell fate. *Nature Mater.* **13**, 645-652 (2014).

183. Sun, Y., Yong, K. M. A., Villa-Diaz, L. G., Zhang, X., Chen, W., Philson, R., Weng, S., Xu, H., Krebsbach, P. H. and Fu, J. Hippo/YAP-mediated rigidity-dependent motor neuron differentiation of human pluripotent stem cells. *Nature Mater.* **In press**, (2014).

184. Connelly, J. T., Gautrot, J. E., Trappmann, B., Tan, D. W. M., Donati, G., Huck, W. T. S. and Watt, F. M. Actin and serum response factor transduce physical cues from the microenvironment to regulate epidermal stem cell fate decisions. *Nat. Cell Biol.* **12**, 711-718 (2010).

185. Schratt, G., Philippar, U., Berger, J., Schwarz, H., Heidenreich, O. and Nordheim, A. Serum response factor is crucial for actin cytoskeletal organization and focal adhesion assembly in embryonic stem cells. *J. Cell Biol.* **156**, 737-750 (2002).

186. Zhou, J., Lee, P. L., Lee, C. I., Wei, S. Y., Lim, S. H., Lin, T. E., Chien, S. and Chiu, J. J. BMP receptor-integrin interaction mediates responses of vascular endothelial Smad1/5 and proliferation to disturbed flow. *J. Thromb. Haemost.* **11**, 741-755 (2013).

187. Du, J., Chen, X., Liang, X., Zhang, G., Xu, J., He, L., Zhan, Q., Feng, X.-Q., Chien, S. and Yang, C. Integrin activation and internalization on soft ECM as a mechanism of induction of stem cell differentiation by ECM elasticity. *Proc. Natl. Acad. Sci. U. S. A.* **108**, 9466-9471 (2011).

188. Faulk, W. P., Matthews, R., Stevens, P. J., Bennett, J. P., Burgos, H. and Hsi, B. L. Human amnion as an adjunct in wound-healing. *Lancet* **1**, 1156-1158 (1980).

189. Kim, J. S., Kim, J. C., Na, B. K., Jeong, J. M. and Song, C. Y. Amniotic membrane patching promotes healing and inhibits proteinase activity on wound healing following acute corneal alkali burn. *Exp. Eye. Res.* **70**, 329-337 (2000).

190. Koob, T. J., Rennert, R., Zabek, N., Massee, M., Lim, J. J., Temenoff, J. S., Li, W. W. and Gurtner, G. Biological properties of dehydrated human amnion/chorion composite graft: implications for chronic wound healing. *Int. Wound J.* **10**, 493-500 (2013).

191. Stern, M. The grafting of preserved amniotic membrane to burned and ulcerated surfaces, substituting skin grafts. *JAMA* **13**, 973-974 (1913).

192. Chung, S., Sudo, R., Vickerman, V., Zervantonakis, I. and Kamm, R. Microfluidic platforms for studies of angiogenesis, cell migration, and cell-cell interactions. Sixth International Bio-Fluid Mechanics Symposium and Workshop March 28-30, 2008 Pasadena, California. *Ann. Biomed. Eng* **38**, 1164-1177 (2010).

193. Izumi, M., Pazin, B. J., Minervini, C. F., Gerlach, J., Ross, M. A., Stolz, D. B., Turner, M. E., Thompson, R. L. and Miki, T. Quantitative comparison of stem cell marker-positive cells in fetal and term human amnion. *J. Reprod. Immunol.* **81**, 39-43 (2009).

194. Miki, T., Marongiu, F., Dorko, K., Ellis, E. C. and Strom, S. C. Isolation of amniotic epithelial stem cells. *Curr. Protoc. Stem. Cell Biol.* **Chapter 1**, Unit 1E 3 (2010).

195. Livak, K. J. and Schmittgen, T. D. Analysis of relative gene expression data using real-time quantitative PCR and the 2(-Delta Delta C(T)) method. *Methods* **25**, 402-408 (2001).

196. Dobin, A., Davis, C. A., Schlesinger, F., Drenkow, J., Zaleski, C., Jha, S., Batut, P., Chaisson, M. and Gingeras, T. R. STAR: Ultrafast universal RNA-seq aligner. *Bioinformatics* **29**, 15-21 (2013).

197. Anders, S., Pyl, P. T. and Huber, W. HTSeq - a Python framework to work with high-throughput sequencing data. *Bioinformatics* **31**, 166-169 (2015).

198. Robinson, M. D., McCarthy, D. J. and Smyth, G. K. edgeR: A Bioconductor package for differential expression analysis of digital gene expression data. *Bioinformatics* **26**, 139-140 (2010).

199. Eisen, M. B., Spellman, P. T., Brown, P. O. and Botstein, D. Cluster analysis and display of genome-wide expression patterns. *Proc. Natl. Acad. Sci. U. S. A.* **95**, 14863-14868 (1998).

200. Saldanha, A. J. Java Treeview - extensible visualization of microarray data. *Bioinformatics* **20**, 3246-3248 (2004).

201. Haas, B. J., Papanicolaou, A., Yassour, M., Grabherr, M., Blood, P. D., Bowden, J., Couger, M. B., Eccles, D., Li, B., Lieber, M., Macmanes, M. D., Ott, M., Orvis, J., Pochet, N., Strozzi, F., Weeks, N., Westerman, R., William, T., Dewey, C. N., Henschel, R., Leduc, R. D., Friedman, N. and Regev, A. De novo transcript sequence reconstruction from RNA-seq using the Trinity platform for reference generation and analysis. *Nat. Protoc.* **8**, 1494-1512 (2013).

202. Love, M. I., Huber, W. and Anders, S. Moderated estimation of fold change and dispersion for RNA-seq data with DESeq2. *Genome Biol.* **15**, 550 (2014).

203. Subramanian, A., Tamayo, P., Mootha, V. K., Mukherjee, S., Ebert, B. L., Gillette, M. A., Paulovich, A., Pomeroy, S. L., Golub, T. R., Lander, E. S. and Mesirov, J. P. Gene set

enrichment analysis: a knowledge-based approach for interpreting genome-wide expression profiles. *Proc. Natl. Acad. Sci. U. S. A.* **102**, 15545-15550 (2005).

204. Wang, X. W., Spandidos, A., Wang, H. J. and Seed, B. PrimerBank: A PCR primer database for quantitative gene expression analysis, 2012 update. *Nucleic. Acids. Res.* **40**, D1144-D1149 (2012).

205. Tadeu, A. M. B., Lin, S., Hou, L., Chung, L. S., Zhong, M., Zhao, H. Y. and Horsley, V. Transcriptional profiling of ectoderm specification to keratinocyte fate in human embryonic stem cells. *PLoS One* **10**, e0122493 (2015).

206. Sankar, S., Tanner, J. M., Bell, R., Chaturvedi, A., Randall, R. L., Beckerle, M. C. and Lessnick, S. L. A novel role for keratin 17 in coordinating oncogenic transformation and cellular adhesion in ewing sarcoma. *Mol. Cell Biol.* **33**, 4448-4460 (2013).

207. Xu, J., Zhu, D. H., He, S. K., Spee, C., Ryan, S. J. and Hinton, D. R. Transcriptional regulation of bone morphogenetic protein 4 by tumor necrosis factor and its relationship with age-related macular degeneration. *FASEB J.* **25**, 2221-2233 (2011).